Photonic Implementation of an Instantaneous Frequency Measurement

A dissertation submitted for the requirements of
Doctor of Philosophy

by
Niusha Sarkhosh
B.Eng. (Electrical Engineering, First Class Honors), RMIT University

School of Electrical and Computer Engineering
Portfolio of Science, Engineering and Technology
RMIT University
March 2009

Declaration

The candidate hereby declares that the work contained in this thesis is her own and that all sources of information have been duly acknowledged. Also, this work has not been submitted previously, in whole or part, with respect of any other award and the work has been carried out since the official date of commencement of the programme.

Niusha Sarkhosh.

Acknowledgements

There are many people, who through the course of this research, have supported me both with aspects of the research itself, but also those who have sustained me personally. I would like to take this opportunity to thank you all.

My sincerest thanks and appreciation goes to my senior supervisor, Associate Professor Arnan Mitchell. His ideas, encouragement and insight were most valuable over the course of this research. I found his knowledge of the field, motivation and enthusiasm for research very inspiring, he made this work an enjoyable experience. I would also like to thank Dr. Lam Bui, and Dr. Thach Nguyen for their interest in this work and for their fruitful discussions.

I sincerely thank Professor Mike Austin, Professor Irena Cosic, Associate Professor Kourosh Kalantar-Zadeh and Mr. Tom Bergin for their strong ongoing support.

I am grateful to all my friends and colleagues in the Optical Lab, for their valuable help and humor, Georgi, Vjay, Ernest, Sumithra, Brenden, Mahyar, Eghan, Yousif and Geeth. Thanks also to my friends Samaneh, Adel, and Janet for their great friendships. To my old and new friends, I would like to thank you all.

My appreciation to the staff members who were extremely helpful at various stage of this work. Associate Professor James Scott, Dr. Alan Harvey, Dr. Heiko Rodolph, Dr. Anthony Holland, Associate Professor Zahir Hussain, Dr. Calude Zorzan, Mr. David Welch and Mr. Yuxun Cao.

To my brother Arshia, my aunty Aghen and my uncles, thanks to the whole of my family. Thank you for being in touch with me at all times and for your moral support. My most heartfelt thanks to my parents and my grandparents, I am grateful for your unconditional love, understanding and encouragement.

Finally, I thank my most precious friend, Hossein. Thank you for your unsparing dedication and continuous support. Without you this project couldn't have been completed.

To all, thank you.

To my Parents, to my Grandma and to the memory of my Grandpa.

Abstract

With the rapid and ongoing developments in telecommunication and electronic warfare technology, faster and more flexible systems are in demand. Wideband signal processing is thus needed to implement such systems. Microwave photonics has been introduced as a tool for achieving such ultra broadband signal processing.

Instantaneous Frequency Measurement (IFM) receivers play an important role in electronic warfare. They have been developed as a means of obtaining a rapid indication of the presence of a threat and to roughly identify the frequency of the threat signals. They also have the advantages of low-cost, compactness and moderate to good sorting capability in an interference-free environment. The main limitation of the traditional RF IFM receivers is constrained bandwidth. Microwave Photonic IFMs have been considered, but the main disadvantages of photonic realization of the recent IFM receiver is cost.

This work aims to propose and demonstrate low-cost photonic IFM receivers with a broad frequency measurement range. The proposed methods are based on the use of photonic mixing to down-convert the RF modulated optical signals to DC. In a RADAR warning receiver, usually a bank of IFMs is required. Increasing the numbers of IFMs requires an increase in the number of photo-detectors. Thus if low-frequency, low-cost detectors can be used, then the net system cost will be reduced significantly. The concept is proven and the issues arising are analyzed. In the proof of concept system, measurement of the RF frequency required advance knowledge of the RF power. Secondly, the use of co-axial RF cables as delay elements, limited the bandwidth and increased bulk.

Using a photonic hybrid approach to achieve orthogonal measurements was demonstrated as a means of identifying both RF frequency and power simultaneously and independently. Employing all optical mixing removed the need for co-axial RF cables delays using non-linear optical devices such as Semiconductor Optical Amplifier (SOA) and Highly Non-Linear Fiber (HLNF).

The last investigation is to improve the sensitivity of the implemented IFM system. The sensitivity of the implemented system is characterized first and a lock-in technique is employed to improve the sensitivity of the system. The final system achieves a sensitivity of -41 dBm which is comparable with the traditional RF IFM receivers.

Contents

List of Figures

List of Tables

Chapter 1

Introduction

1.1 Motivation

Advanced signal processing techniques are important for modern wireless communication [1] and electronic warfare systems. Modern systems often operate anywhere in the (0-20 GHz) region [2] and can be required in the 2-40 GHz range [3]. Wideband signal processing is essential to increase the RF spectrum efficiency and improve the quality of these systems. For instance an approach in communication systems could be smart antennas [4]. Smart antennas exploit the space domain to increase the capacity of communication systems. These systems require adaptive signal processing algorithms to track the desired signals continuously, as well as identify and remove any interference. An important element in military strategy is electronic warfare in which RADAR plays a primary role [5, 6]. Similar to smart antennas, application of advanced signal processing techniques are crucial for locating the enemy RADAR both in space and frequency so that the appropriate counter measure can be precisely deployed.

Technologies used for signal processing, include conventional direct Radio Frequency (RF) techniques, digital techniques, intermediate frequency (IF) techniques and photonic techniques [2, 7]. Direct RF techniques suffer an increased loss, high dispersion, and unwanted radiation problems in high frequencies. The systems that use traditional RF techniques can be bulky and often lack the agility required to perform advanced signal processing in rapidly changing environments. Digital techniques, although very flexible, are currently limited by analogue to digital conversion rates of only few GHz. IF techniques are implemented using mixers to segment broadband spectra in to GHz slices and then mix this down to a lower frequency where digital sampling techniques can be employed. Image and intermodulation frequency generation, and non-linear frequency dependent conversion gain are typical problems. The need for multiple parallel systems for each component of the broadband spectrum is also a problem, for instance; 40 IF

stages with 1 GHz bandwidth would be needed to cover the 0-40 GHz band. In traditional defence applications, IF and digital techniques are very popular; however, the significant hardware associated with the transport and processing of multiple IF signals, specifically cabling, can introduce considerable cost, bulk and weight [2, 8].

A new signal processing technique which has recently been developed is microwave photonic signal processing [9]. The attractive features of this technique are handling broadband signals directly therefore avoiding problems associated with the limited frequency range of digital implementations and the parallel implementations used in IF processing for frequency down conversion. Microwave photonic also offers frequency independent loss, elimination of the need for matching networks, and immunity to electromagnetic interference. It is possible to perform some signal processing operations directly in the photonic domain [8, 10].

Microwave photonic signal processing has already been demonstrated in applications such as phase shifters [11–13], true time delay beamforming/steering [14, 15], microwave filters [16–18], and nullforming/steering systems [19, 20] to name a few. Several papers provide a review on this topic [10, 21–26].

Many of these reported microwave photonic systems aim to identify and control RADAR signals in space. It is equally important to identify the location RADAR threats in frequency. One system dedicated to this task is the Instantaneous Frequency Measurement (IFM) receiver.

Several configurations of IFM receivers have been reported over the past decades. A review of IFM receivers attempted in the literature follows.

1.2 Review of Instantaneous Frequency Measurement Receivers

RADAR warning receivers are designed to detect and classify potential threats in an electronic warfare environment. RF signal processing techniques are exceptionally incisive; however, they can require some advance knowledge of the threat and can also require significant computation resources and time for processing. Instantaneous Frequency Measurement (IFM) systems have been developed as a means of obtaining a rapid indication of the presence of a potential threat and to roughly identify the frequency of the threat signals, suggesting the frequency range in which to focus more sophisticated signal acquisition and processing resources. The major advantages of IFM sytems are good frequency accuracy, low-cost, compactness and moderate to good sorting capability in an interference-free or low-signal-density environment. IFMs are not confused by

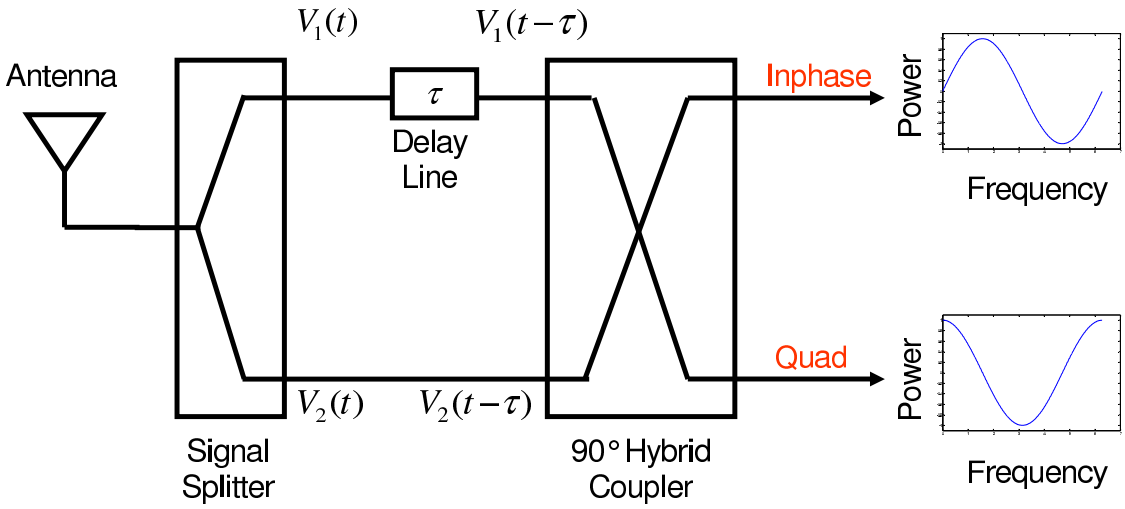

Figure 1.1: RF IFM receiver

wide bandwidth modulations such as chirp and frequency hopping. The IFM is a good compromise between channelized and crystal video intercept receivers [27–29].

For clarity, it will be useful to explain the operation of IFM receivers and the types of these receivers. Figure 1.1 shows a simple block diagram of an electronic IFM. The antenna receives the RF signal (e.g. from the guiding RADAR). This signal is then split into two equal portions using a wideband power splitter. One portion is time delayed by amount τ, relative to the other portion. Both portions were then combined with a 90° RF hybrid coupler. The output of the hybrid coupler consists of frequency dependent amplitude RF signals with 90° phase shift respect to each other. By dividing one output by the other, it is possible to find the RF angular frequency.

Traditional IFM receivers have been deployed for many years [30, 31]. They provide good frequency measurement range (0.5-18 GHz) with sensitivity down to -50 dBm [32]. Traditional IFM receivers have been implemented simply using interferometers formed from microwave hybrid couplers and RF delay lines [33–35].

In recent years, electronic warfare systems operating in the millimeter wave regime (0.5-40 GHz) have become desirable. It is difficult to realize traditional microwave implementations that can provide such broad bandwidth operation [36, 37]. Attempts have been made to improve IFM receiver bandwidth and efficiency. In one work, a frequency measurement range of 6-18 GHz was demonstrated [34]. A multiple delay line IFM design based on a phase discriminator topology was implemented in a co-planar waveguide which enabled dispersion issues to be overcome, but was still subjected to frequency dependent signal fading due to conductor loss.

In another attempt, an IFM receiver with only two delay lines has been demonstrated based on the Chinese remainder theorem [38]. It featured fine frequency resolution and

wide input frequency range. Also improvements in bandwidth have been through phase shifted sampling [39,40]. However, it has stringent fabrication tolerance and could not be reconfigured.

High resolution IFM receivers have also been achieved. A diode ring was used in one IFM and only power dividers in another. Conversion techniques of the output signals were used. These IFMs can achieve frequency resolution better than 1 MHz which depends on the structure of the subsystems and the length of the delay lines [41]. However, this implementation has limited bandwidth and limited reconfigurability.

RF devices can be somewhat bulky and rely on multi-octave RF componentry which can be difficult to implement. Usually banks of the devices are required and they are positioned close to the receiving antenna to ensure the best sensitivity and dynamic range. Lately researchers have endeavored to incorporate emerging microwave photonic technology in order to realize the system that enjoy the merits of both RF and photonic systems [9,42].

1.3 Microwave-Photonics

Microwave photonics is a new technology which uses photonics to manage broadband microwave signals. It has been introduced as a useful tool of increasing the bandwidth of microwave signal processing systems [9, 10, 22, 43–47]. It provides the opportunity to work with ultra broad bandwidths, specifically much greater than typically possible with electrical circuits.

Many researchers have investigated microwave photonics as a replacement for traditional microwave implementations. Remoting is one of the applications of microwave photonics [48]. Applications in which point-to-point routing of analog signals were required have benefited from the excellent propagation characteristics of optical fiber when compared to co-axial cables. Fiber-optic links that remote RF signals to and from phased-array RADAR antennas must meet especially stringent performance requirements. Precisely maintaining both amplitude and phase of the reduced signals over $100's$ of meters. In the past decade, there has been significant progress in the performance of the fiber-optic links that distribute RF signals in antenna-remoting applications, as well as in cellular communications [49,50] and cable television signal distribution networks [51,52].

In another application, microwave photonic techniques have been used, to implement antenna beam forming networks [53]. This system was based on an optical Butler matrix. It allowed simultaneous multi-beam generation capability. This system enabled 40 GHz RF phase measurements with low ripple and high linearity. This showed the ability of microwave photonics to achieve broadband frequency operation.

In various communications systems microwave photonics facilitates achieving broader bandwidths [54]. It enables broadband signal processing which is increasingly needed in high capacity networks as well as electronic warfare systems. Considering this, it may be a good candidate to be employed to implement a photonic IFM receivers which offers broad bandwidth.

One major complaint against microwave photonics is system cost. Therefore some researchers have endeavored to reduce the cost of the microwave photonic systems through the use of low-cost sources. In one work two configurations of tunable and reconfigurable photonic filters were proposed where low-cost optical sources were employed to minimize the total cost of the system [55]. There were two options, one option was a high power configuration based on fixed lasers. The second was a low power configuration based on spectral slicing of a broadband source. A review of photonically implemented IFM receivers attempted in the literature follows.

1.4 Review of Photonic Frequency Measurement

As discussed in Section 1.3 microwave photonics has been demonstrated as a suitable platform for broadband signal processing. Microwave photonics provides low loss, high isolation, and low dispersion. It could be useful for implementing an IFM system and may address many of the issues identified for RF IFM receivers.

Attempts have been made to implement microwave photonic frequency measurement. One of the first works, was done by L. Nguyen [56] where a frequency measurement concept has been demonstrated based on the amplitude comparison of power fading functions generated by double sideband modulated optical carriers propagating through a dispersive medium. A 100 MHz accuracy was achieved over a 4-12 GHz frequency range in a spectrally uncluttered environment with near real time response. This concept was extended to meet the requirements for receivers of this type while offering the potential for wide operating bandwidths and lightweight compact packaging. In a practical RADAR warning receiver, a bank of IFM systems are usually needed. This will result in the need for employing many photo-detectors. Since a broad band high performance photo-detector was employed in this implementation, the total cost of the system could be relatively high, specifically when implementing multiple IFM system.

1.4.1 Optical Power Monitoring

One approach is to employ optical power monitoring. In one work RF frequency measurement has been achieved based on monitoring the optical power [57]. The RF signal

to be measured was modulated onto two optical carriers with their wavelengths set at one peak and one valley of the spectral response of a sinusoidal filter. A Mach-Zehnder Modulator (MZM) biased at a null was employed to perform intensity modulation with suppressed carrier. A mathematical model was developed to establish a relation between the optical powers from each of the two wavelength channels and the microwave frequency to be measured. The microwave frequency was thus evaluated by simply monitoring the optical powers at the outputs of the two wavelength channels [57]. However, this system has limited stability as it employed a Sagnac loop filter and sensitivity due to the poor gain of the null-biased MZM.

In another attempt to utilize optical power monitoring, the measurement of microwave frequency in the optical domain has been demonstrated with adjustable measurement range and resolution. Two optical wavelengths with a large wavelength spacing were modulated by an unknown microwave signal in a MachZehnder Modulator (MZM). The optical output from the MZM was sent to a dispersive fiber to introduce chromatic dispersion, leading to different microwave power penalties for different frequencies. The two wavelengths were then separated, with the microwave powers measured by two photodetectors. A fixed relationship between the microwave power ratio and the microwave frequency was established. The microwave frequency was estimated by measuring the two received microwave powers. The frequency measurement range and resolution could be adjusted by tuning the wavelength spacing [58]. This implementation relied on using a long length of dispersive fiber which could limit the stability and latency of the system. Also broadband photo-detectors were required.

Another approach to measure the RF frequency photonically, was proposed in [59]. It was based on optical power monitoring using a complementary optical filter pair. An optical carrier was modulated by an RF tone using an MZM biased at null to achieve carrier suppression. The suppressed carrier optical signal was then sent to a complementary optical filter pair. The powers from the complementary filters were then measured using two optical power meters. A mathematical expression establishing a relation between RF frequency and the optical powers was then developed and experiments were performed to verify the effectiveness of the proposed approach. Up to 15 GHz frequency measurement was achieved; however, the author indicated that the measurement were poorly accurate. This could be due to the limitations constraint by the complementary optical filter pair where two optical filters must be implemented with exact center frequencies.

1.4.2 Phase Modulation

Phase modulation has also been employed to achieve microwave photonic frequency measurement. In one attempt, a photonic approach for microwave frequency measurement is

proposed in [60]. An optical carrier was modulated by an RF tone to be measured. This was done using a 12 GHz phase modulator. The modulated optical signal is then split into two parts. The first part, passed through a spool of Polarization Maintaining (PM) fiber while the second part traversed through dispersion compensation fiber. This allow introduction of different microwave power penalties. The microwave powers of both parts were then measured by two photo-detectors. A fixed frequency to power mapping was established by obtaining an amplitude comparison function. A proof of concept experiment demonstrated frequency measurement over a range of .5-10.5 GHz, with measurement error less than ± 0.07 GHz. The frequency to power map gained by this technique is polarization dependent, and thus it could be hard to be employed in the harsh battle environment. Furthermore, using spools of PM and dispersion compensated fiber could be cost ineffective when a bank of IFM required.

In a further attempt to employ phase modulation, a technique for instantaneous microwave frequency measurement using an optical phase modulator was proposed and demonstrated practically in [61]. An RF tone with an unknown frequency to be measured was modulated onto two optical carriers with different wavelengths using a phase modulator. The phase-modulated optical carriers then traversed through a spool of dispersive fiber to experience different delays. The delayed signal were then separated and detected at two photo-detectors. Due to the chromatic dispersion of the dispersive fiber, the two RF tones experience different power fading. This results in different power versus frequency functions. A fixed relationship between the RF frequency and the RF powers was then established. The RF frequency was then estimated using this pair of power measurement. The system exhibits less loss compared with the techniques using intensity modulation. Since no bias is needed the system has a better stability, which is highly expected for defense applications. The system was capable of measuring RF frequencies from 7.3-15.05 GHz with 500 MHz accuracy. The noise generated in the phase modulator was identified as the major source of error.

1.4.3 Hi-Resolution IFM Systems

Attempts to improve frequency measurement range and resolution have also been reported. A photonic assisted approach to microwave frequency measurement is proposed based on frequency to power mapping with the help of the so-called amplitude comparison function [62]. The key component was a dual output MZM working at chirped modulation. The proposed scheme was characterized as having simplicity, higher resolution, and tunable measurement range. A frequency accuracy of 50 MHz was achieved beyond 7 GHz. High frequency photo-detectors (25 GHz) were employed which could increase the cost of the IFM system where bank of IFMs required. Also since the system

required using a tunable laser and measuring the response for different optical powers, it can not respond instantaneously, therefore it could have a poor latency and thus not able be practically employed as an IFM system.

In another work, an approach is proposed and demonstrated to improve the measurement range and resolution of a microwave frequency measurement system [63]. Two optical carriers were modulated by a microwave signal using an MZM. The optical output from the MZM was then sent to a dispersive fiber to introduce different chromatic dispersions, leading to different microwave power penalties. A fixed relationship between the microwave power ratio and the microwave frequency was established. The microwave frequency was then estimated by measuring the microwave powers. A frequency measurement accuracy was achieved; however, the frequency measurement range was very limited 9.9-12.2 GHz which could make the system unpractical.

In another attempt to measure the microwave frequency, a photonic RF instantaneous frequency measurement system was proposed and experimentally demonstrated [64]. A frequency measurement independent of the optical input power and microwave modulation index was achieved by using the constructive and destructive ports of a polarization domain interferometer. A single laser diode was used to produce an optical carrier modulated by a Mach-Zehnder Modulator (MZM) biased at null. The output of the MZM then became rotated by 45° and traversed through a PM fiber. A polarization beam splitter was then employed to extract TE and TM components of the carrier and each component was them measured using optical power meters. Experimental tests yielded a peak to peak frequency error lower than 200 MHz for a frequency range of 1-18 GHz. Since the MZM modulator was biased at null, poor sensitivity was inevitable therefore an RF amplifier was used to amplify the input RF power up to 16 dBm. This amount of power may be not practically achievable. Also the system relied on polarization of the carrier which again may reduce the sensitivity in the battle environment.

1.4.4 The Other Attempts

A further approach based on a monolithically integrated echelle diffractive grating was proposed and demonstrated practically [65]. An optical carrier was modulated by an RF tone using an MZM. To suppress the optical carrier, the MZM was biased at null. One of the sidebands was then filtered out using a fiber Bragg grating, while the other sideband was characterized by an echelle diffractive grating based interrogator. the resolution of the integrator was better than 1 pm, therefore it was possible to measure the center wavelength of the sideband accurately. The acquired data, together with the wavelength of the optical carrier, was then used to calculate the the frequency of the RF tone. Relying on a fiber Bragg grating, this system exhibits a frequency measurement accuracy of 200 MHz which

may not be enough for an IFM system. Also a very narrow line-width laser would be needed to get this accuracy which in practice could increase the cost of the whole system as well as latency. This laser should also be tunable as it has to scan the band. Although this system could be employed as a scanning receiver, its low latency makes it difficult to be utilized as an IFM system.

A technique directly maps the frequency information of the incoming simultaneous microwave signals to a distinct set of relative time delays utilizing a dispersive medium was recently demonstrated in [66]. The dispersive medium was a chirped fiber Bragg grating with a reflection bandwidth of .8 nm and a dispersion on 1000 ps/nm. The measurement of the observed time delay directly equates to the value of the input signal frequency. The operation of this technique was successfully verified for two simultaneous signals at 20 and 40 GHz with 1.56 GHz error, demonstrating a potential capability for use in a spectrally cluttered environment.

1.4.5 Summary

In summary, a review of microwave frequency measurement techniques based on photonic approaches has been conducted. High frequency photo-detectors are needed to achieve microwave frequency measurement in some cases. Where multiple IFMs are needed, this approach will not be cost efficient. Also the measurements rely on knowledge of the microwave signal power, which is always unknown in defense applications. Therefore, there is still the need to realize RF frequency measurement independent of RF power level. It would thus be advantageous to implement a cost effective photonic IFM system which is able to measure both RF power and frequency simultaneously.

1.5 Thesis Objective

Traditionally realized IFM receivers must overcome a number of limitations prior to their practical use. The main limitations are bulk, complexity, limited bandwidth, narrow tunability and insufficient reconfigurability. The authors of several publications specifically emphasized the importance of achieving broadband and reconfigurability simultaneously if these IFMs are to meet their applications [31, 33]. To date, none of the concepts reviewed in Section 1.2 have been able to address these limitation adequately and simultaneously.

The objective of this work is to propose, evaluate, realize and characterize a photonic Instantaneous Frequency Measurement receiver with simultaneously broadband and reconfigurable frequency response, while reducing system complexity and cost. A tech-

nique based on using optical mixers to down convert the RF frequency to be measured, will be investigated. The design is anticipated to exhibit broader frequency range when compared to traditional IFM receivers while minimizing complexity and cost. Although the mixing concept and measuring the DC have been previously used as a method to measure the frequency, to the best of our knowledge, this is the first time this method is used to implement a photonic IFM receiver.

1.6 Thesis Overview

This thesis consists of six Chapters. Chapter 2 focuses on photonic implementation of IFM system. Chapter 2 begins with an overview of frequency measurement in general and then describes the concepts and configuration of the new photonic IFM receiver. A reduced cost photonic IFM receiver based on the mixing concept is introduced and developed. Mathematical models are developed to predict the exact system behavior. A proof of concept experiment is developed and results validate the proposed concept.

Chapter 3 moves to configure the IFM system with orthogonal measurements, to be able to measure both RF frequency and power simultaneously while maintaining the main goals of this work of a low-cost and broadband system. Chapter 3 also focuses on employing a photonic hybrid coupler to achieve orthogonal measurements. It is shown that with a slight increase in complexity the system can measure both frequency and RF power independently.

In Chapter 4, the approach of Chapter 2 is modified to improve the operation of the IFM receiver. This Chapter seeks to eliminate the limitations of the experiment of Chapter 2 employing all optical mixing. This is done using non-linear devices such as Semiconductor Optical Amplifier (SOA) or Highly Non-Linear Fiber (HNLF) as all optical mixers. This implementation exhibits greatly improved bandwidth, reduces system complexity and improved system stability.

Chapter 5 investigates the sensitivity of the demonstrated systems and improves the noise floor of the system. Different noise sources and their effect on the performance of the system sensitivity are identified. Lock-in techniques are employed to improve the noise floor of the system. A noise floor of -41 dBm is demonstrated for a photonic IFM system with 10 GHz bandwidth. This sensitivity is comparable to traditional RF IFM receivers.

Chapter 6 summarize the overall achievement of this research and highlights a pathway for future work.

1.7 Original Contributions

The original contributions of this Thesis are as follows:

1. Proposed and demonstrated a photonic Instantaneous Frequency [67] which based on the calculation of [68]. This design provides insight into the practical issues encountered when realizing this system.

2. Proposed and demonstrated a method of all non-linear mixing to implement a Instantaneous Frequency Measurement Receiver. The method is used a Semiconductor Optical Amplifier [69].

3. Design and demonstration a wideband microwave photonic Hilbert transformer [70] which based on the calculation of [71]. This demonstration shows the ability of photonic signal processing to generate wideband in-phase and quadrature-phase.

4. Design and demonstrated a sensitivity improved Instantaneous Frequency Measurement Receiver [72]. This demonstration is based on employing lock-in technique and shows the ability to improve noise floor up to -41 dBm .

Chapter 2

Photonic Measurement Instantaneous Frequency Measurement (IFM) System

2.1 Introduction

Frequency measurement is a critical component of modern electronic warfare systems as described in Chapter 1. Instantaneous Frequency Measurement (IFM) receivers have been widely used in electronic warfare for many years. These receivers detect the frequencies of threat signals. IFMs provide an early indication of threat classification and also suggest frequency ranges in which to focus more sophisticated spectrum analysis resources.

Rigorous spectrum analysis is usually achieved via a scanning receiver [73]. Here an extremely narrow oscillator tone is tuned across the measurement band and this is mixed with the signal. Only the DC component is measured. This scanning process is very precise and has exceptional noise rejection, but it is essentially serial in nature. It is possible that a smart threat could operate only when the scanning receiver is not looking at a particular frequency. In this case the threat might be missed. To ensure a 100% probability of intercept, a technique must be able to monitor the full spectrum continuously and identify potential threat signals instantaneously. Since identifying the exact frequency spectrum of a threat could require a significant scan time, it is important to narrow the frequency range to reduce the scan time as much as possible. Scanning receivers could then be used to find the exact RADAR threat spectrum. Having the exact spectrum of the threat, it is possible to pattern match this spectrum against a database of known threats to obtain a recommended countermeasure and to take further appropriate action to mislead the threat.

Figure 2.1 shows a missile (threat) targeting an aeroplane being guided by a RADAR on a tank. An IFM receiver is required to instantaneously detect the RADAR signal and direct counter measures to mislead the RADAR. Although IFM systems are common in

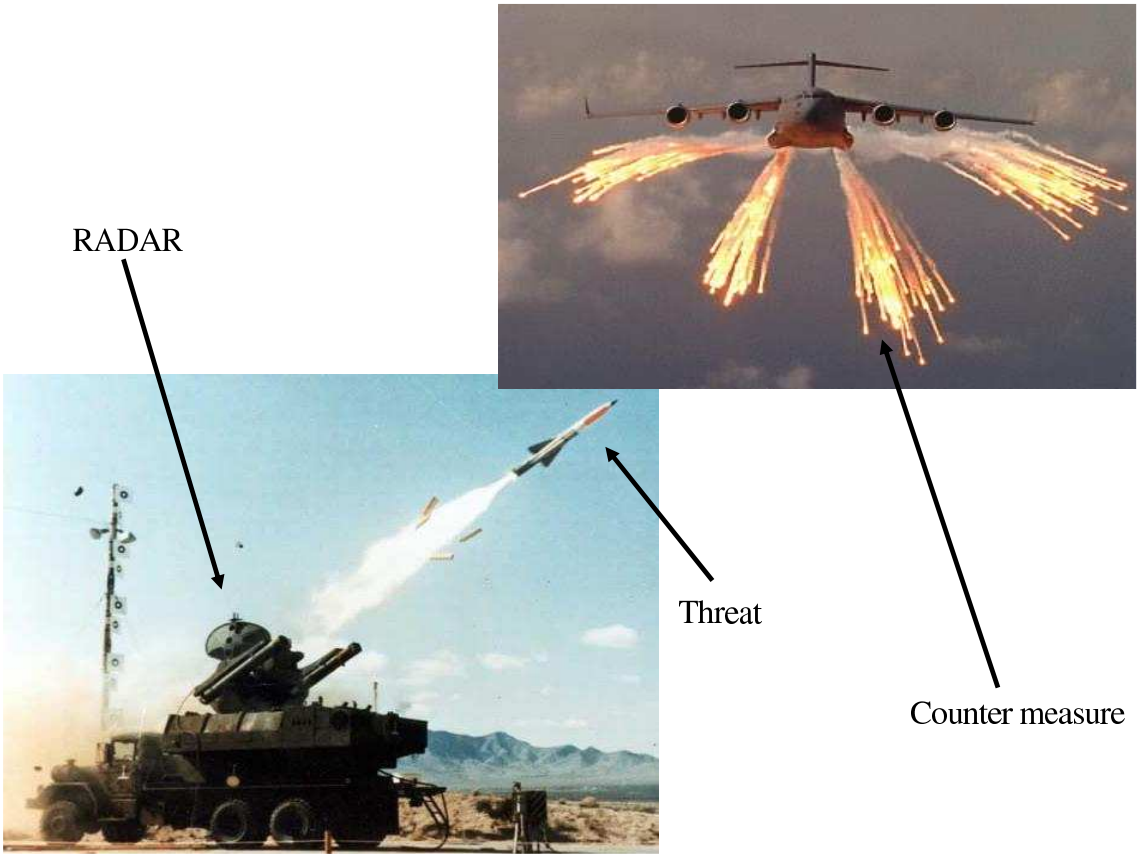

Figure 2.1: The asset (Aeroplane) is being threaten by a threat (missile) being guided by a RADAR.

traditional RF systems, they can have significant limitations. Microwave photonics can help, but systems proposed thus far require expensive high frequency, photo-detectors.

This Chapter investigates the possibility of realizing an IFM receiver using photonics, but in a way that only requires inexpensive low-frequency photo-detectors.

For clarity, the operation of IFM receivers and the types of these receivers are first reviewed in Section 2.2. Both passive and active versions of IFM are identified and microwave photonic IFM receivers introduced as a solution to the bandwidth limitation. In Section 2.3 a new microwave photonic IFM concept is introduced based on using optical modulators as mixers to enable the use of low frequency photo-detectors, in order to reduce the system cost. A photonic IFM system based on this new concept is designed, modelled and demonstrated practically in Section 2.4. Section 2.5 proposes and demonstrates a high frequency version of this low-cost photonic IFM system. Section 2.6 draws conclusions on the practicality of the proposed photonic IFM system and suggests the research focus required for subsequent Chapters. The findings of this Chapter have been published in [67, 68].

2.2 IFM Concept

Traditional IFM systems have been in use for more than 55 years [74]. Traditional RF implementations can be limited in terms of bandwidth, bulk, and cost. Specifically, implementing some components such as wideband splitters and delays is difficult in the RF domain as discussed in Section 1.2.

To understand the limitations and opportunities for IFM systems it will be valuable to review reported implementations. There are two main types of IFM receivers. They can be divided in passive and active versions.

2.2.1 RF Passive IFM

Figure 2.2 shows a simple block diagram of an electronic IFM. An RF signal $v_{in}(t)$ is received from an antenna. This signal is then split into two equal portions using a wideband power splitter. One portion is time delayed by amount τ, relative to the other portion. Both portions are then *summed* with a combiner. The output of the combiner will be an RF signal with an amplitude that depends on frequency. To gain insight into the IFM operation it will be useful to describe it mathematically.

The input signal can be described as :

$$v_{in}(t) = V_\circ \cos \Omega t \tag{2.1}$$

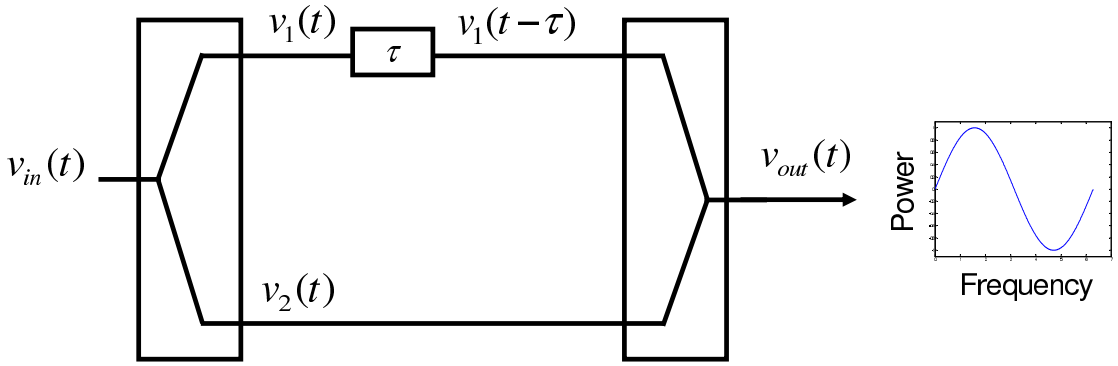

Figure 2.2: Passive RF IFM receiver

where $V_\circ$ and Ω are the amplitude and angular frequency of the RF signal, respectively. The RF signal is then divided into two equal portions using an RF power divider. The voltage at each output of the power divider can be described as:

$$v_1(t) = v_2(t) = \frac{V_\circ}{\sqrt{2}} \cos \Omega t \tag{2.2}$$

The first portion $v_1(t)$, is then delayed by amount τ relative to the second portion $v_2(t)$. Thus:

$$v_1(t-\tau) = \frac{V_\circ}{\sqrt{2}} \cos \Omega(t-\tau) \tag{2.3}$$

The two portions are then *summed* together using a combiner. The summed signals can then be written as:

$$v_m(t) = \frac{V_\circ}{\sqrt{2}} cos\Omega t + \frac{V_\circ}{\sqrt{2}} \cos \Omega(t-\tau) \tag{2.4}$$

Using trigonometric relations, the Equation (2.4) can be rewritten as:

$$v_m(t) = \sqrt{2} V_\circ \cos \frac{\Omega\tau}{2} \cos \Omega(t - \frac{\tau}{2}) \tag{2.5}$$

This output signal is a tone at frequency Ω with amplitude of $\sqrt{2}V_\circ \cos \frac{\Omega\tau}{2}$. This amplitude oscillates with frequency and thus, provided τ is chosen such that the amplitude traces a single period over the desirable frequency range, it is possible to measure the RF frequency by measuring the amplitude of the output signal.

However, to be able to measure the amplitude of this RF tone, an RF power meter must be employed. The RF power meter must measure the amplitude at the frequency of the threat signal (Ω). This may place limitations on the IFM system, especially at ultra high frequencies (40 GHz). Therefore it would be advantageous to develop an IFM system which provides low frequency signals at the output.

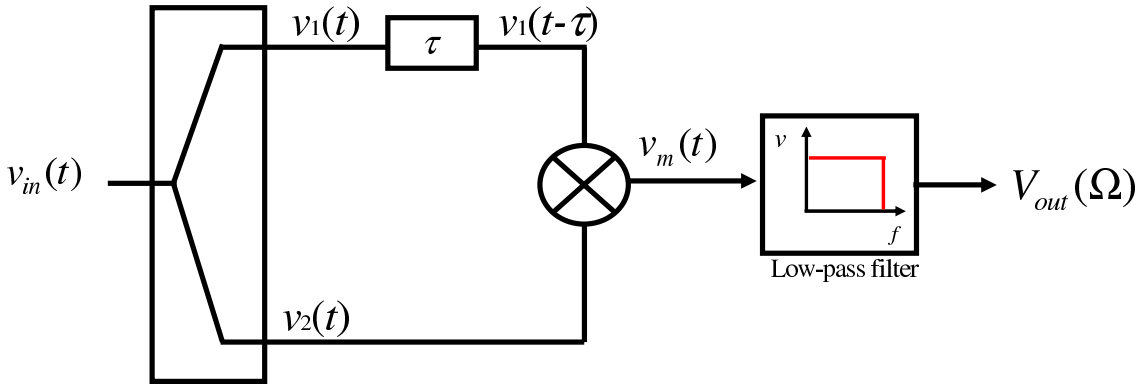

Figure 2.3: Block diagram of a Mixed IFM system.

2.2.2 RF Active/Mixed IFM

In this Section a simple IFM system is presented which uses a DC voltage to measure RF frequency therefore, eliminating the need of using an RF power meter.

Figure 2.3 shows a block diagram of a simplified active IFM system. Similar to the system of Section 2.2.1 and Figure 2.2 a single RF tone $v_{in}(t)$ is divided into two equal portions. One portion is delayed relative to the other by time τ. The two portions are then *multiplied* together. The result is then low-pass filtered. The advantage is that the output should be a DC signal regardless of the RF threat frequency. Hence very simple electronics can be used for detection.

Again to gain further insight it will be valuable to describe IFM operation mathematically. The RF tone can be described as :

$$v_{in}(t) = V_\circ \cos \Omega t \tag{2.6}$$

where $V_\circ$ and Ω are the amplitude and angular frequency of the RF tone, respectively. The RF tone is divided into two equal portions using a wideband power divider. Therefore the voltage at each output of the power divider can be described by:

$$v_1(t) = v_2(t) = \frac{V_\circ}{\sqrt{2}} \cos \Omega t \tag{2.7}$$

The first portion $v_1(t)$, is then delayed by amount τ relative to the second portion $v_2(t)$. Thus:

$$v_1(t-\tau) = \frac{V_\circ}{\sqrt{2}} \cos \Omega(t-\tau) \tag{2.8}$$

Unlike the configuration of Figure 2.2 the two portions are then *multiplied* together. The result of this multiplication can be written as:

$$v_m(t) = \frac{1}{2} V_\circ^2 \cos \Omega t \times \cos \Omega(t-\tau) \tag{2.9}$$

Using trigonometric relations, Equation (2.9) can be written as:

$$\frac{1}{4}V_\circ^2 \cos\Omega(2t-\tau) + \frac{1}{4}V_\circ^2 \cos\Omega\tau \tag{2.10}$$

A low-pass filter, removes the high frequency term $\frac{1}{4}V_\circ^2 \cos\Omega(2t-\tau)$. The remaining voltage present at the output of the interferometer, can then be described as :

$$V_{out}(\Omega) = \frac{1}{4}V_\circ^2 \cos\Omega\tau \tag{2.11}$$

This voltage varies with input RF frequency (Ω), but is not time dependent, hence can be measured using a DC voltmeter. This removes the need for a broadband power meter significantly reduce the cost and complexity of the receiver electronics. However, this IFM system requires a broadband mixer. As discussed in Chapter 1 implementing such mixers and delays could be challenging in the RF domain.

2.2.3 Practical IFM Systems

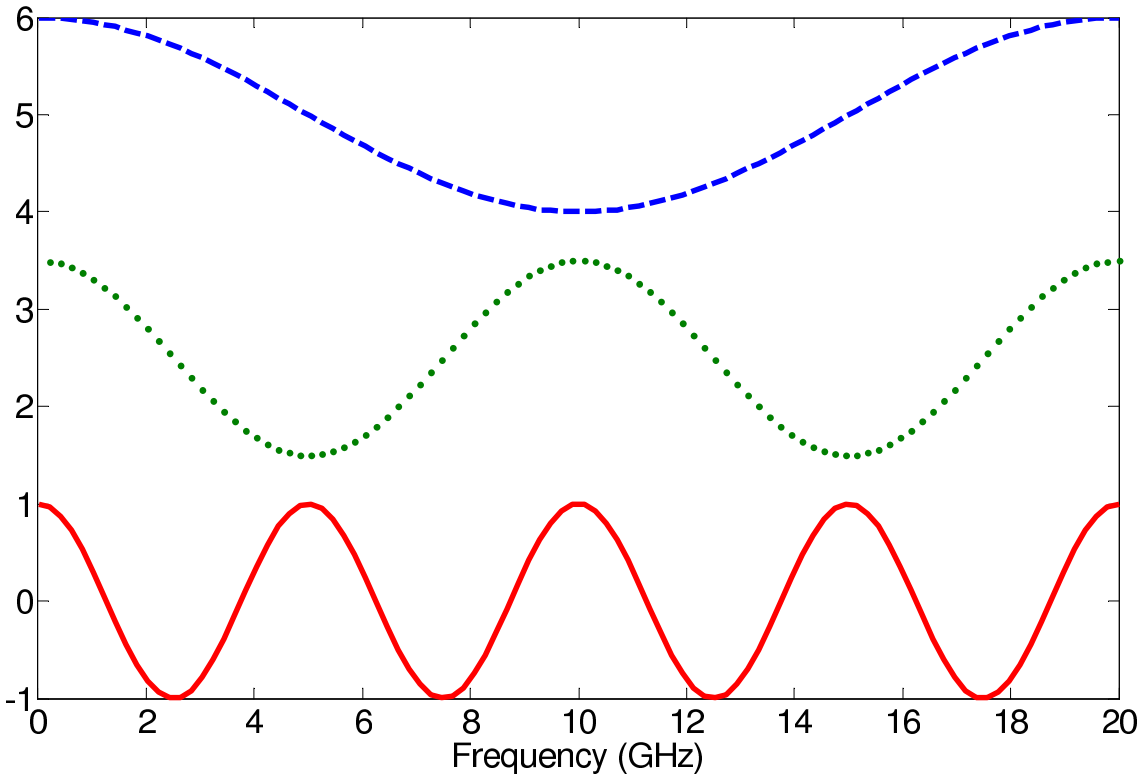

Figure 2.4: The response of a bank of 3 photonic IFM systems which gives 3 bits of resolution.

As Equation (2.5) and Equation (2.11) indicated, the response of the IFM receivers are periodic; therefore, employing only one IFM receiver is not practical if high resolution, multi octave measurements are required. Frequencies within different periods may be indistinguishable. This limitation can be overcome by using banks of IFMs.

Figure 2.4 shows the concept of a bank of IFMs sytems which could be used to measure an RF frequency in a 0.5-20 GHz frequency range. Each IFM system is designed to cover a particular frequency band. This is done using different delays inside each interferometer. Each IFM is designed such that it exhibits responses with decremented bandwidth. The system works based on narrowing the frequency detection region. The first IFM (dashed curve) determines whether the RF frequency is more or less than 5 GHz. The second IFM (dotted curve) then determines whether the RF frequency is below or higher than 2.5 GHz (in a 5 GHz frequency range). Finally the third IFM (solid curve) determines if the RF frequency is less or higher than 1.25 GHz (in a 2.5 GHz frequency range). This could be continued until the desired resolution is achieved.

Banks of IFMs are also required if multiple RF tones are present simultaneously. In this case the same numbers of IFMs are required as separate tones that must be identical.

2.2.4 RF IFM Example

A high resolution IFM receiver employing multiple interferometers has been reported in the literature. A five bit superconductive digital IFM subsystem has been demonstrated in [75, 76]. It has a center frequency of 4 GHz and a bandwidth of 500 MHz. The subsystem contained a cryogenic section with five discriminator modules utilizing superconductive delay lines, GaAs mixers, and power dividers. The subsystem also had a room-temperature GaAs limiting amplifier and a silicon postprocessor.

As evident from [75, 76] traditional IFM receivers can be implemented using interferometers formed from microwave hybrid couplers and RF delay lines. Such implementations can be challenging in the RF domain requiring fairly exotic superconductive elements and hybrid GaAs technology, even to obtain the modest bandwidth reported. RF systems may also incur unwanted radiation at the higher frequencies (10 GHz) which occur inside microwave devices, and can be bulky as well. The dispersive nature of the microwave devices further limit their frequency range. Microwave photonics may have the ability to overcome these problems and thus some research effort has been employed to achieve microwave photonic IFMs.

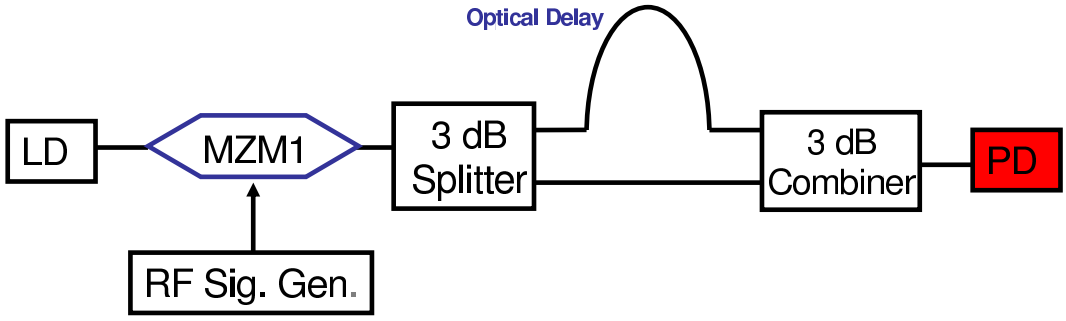

Figure 2.5: Block diagram of the photonic IFM system.

2.2.5 Microwave Photonic IFM

Microwave photonics can handle ultra broad bandwidths (40 GHz and beyond) and may overcome some of the limitations identified with traditional RF systems. In particular attempts have been made to realize photonic IFMs systems in order to harness the broadband features of photonics.

Attempts have been reported to realize a photonic IFM system [56, 77]. Figure 2.5 shows an experimental diagram from one recent investigation into photonic IFMs . A RF tone was provided by an RF signal generator. A laser diode (LD) provided the optical carrier. The RF signal and the optical carrier were mixed using an MZM. At the output of the MZM there was an interferometer. Consisting of a 3dB optical splitter, optical delay lines and a 3dB optical combiner. The output signal of the MZM was equally divided in to two portions by the 3dB optical splitter. One portion was delayed with respect to the other by the optical delay line. The two portions were then combined by the 3dB optical combiner. The signal was then detected by a broadband photo-detector and the RF signal amplitude was measured using an RF power meter.

Comparing this photonic example with the RF passive IFM in Section 2.2.1 (Figure 2.2), it is evident that the two systems are similar. The RF signal splitter is replaced with the 3dB optical splitter. For the delay, instead of using the RF delay lines, optical delay lines were used. These optical devices have GHz and even THz bandwidth, low weight and low-cost. A 3dB optical combiner was used instead of the RF coupler to sum the signals. Since the system is equivalent to a passive IFM receiver, an RF power meter must be employed to measure the output of the broadband photo-detector.
As discussed in Section 2.2.4, there is a need for banks of these IFMs in order to make high resolution measurements over broad bandwidths and identify multiple tones. Due to the high cost of broadband photo-detectors, implementing banks of these devices would be prohibitively expensive. As discussed in Chapter 1, IFM should be cost effective; therefore, it would be advantageous to implement an IFM system that requires only low frequency photo-detectors and thus becomes inexpensive.

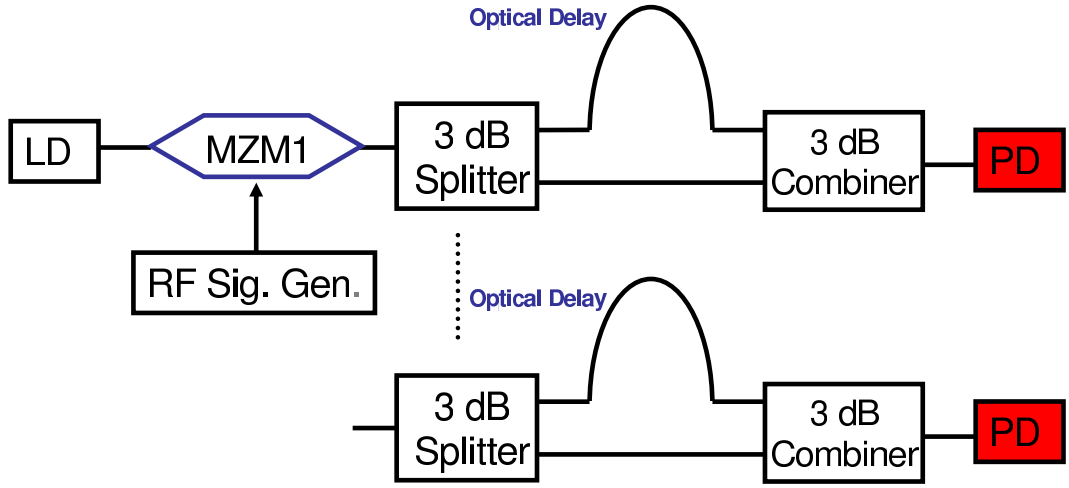

Figure 2.6: Block diagram of the bank photonic IFM system.

2.3 Photonic Mixed IFM Concept

The aim of this Section is to implement a photonic IFM receiver, which is comparable in performance with existing IFM receivers but requires only low-cost photo-detectors. This system will inherit the cost effectiveness from the mixed IFM system of Section 2.2.2 and the broad bandwidth from photonics of Section 2.2.5.

Figure 2.7 shows a block diagram of the proposed photonic IFM system. An RF tone is divided into two equal parts. The first part modulates an optical carrier (Figure 2.7 inset a)). Therefore two sidebands are added to the optical carrier (Figure 2.7 inset b)). The

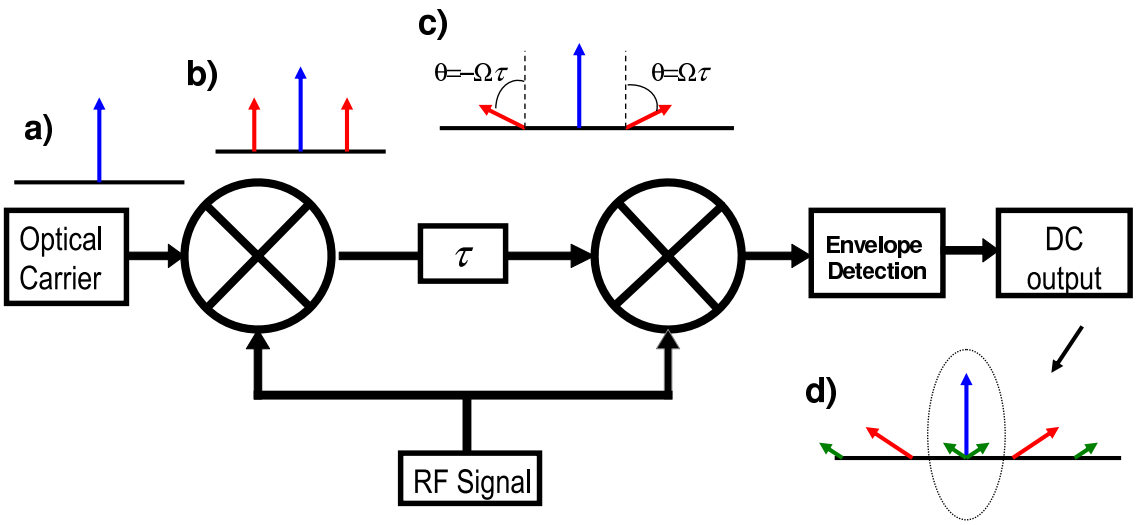

Figure 2.7: Block diagram of the proposed photonic IFM system.

modulated optical carrier then experiences a delay of τ which causes a phase rotation of $\theta = \Omega\tau$ on the sidebands, where Ω is the RF tone angular frequency (Figure 2.7 inset c)). This signal is then re-modulated by the second portion of the RF tone and as a result, each sideband becomes the carrier of its own sidebands (Figure 2.7 inset d)). Using a DC detector, only the optical power is detected; however, the optical carrier has two phase shifted sidebands coherently summed with it. The power may thus be increased or decreased depending on the phase of the sidebands. Since the sideband phase shift (θ) is frequency dependent, the amount of DC voltage at the output of the DC photo-detector is also frequency dependent. This system should thus enable frequency measurement with only DC detection.

2.3.1 Photonic Mixed IFM Model

To gain a better understanding of the proposed system of Figure 2.7, a simple mathematical model is developed in this Section. The simple aspect of the model is that ideal elements are used. The optical carrier $e(t)$ can be expressed as:

$$e(t) = E_\circ e^{j\omega_\circ t} \tag{2.12}$$

where $E_\circ$ and $\omega_\circ$ are the amplitude and angular frequency of the electrical field of the optical carrier. The RF tone $v_{in}(t)$ can be written as:

$$v_{in}(t) = V_\circ \cos \Omega t \tag{2.13}$$

where $V_\circ$ and Ω are the amplitude and angular frequency of the RF tone. The RF tone is divided equally into two portions, therefore the voltage of each portion can be written as:

$$e_1(t) = e_2(t) = \frac{1}{\sqrt{2}} V_\circ \cos \Omega t \tag{2.14}$$

After the first modulator, the modulated carrier can be described as:

$$e_1(t) = \frac{1}{\sqrt{2}} E_\circ V_\circ e^{j\omega_\circ t} \cos \Omega t \tag{2.15}$$

The modulated carrier (Equation (2.15)) is then delayed by τ, and thus can be written as:

$$e_1(t-\tau) = \frac{1}{\sqrt{2}} E_\circ V_\circ e^{j\omega_\circ (t-\tau)} \cos \Omega (t-\tau) \tag{2.16}$$

This signals of Equation (2.14) and Equation (2.3.1) are then multiplied to produce:

$$e_2(t) = \frac{1}{2}E_\circ V_\circ^2 e^{j\omega_\circ(t-\tau)} \cos\Omega(t-\tau) \times \cos\Omega t \tag{2.17}$$

At the output an envelope detector measures the power. The output signal from this envelope detection is thus:

$$I = r * e_2 \times e_2^* = \frac{1}{4}rE_\circ^2 V_\circ^4 \cos\Omega^2(t-\tau) \times \cos^2\Omega t \tag{2.18}$$

where r is the detector responsivity index. Equation (2.18) can be expanded as:

$$I = \frac{1}{4}rE_\circ^2 V_\circ^4 \frac{1+cos2\Omega(t-\tau)}{2} \times \frac{1+cos2\Omega t}{2} \tag{2.19}$$

Using trigonometric equations, Equation (2.19) can be written as:

$$I = \frac{1}{4}rE_\circ^2 V_\circ^4 \left[\frac{1}{4} + \frac{1}{8}\cos 2\Omega(2t-\tau) + \frac{1}{8}\cos 2\Omega\tau\right] \tag{2.20}$$

A filter isolates the DC term. Equation (2.20) thus becomes:

$$I = \frac{1}{16}rE_\circ^2 V_\circ^4 + \frac{1}{32}rE_\circ^2 V_\circ^4 \cos 2\Omega\tau \tag{2.21}$$

Equation (2.21) clearly shows the frequency dependence of the DC output of the detector, and also shows the DC output has a cosine shape and is in proportion to the optical power. This DC output could thus be used to measure the RF frequency.

Having conceived a mixed IFM system that could be implemented photonically, it is now possible to develop a practical photonic mixed IFM system that is able to measure RF frequencies using DC photo-detectors.

2.3.2 Practical Photonic IFM System Configuration

This Section aims to implement the configuration of Figure 2.7 as a practical system. Figure 2.8 shows the experimental setup of the proposed photonic IFM system. The input signal was provided with an RF signal generator, which was divided equally into two parts using an RF Wilkinson power divider feeding the two arms of the IFM system. One part of the RF signal was input to the first MZM (MZM1). This signal was then mixed with the optical carrier which was provided by a laser diode (λ_1). The modulated optical carrier then experienced a delay through a length of optical fiber. The second part of the RF signal was input to the second MZM (MZM2) at the far end of the optical delay. The re-modulated signal was then amplified using an EDFA and filtered using an AWG to remove unwanted spontaneous emission introduced by the EDFA. The DC output signal

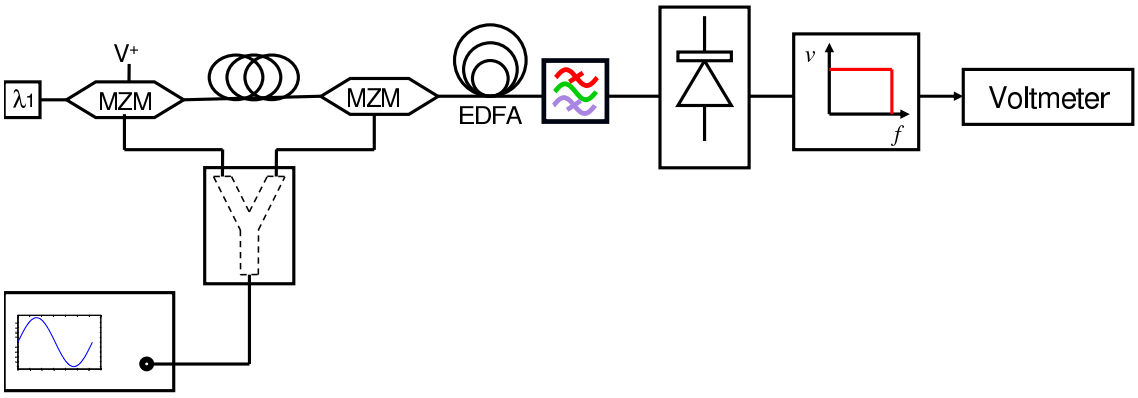

Figure 2.8: Experimental setup of proposed photonic IFM system

was then detected by a photo-detector. The electrical output was low-pass filtered and recorded using a digital voltmeter.

Having conceived a practical photonic IFM system configuration, a more realistic theoretical model should be developed to accurately predict the frequency dependence of the DC term of the photo-detector output voltage as a function of predicted system parameters.

2.3.3 Practical Photonic IFM Model

As with previous sections, further insight into the system of Figure 2.8 will be gained by describing its operation mathematically. The aim of this Section is to develop an accurate model predicting the components that determine the value of DC output of the photo-detector of the system of Figure 2.8.

The single RF tone can be written as:

$$v_{in}(t) = V_\circ \cos \Omega t \tag{2.22}$$

where Ω is the angular frequency of the RF tone,and

$$V_\circ = \sqrt{2 Z_{in} P_{RF}} \tag{2.23}$$

is the amplitude of the RF tone, where Z_{in} is the input impedance of MZM1 and P_{RF} is the RF input tone power present at the RF port of MZM1. The RF tone modulates an optical carrier which can be described as:

$$e(t) = E_\circ e^{j\omega t} \tag{2.24}$$

where $E_\circ$ and ω are amplitude and angular frequency of the electrical field of the optical carrier respectively. Provided MZM1 operates in push-pull mode (ideally with zero

chirp),the output signal of MZM1 can then be described as:

$$e_1(t) = \sqrt{L_1}E_\circ e^{j\omega t}\cos[\frac{\pi(v_{in}(t)+V_{B_1})}{2V_{\pi_1}}] \tag{2.25}$$

where L_1 is the loss of MZM1 including fiber patch, V_{B_1} is DC bias of MZM1 , and V_{π_1} is MZM1 half wave voltage. Substituting Equation (2.22) in Equation (2.25), it can be deduced that:

$$e_1(t) = \sqrt{L_1}E_\circ e^{j\omega t}\cos[\frac{\pi(V_\circ\cos\Omega t+V_{B_1})}{2V_{\pi_1}}] \tag{2.26}$$

Equation (2.26) can be expanded as:

$$e_1(t) = \sqrt{L_1}E_\circ e^{j\omega t}\left[\cos\left(\frac{\pi V_\circ}{2V_{\pi_1}}\cos\Omega t\right)\times\cos\frac{\pi V_{B_1}}{2V_{\pi_1}} - \cos\left(\frac{\pi V_\circ}{2V_{\pi_1}}\sin\Omega t\right)\times\sin\frac{\pi V_{B_1}}{2V_{\pi_1}}\right] \tag{2.27}$$

In order to isolate the frequency components of the Equation (2.26) a Fourier decomposition is used. The following equations are useful:

$$\begin{aligned}\cos(a\cos\Omega t) &= J_\circ(a) + 2\sum_{m=1}^{\infty}J_{2m}(a)\sin 2m\Omega t\\ \cos(a\sin\Omega t) &= 2\sum_{m=1}^{\infty}J_{2m+1}(a)\cos(2m+1)\Omega t\end{aligned} \tag{2.28}$$

where J_k is the Bessel function of the first kind. Defining $a = \frac{\pi V_\circ}{2V_{\pi_1}}$ and substituting Equation (2.28) in to Equation (2.27), yields:

$$\begin{aligned}e_1(t) = \sqrt{L_1}E_\circ e^{j\omega t}\ \Bigg\{&cos\tfrac{\pi V_{B_1}}{2V_{\pi_1}}\left[J_\circ(\tfrac{\pi V_\circ}{2V_{\pi_1}}) + 2\sum_{m=1}^{\infty}J_{2m}(\frac{\pi V_\circ}{2V_{\pi_1}})\sin 2m\Omega t\right]\\ &-2\sin\tfrac{\pi V_{B_1}}{2V_{\pi_1}}\sum_{m=0}^{\infty}J_{2m+1}(\frac{\pi V_\circ}{2V_{\pi_1}})\cos(2m+1)\Omega t\Bigg\}\end{aligned} \tag{2.29}$$

To simplify Equation (2.29), note that distant threat signals have low power, therefore contribution of harmonics components is insignificant except the fundamental at Ω and the DC component. These harmonics can thus be neglected and Equation (2.29) can approximated as:

$$e_1(t) \approx \sqrt{L_1}E_\circ e^{j\omega t}\left[\cos\frac{\pi V_{B_1}}{2V_{\pi_1}}J_\circ(\frac{\pi V_\circ}{2V_{\pi_1}}) - 2sin\frac{\pi V_{B_1}}{2V_{\pi_1}}J_1(\frac{\pi V_\circ}{2V_{\pi_1}})\cos\Omega t\right] \tag{2.30}$$

Equation (2.30) is the closed form of the output electrical field of the MZM1 which only includes the fundamental and DC components.
The signal is then optically delayed, to become:

$$e_1(t-\tau) \approx \sqrt{L_1}E_\circ e^{j\omega(t-\tau)}\left[\cos\frac{\pi V_{B_1}}{2V_{\pi_1}}J_\circ(\frac{\pi V_\circ}{2V_{\pi_1}}) - 2sin\frac{\pi V_{B_1}}{2V_{\pi_1}}J_1(\frac{\pi V_\circ}{2V_{\pi_1}})\cos\Omega(t-\tau)\right] \tag{2.31}$$

This optically delayed signal is then input to MZM2 where it is multiplied by the RF tone again. This RF tone has been delayed through a length of co-axial cable. The time delay τ depends on the relative delay between optical fiber path and co-axial cable path as shown in Figure 2.8. To express mathematically the relative phase difference is labelled $\phi(\Omega)$. Note that due to dispersion of the co-axial cable, $\phi(\Omega)$ can be a nontrivial function of RF frequency resulting in frequency dependent delay. Therefore the second portion of the RF signal present at the input of MZM2 can be described as:

$$\frac{1}{\sqrt{2}} M(\Omega) V_\circ \cos[\Omega t + \phi(\Omega)] \tag{2.32}$$

where $M(\Omega)$ is the absolute magnitude response of the RF Path and $\phi(\Omega)$ is the phase response of the RF Path relative to the Optical Path. For brevity M and ϕ will be used instead of $\phi(\Omega)$ and $M(\Omega)$, respectively.

After modulation by MZM2, Equation (2.31) becomes:

$$\begin{aligned} e_2(t) = \sqrt{L_1 L_2} E_\circ e^{j\omega t} &\left[\cos\frac{\pi V_{B_1}}{2V_{\pi_1}} J_\circ(\frac{\pi V_\circ}{2V_{\pi_1}}) - 2\sin\frac{\pi V_{B_1}}{2V_{\pi_1}} J_1(\frac{\pi V_\circ}{2V_{\pi_1}})\cos\Omega t\right] \times \\ &\left[\cos\frac{\pi V_{B_2}}{2V_{\pi_2}} J_\circ(\frac{\pi M V_\circ}{2V_{\pi_2}}) - 2\sin\frac{\pi V_{B_1}}{2V_{\pi_2}} J_1(\frac{\pi M V_\circ}{2V_{\pi_2}})\cos(\Omega t + \phi)\right] \\ &= e^{j\omega t}[A + B\cos(\Omega t + \phi)][C + D\cos\Omega t] \end{aligned} \tag{2.33}$$

where A, B, C, and D are:

$$\begin{aligned} A &= \sqrt[4]{L_1 L_2 E_\circ^2}\cos(\tfrac{\pi V_{B_1}}{2V\pi_1}) J_\circ(\tfrac{\pi V_\circ}{2V_{\pi_1}}) \\ B &= -2\sqrt[4]{L_1 L_2 E_\circ^2}\sin(\tfrac{\pi V_{B_1}}{2V\pi_1}) J_1(\tfrac{\pi V_\circ}{2V_{\pi_1}}) \\ C &= \sqrt[4]{L_1 L_2 E_\circ^2}\cos(\tfrac{\pi V_{B_2}}{2V\pi_2}) J_\circ(\tfrac{\pi M V_\circ}{2V_{\pi_2}}) \\ D &= -2\sqrt[4]{L_1 L_2 E_\circ^2} sin(\tfrac{\pi V_{B_2}}{2V\pi_2}) J_1(\tfrac{\pi M V_\circ}{2V_{\pi_2}}) \end{aligned} \tag{2.34}$$

This signal of Equation (2.33) is detected by the photo-detector and the output voltage can be described as:

$$v(t) = r Z_{PD} G_{PD}\ e_2(t) \times e_2(t)^* = r Z_{PD} G_{PD}[A + B\cos(\Omega t + \phi)]^2 [C + D\cos\Omega t]^2 \tag{2.35}$$

where Z_{PD}, r and G_{PD} are output impedance, responsivity and gain of the photo-detector respectively. Since the DC component of the output voltage of the photo-detector is of interest, it is necessary to expand Equation (2.35).

$$\begin{aligned} v(t) &= r Z_{PD} G_{PD}\left[A^2 + B^2\cos^2(\Omega t + \phi) + 2AB\cos(\Omega t + \phi)\right] \\ &\quad \times \left[C^2 + D^2\cos^2\Omega t + 2CD\cos\Omega t\right] \\ &= r Z_{PD} G_{PD}\left[A^2 + \frac{B^2}{2} + \frac{B^2}{2}\cos 2(\Omega t + \phi) + 2AB\cos(\Omega t + \phi)\right] \\ &\quad \times \left[C^2 + \frac{D^2}{2} + \frac{D^2}{2}\cos 2\Omega t + 2CD\cos\Omega t\right] \end{aligned} \tag{2.36}$$

The DC component of the photo-detector output voltage can be isolated by taking the time invarient components of Equation (2.36) resulting in:

$$V_{DC} = rZ_{PD}G_{PD}\left[\left(A^2 + \frac{B^2}{2}\right)\left(C^2 + \frac{D^2}{2}\right) + 2ABCD\cos\phi + \frac{B^2D^2}{8}\cos 2\phi\right] \tag{2.37}$$

This equation shows that the DC part of the output voltage of the photo-detector consists of a constant DC offset and also some frequency dependent terms. To establish the relative scales of these components and the system parameters that they depend on, some simplifications can be made. The same half-wave voltage is assumed for MZM1 and MZM2 ($V_{\pi_1} = V_{\pi_2} = V_\pi$) and quadrature bias is assumed for both MZMs, ($V_{B_1} = V_{B_2} = \frac{V_\pi}{2}$).

Thus:

$$\cos\tfrac{\pi V_{B_1}}{2V_{\pi_1}} = \sin\tfrac{\pi V_{B_1}}{2V_{\pi_1}} = \cos\tfrac{\pi V_{B_2}}{2V_{\pi_2}} = \sin\tfrac{\pi V_{B_2}}{2V_{\pi_2}} = \tfrac{1}{\sqrt{2}} \tag{2.38}$$

Also making the small signal approximation $\frac{\pi V_\circ}{2V_\pi} \ll 1$ and since transmission through the RF cable does not supply gain, thus $M < 1$:

$$\begin{array}{ccc} J_\circ(\frac{\pi V_\circ}{2V_{\pi_1}}) \approx 1 & , & J_\circ(\frac{\pi MV_\circ}{2V_{\pi_2}}) \approx 1 \\ J_1(\frac{\pi V_\circ}{2V_{\pi_1}}) \approx \frac{\pi V_\circ}{4V_\pi} & , & J_1(\frac{\pi MV_\circ}{2V_{\pi_2}}) \approx \frac{\pi MV_\circ}{4V_\pi} \end{array} \tag{2.39}$$

Therefore, Equation (2.34) can be simplified as:

$$\begin{array}{c} A = C = \sqrt[4]{\frac{L_1L_2E_\circ^2}{4}} \\ B = \frac{1}{M}D = -\sqrt[4]{\frac{L_1L_2E_\circ^2}{4}}\frac{\pi V_\circ}{2V_\pi} \end{array} \tag{2.40}$$

Thus Equation (2.37), becomes:

$$V_{DC} = rZ_{PD}G_{PD}\left[A^4 + \frac{M^2B^4}{4} + \frac{1}{2}(1+M^2)A^2B^2 + 2MA^2B^2\cos\phi + \frac{M^2B^4}{8}\cos 2\phi\right] \tag{2.41}$$

Further simplification is possible by noting the small signal approximation $\frac{\pi V_\circ}{2V_\pi} \ll 1$, and since $M < 1$, infers that $A \gg B$, therefore $A^4 \gg \frac{1}{4}M^2B^4$, and $2MA^2B^2 \gg \frac{1}{8}M^2B^4$. Equation (2.41) can now be written:

$$V_{DC} = rZ_{PD}G_{PD}\left[A^4 + \frac{1}{2}(1+M^2)A^2B^2 + 2MA^2B^2\cos\phi\right] \tag{2.42}$$

Assuming the modulators have identical loss $L_1 = L_2 = L$. A factor G can be defined,

$$G = rG_{PD}L^2 \tag{2.43}$$

Also $E_\circ$ can be described as a function of laser power $P_\circ$, as below:

$$E_\circ = \sqrt{P_\circ} \tag{2.44}$$

Substituting the Equation (2.40) in Equation (2.41), the output voltage can be written as:

$$V_{DC} = \frac{1}{4}GZ_{PD}P_\circ\left[1 + \frac{\pi^2(1+M^2)Z_{in}P_{RF}}{4V_\pi^2} + \frac{\pi^2}{V_\pi^2}MZ_{in}P_{RF}\cos\phi\right] \tag{2.45}$$

This equation shows the DC voltage at the photo-detector. Expanding Equation (2.45):

$$V_{DC} = \frac{1}{4}GZ_{PD}P_\circ + \frac{1}{4}GZ_{PD}P_\circ\frac{\pi^2(1+M^2)Z_{in}P_{RF}}{4V_\pi^2} + \frac{1}{4}GZ_{PD}P_\circ\frac{\pi^2}{V_\pi^2}MZ_{in}P_{RF}\cos\phi \tag{2.46}$$

As can be seen, Equation (2.46) has three terms. The first term is:

$$\frac{1}{4}GZ_{PD}P_\circ \tag{2.47}$$

which is a function of the laser power and is independent of the input RF power and frequency. This term is background interference as it does not vary with frequency. The second term is:

$$\frac{1}{4}GZ_{PD}P_\circ\frac{\pi^2(1+M^2)Z_{in}P_{RF}}{4V_\pi^2} \tag{2.48}$$

which is a function of both optical and RF powers. In theory it should be independent of RF frequency but as the RF cable has a frequency dependent loss $M(\Omega)$, this term also has some nontrivial frequency dependence. The third term is:

$$\frac{1}{4}GZ_{PD}P_\circ\frac{\pi^2}{V_\pi^2}MZ_{in}P_{RF}\cos\phi \tag{2.49}$$

which is a function of both optical and RF powers and is also sinusoidal function of the phase delay ϕ. The term $\phi(\Omega)$ is proportional to the RF frequency and is the term that should be measured.

If the system has identical loss for both the optical path and the RF path then M=1. By substituting M=1 in the Equation (2.45) the DC output voltage will be:

$$V_{DC} = \frac{1}{4}GZ_{PD}P_\circ\left[1 + \frac{\pi^2(2)Z_{in}P_{RF}}{4V_\pi^2} + \frac{\pi^2}{V_\pi^2}Z_{in}P_{RF}\cos\phi\right] \tag{2.50}$$

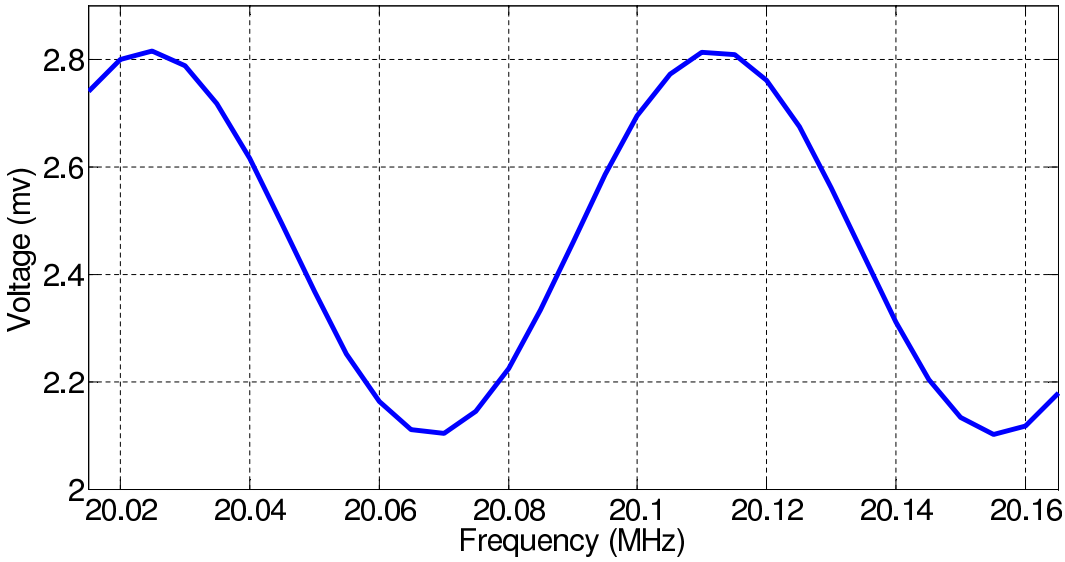

Figure 2.9: Predicted photo-detector DC voltage.

To gain insight into the behavior of the IFM system described by Equation (2.50), typical values are provided as follows: $P_\circ$=5.4 dBm, P_{RF}=13 dBm, Z_{in}=Z_{PD}=50Ω, V_π=5, L=2.345Km which correspond to τ=8.93μs, and the factor G was calculated to be 1.2.

Figure 2.9 shows the prediction result. A sinusoidal relationship is superimposed on a DC offset. In this example, frequency measurement could be made between 20.02 and 20.07 MHz. This narrow frequency range is due to the long length assumed for the optical fiber delay (τ). The example does show however that a frequency measurement system should be possible with the configuration of Figure 2.8. In the next Section the proof of concept will be implemented and characterized.

2.4 Photonic IFM Proof of Concept Demonstration

Having established a relationship in Section 2.3.3 between the DC output voltage of the photo-detector and input RF frequency for the practical mixed photonic IFM system of Figure 2.8, it should now be possible to demonstrate frequency measurement for the proposed mixed photonic IFM system of Figure 2.8.

The system was configured as depicted in Figure 2.8, the laser power was set to $P_\circ$=5.4 dBm and the EDFA gain was maximized (20 dB). An Arrayed Waveguide grating (AWG) with channel width of 0.8 nm was used as the optical filter. RF Signal powers of 10 dBm and 13 dBm were used at the input, Separate measurements were taken. The DC voltage was measured at the output as a function of frequency. Figure 2.10 presents the measured results obtained for this system along with the predicted response of Equation (2.50). Excellent agreement is evident.

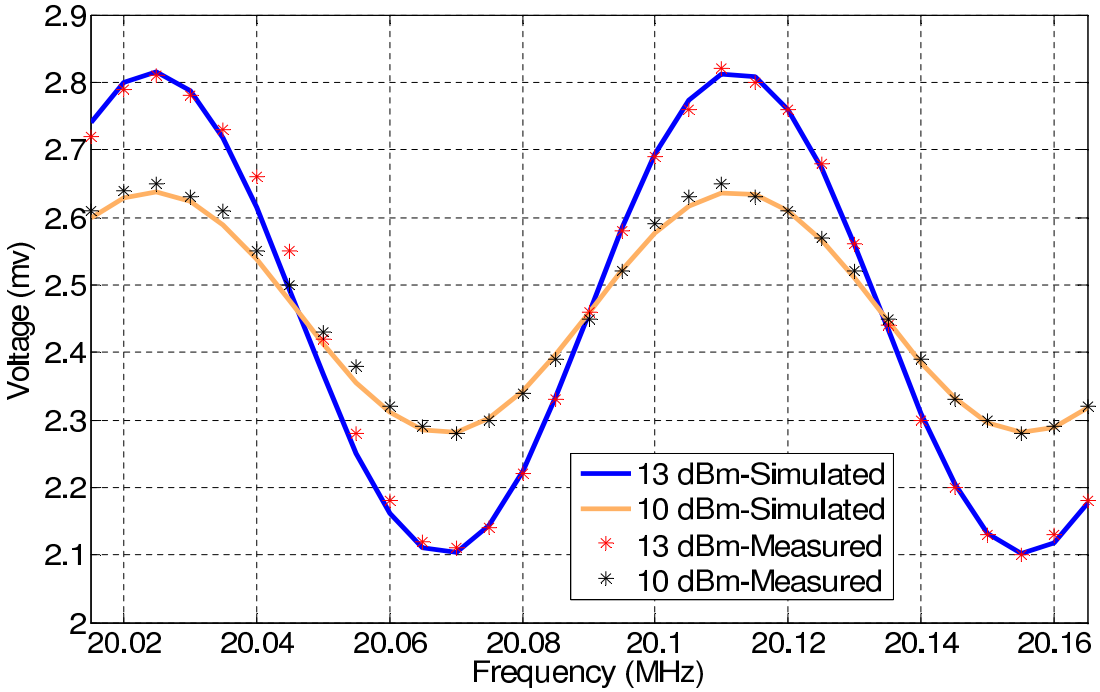

Figure 2.10: Measured and predicted photo-detector DC voltage.

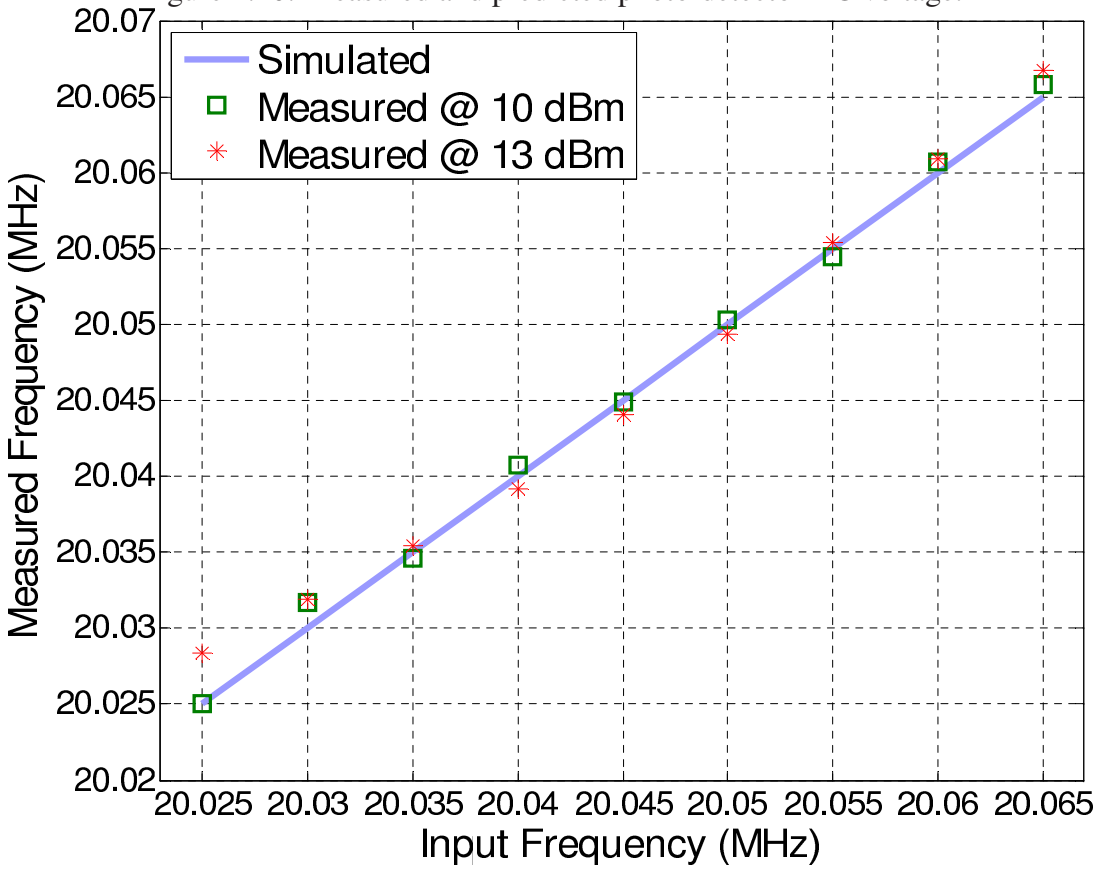

Figure 2.11: Measured frequency vs. input frequency.

The DC level measured at the output can clearly be seen to vary sinusoidally as the input frequency is varied. The oscillation period and amplitude are also very close to those predicted by Equation (2.50) thus this model is validated.
The voltage from Figure 2.10 must be interpreted to predict the input frequency. Equation (2.50) can be used to calculate frequency Ω since:

$$\phi = \Omega\tau \tag{2.51}$$

Due to the oscillatory nature of Equation (2.50), unambiguous frequency measurement is only possible within each half a period of Figure 2.10. The inverted responses are presented in Figure 2.11. Excellent agreement between interpreted measurement and actual frequency is evident. The systems shows the ability to measure frequencies in the frequency range of 20-20.06 MHz.

2.4.1 Discussion

In this Section a mixed photonic approach to measure the frequency of RF signals using only DC photo-detectors was achieved. An experiment along with a comprehensive theoretic model was developed to demonstrate the functionality of the proposed system. The system exhibited a DC voltage which was a function of frequency. The output require a measurement of DC optical power only enabling the use of low-cost photo-detectors.
The demonstrated system was only able to measure RF frequencies in the MHz range. This was attributed to the large length difference between the optical and RF paths. It is desirable to measure the higher frequency range up to 40 GHz. To achieve this, the differential time τ should be decreased (Figure 2.7). One approach would be to introduce an RF delay to the system which will compensate for the optical delay. Having established the need for a higher frequency measurement, the next Section will explore how a GHz frequency measurement can be practically achieved.

2.5 High Frequency IFM System Demonstration

The aim of this Section is to implement a high frequency mixed photonic IFM system. Figure 2.12 shows the experimental setup of the proposed high frequency mixed photonic IFM system. This setup is similar to Figure 2.8 but has a length of co-axial cable inserted. Due to the significant RF losses at 10 GHz plus frequencies the optical path has also been made as short as possible such that the RF cable can also be as short as possible to compensate.

As in Section 2.3, an RF signal generator produced a single RF tone which was divided equally into two portions using an RF Wilkinson power divider feeding two arms of the

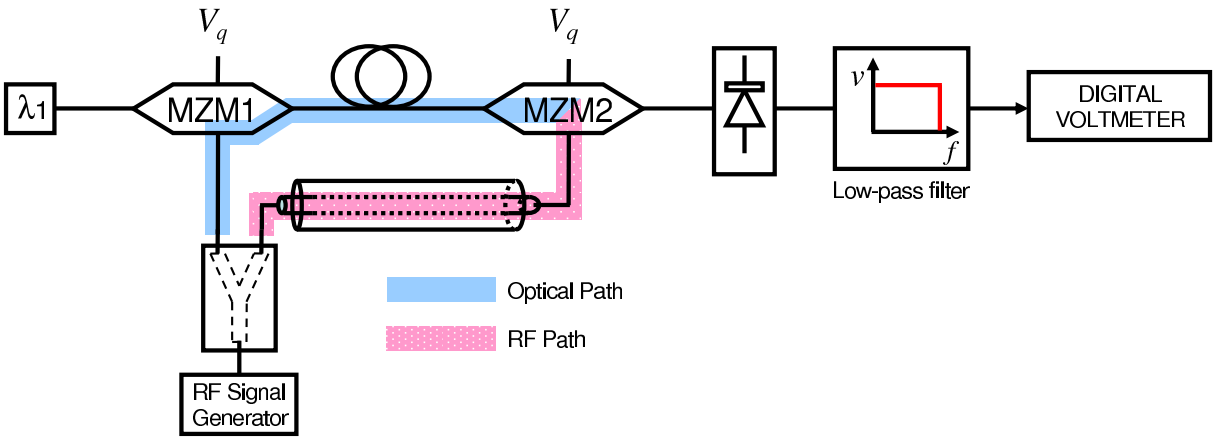

Figure 2.12: Experimental setup of proposed photonic IFM system

IFM system. These two arms were labelled the "Optical Path" and the "RF Path" on Figure 2.12. The RF tone in the Optical Path was input to MZM1 which was biased at quadrature. An optical carrier with wavelength of λ_1 produced by a laser diode. This carrier was modulated by MZM1, then the modulated carrier traversed the fiber patch cord and experienced an optical delay. The second portion of the RF tone entered the RF Path and was delayed using a length of co-axial cable. The delayed RF signal was input to a second modulator MZM2 (biased at quadrature) which modulates the optical carrier a second time. The twice-modulated signal was then detected by a photo-detector. The output of the photo-detector was then low-pass filtered and measured by a DC digital voltmeter.

This system can be modelled as discussed in Section 2.3.3; however, in this case, the phase (ϕ) and the amplitude (M) response of the co-axial cable cannot be trivialized. Hence the DC output voltage from Equation (2.46) will be:

$$V_{DC} = \frac{1}{4} G Z_{PD} P_{\circ} \left[1 + \frac{\pi^2 (1 + M^2) Z_{in} P_{RF}}{4 V_{\pi}^2} + \frac{\pi^2}{V_{\pi}^2} M Z_{in} P_{RF} \cos\phi \right] \tag{2.52}$$

It should now be possible to demonstrate frequency measurement; however, as each parameter in Equation (2.52) is known, except for the RF path parameters M, and ϕ, these parameters must first be empirically characterized.

2.5.1 RF Path Characterization

As Equation (2.52) suggests, to predict the DC voltage of the photo-detector, it is necessary to know the absolute magnitude response of the RF Path (M) and phase response of the RF Path relative to the Optical Path (ϕ). Due to dispersive nature of the co-axial cable, the frequency dependence of (M), and (ϕ) will be non-trivial, and therefore must be measured empirically.

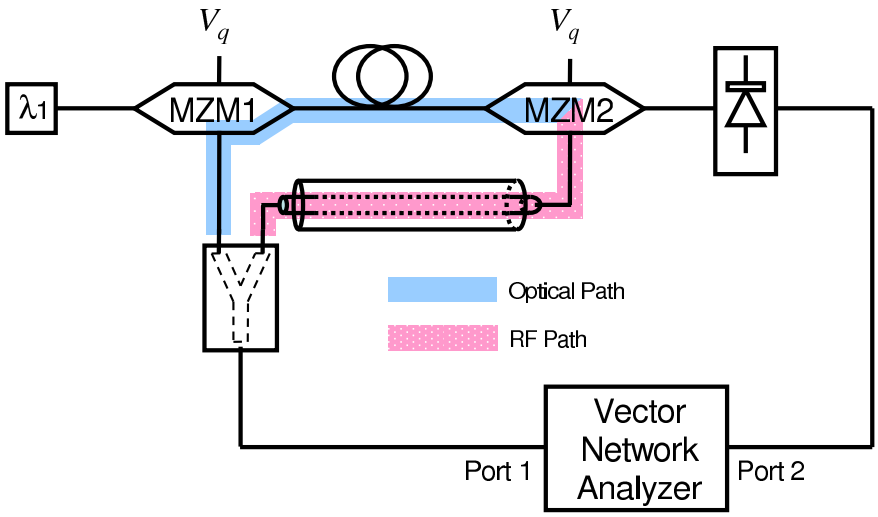

Figure 2.13: Experimental setup for the RF Path characterization.

To measure the amplitude (M) and phase response (ϕ) of the co-axial cable, the system was configured as shown in Figure 2.13. The laser wavelength and power were set to $\lambda_1 = 1550\ nm$ and $P_\circ = 11.7\ mW$ (10.7 dBm) respectively. The factor G was calculated to be $G = 1.2$. The input impedance of both MZMs (Z_{in}) and the output impedance of the photo-detector (Z_{PD}) were $50\ \Omega$. The V_π of the both MZMs was 5V.

A Vector Network Analyzer (VNA) was used to characterize the RF Path. To measure the phase difference (ϕ) of the RF Path relative to the Optical Path, Port 1 of the VNA was connected to the input of Wilkson power divider and Port 2 of the VNA was connected to the output of the photo-detector. The VNA was then calibrated while the two ends of the co-axial cable were disconnected and replaced by two matched loads.

The co-axial cable returned while the input of MZM1 was disconnected and the Wilkinson power divider terminated with a matched load. The VNA then measured the phase response of the RF Path with respect to the Optical Path (ϕ). The absolute response of the RF Path (M) was also measured by the VNA no referenced back to the Optical Path.

Figure 2.14 shows the measured magnitude of the forward transmission of the RF Path. The magnitude response decreased with increasing frequency. A resonance point at a frequency of 5.5 GHz is evident which can be attributed to the onset of higher order modes in the co-axial cable. To use these measurements in the experiment, it had been ensured that the cable was completely mechanically immobilized as the resonance frequency could vary due to vibration. Figure 2.15 shows the measured phase of the RF Path relative to the Optical Path. The phase response was almost linear over the whole band although there are some deviations for frequencies higher than 5.5 GHz.

The results of Figure 2.14 and Figure 2.15 show that the amplitude and phase of the

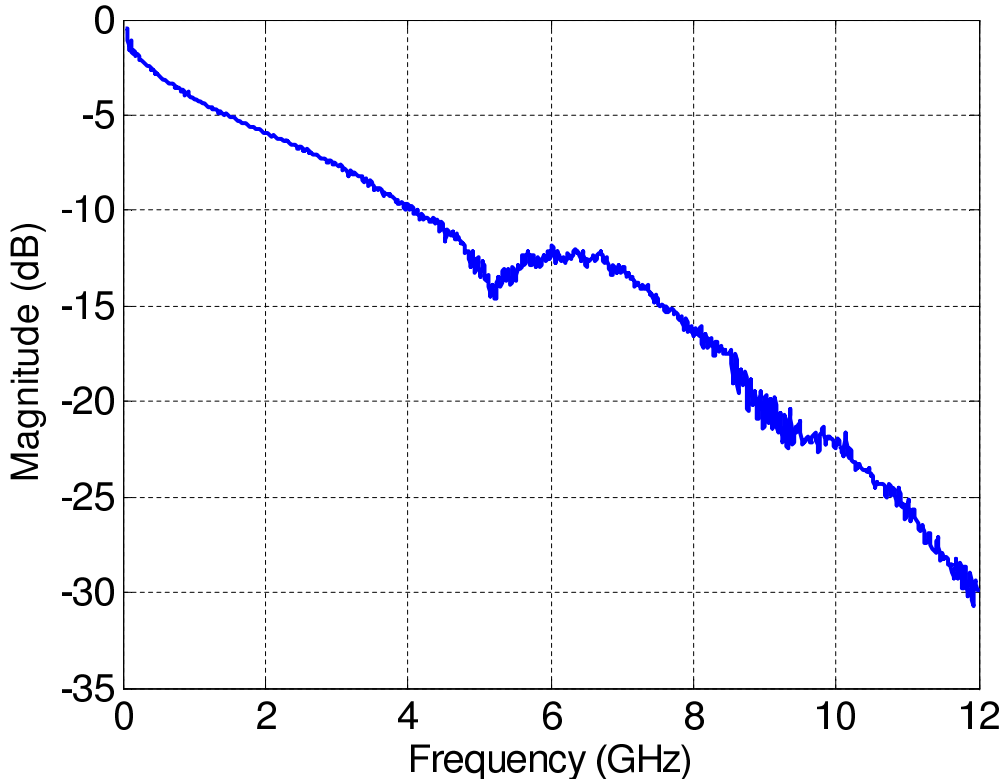

Figure 2.14: Absolute magnitude response of the RF Path.

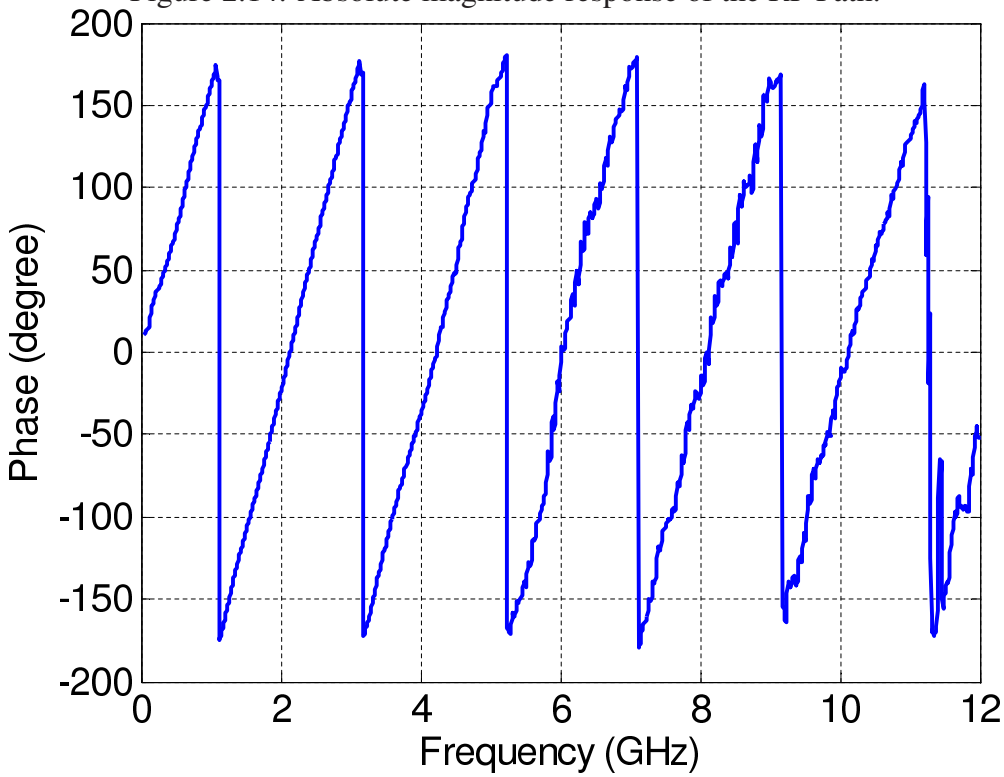

Figure 2.15: Phase response of the RF Path relative to the Optical Path.

RF Path were well-behaved below 5 GHz, and importantly, that the relative phase between the paths had an almost linear dependance on frequency in that range. The system should thus be suitable for frequency measurement in the 0-5 GHz frequency range.

2.5.2 IFM Characterization

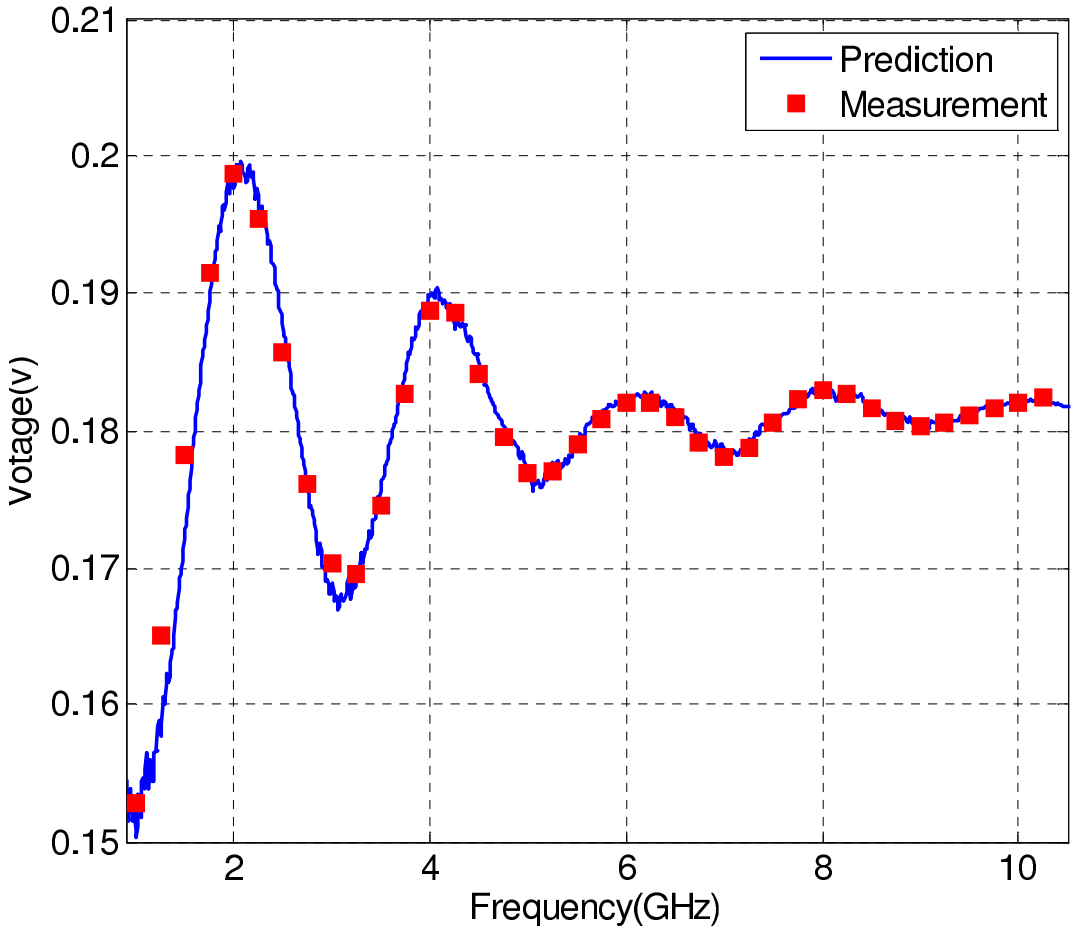

Figure 2.16: Measured and predicted photo-detector DC voltage.

Having established all of the parameters in Equation (2.52), the operation of the IFM system was then demonstrated. The system was configured as depicted in Figure 2.12 with $\lambda_1 = 1550\ nm$, $P_\circ = 11.7\ mW$, $G = 1.2$, and $P_{RF} = 8mW$ as used in the RF Path characterization. The DC voltage was measured as a function of RF input frequency as presented in Figure 2.16.

Clear oscillatory behavior was observed as predicted. Attenuation of the envelope is evident towards high frequency. The response predicted using Equation (2.52) is also presented in Figure 2.16. Excellent agreement is evident. The attenuation observed is also predicted by Equation (2.52) and thus this attenuation can be attributed to the RF loss in

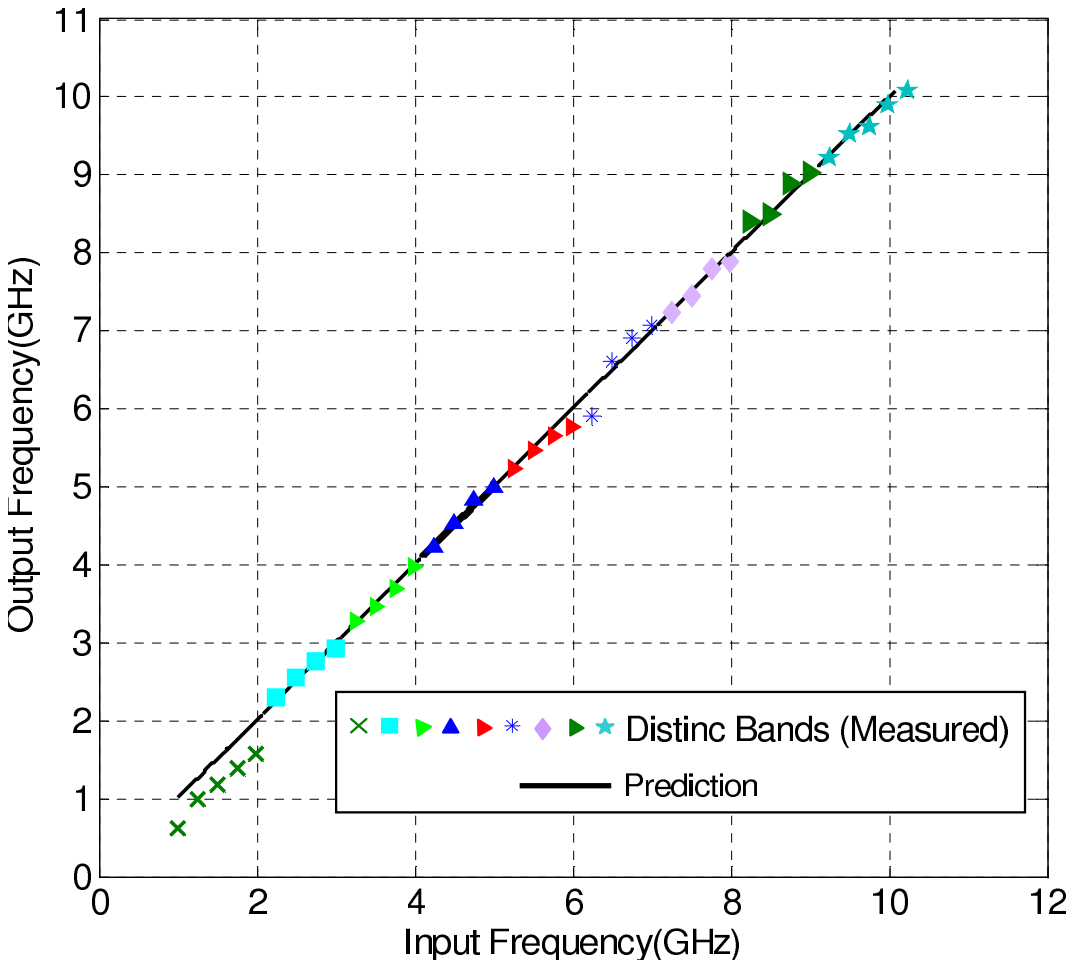

Figure 2.17: Measured frequency vs. input frequency.

the co-axial cable and the frequency response of the MZMs. Therefore, the sensitivity at lower frequencies would be better.

To perform the frequency measurement, a look up table was generated using Equation (2.52) and the empirically measured co-axial cable magnitude and phase response (M and ϕ) of Figure 2.14 and Figure 2.15. This table mapped each measured voltage to an input frequency. This look-up table was then used to invert the response to find the input frequencies that correspond to measured DC outputs. Due to the oscillatory nature of Equation (2.52), unambiguous frequency measurement was only possible within each half a period of Figure 2.16. Therefore, there were nine distinct bands within which conclusive frequency measurement was possible.

Figure 2.17 presents the inverted response for each of these bands. Excellent agreement between interpreted measurement and actual frequency is evident. Due to the zero gradient at peaks and nulls of Equation (2.52), sensitivity is less at the these frequencies. Deviation observed around 6 GHz can be attributed to the non-ideal behavior of the co-axial cable.

Figure 2.16 shows that oscillations in Equation (2.52) can be detected up to about 10 GHz. Beyond this frequency, losses in the co-axial cable become excessive, damping the oscillations. The co-axial cable in this demonstration was over 5m long to match the length of the optical fiber patch cords. The RF losses could be reduced by making both Optical and RF Paths shorter. In the simulations, it was assumed that both MZMs used in the setup were identical; however, in practice, there may be slight different parameters such as V_π. This could result in some small discrepancies between the measured and predicted results. Also as time passes drifts in modulators biases could account for errors in the measurements. Bias controllers could be employed to ensure no MZM bias drift. An integrated system could have path lengths in the order of only millimeters and would significantly improve the upper limit of frequency measurement and also minimize sensitivity to vibration and thermal fluctuations. The fractional bandwidth of the measurement window could be extended by decreasing the relative delay between the RF Path and the Optical Path which will increase the period of oscillation in Equation (2.52) and Figure 2.16. This way, it would be possible to cover the whole desired frequency measurement range by only one band and thus the frequency measurement would be conclusive within 1-10 GHz frequency range. This however, would reduce the gradient and hence the sensitivity.

2.5.3 Summary

In this Section a photonic approach to measure high frequency (GHz) RF signals was demonstrated. The experimental setup of Section 2.3.2 was modified to achieve high frequency measurement. This was done by adding an RF delay using a length of co-axial cable to compensate the optical delay. The mathematical model of Section 2.3.3 was modified to predict the behavior of the system accurately considering the frequency dependent characteristics of the co-axial cable. The system was then characterized to demonstrate the high frequency performance. The system exhibited a DC voltage which was a function of frequency and measurements were performed using only a low-cost, low-frequency photo-detector. Since in practical RADAR warning receivers, a bank of IFMs is required. Therefore increasing the number of IFMs requires an increase in the number of photo-detectors, this would reduce the cost of the whole system. The system had a frequency measurement range of 1-10 GHz. This shows the ability of microwave photonics to achieve high frequency signal processing while using only low-cost DC photo-detectors.

2.6 Conclusion

In this Chapter, a novel technique was demonstrated to implement a photonic IFM receiver which uses only low-cost DC photo-detectors. By using the concept of mixing, this photonic configuration was able to exhibit a frequency dependent DC output. This enables high frequency measurement using low frequency and thus inexpensive photo-detectors. This design is specifically important if there is a need to implement a bank of IFMs to identify multiple threat signals independently or resolve threats spectra with increased precision over a broad bandwidth. The previously demonstrated system needed expensive broadband photo-detectors. As stated in Section 2.3.3 the mathematical model describing he behavior of the system, was based on small signal assumptions. Since distant threats signals are of low power nature. For larger threat signals the small signal assumption are no longer valid; however, since the final measurement is based on a look up table this does not affect the performance of the system. To predict the dynamic range of this IFM system the large signal behavior describing by Equation (2.29) should thus be used.

The system demonstrated in this Chapter exhibited a frequency range of 1-10 GHz. This limitation was due to the fact that a co-axial cable used in the system introducing an RF delay to match the photonic delay. The co-axial cable had a relatively long length, which caused a high loss for frequencies higher than 10 GHz. Therefore the system could still suffer from the RF domain limitations such as frequency dependent loss.

Another disadvantage of the system is that the output measurement depends on both RF signal frequency and amplitude. A single measurement could not isolate these two unknowns and thus another set of measurement is required in order to independently measure the RF frequency and RF power.

These two identified limitations of the demonstrated system will be addressed in the following Chapters. Chapter 4 examines an all optical mixed IFM that eliminates the co-axial cable and thus significantly extends the system bandwidth and sensitivity at higher frequencies. Chapter 3 introduces a photonic hybrid coupler based on Hilbert transform concept to achieve two orthogonal measurements. This enables independent quantification of RF signal frequency and amplitude.

Chapter 3

Orthogonal Measurement Photonic Instantaneous Frequency Measurement (IFM) System

3.1 Introduction

Chapter 2 introduced and demonstrated a new photonic IFM system, which could measure RF frequencies in the GHz range that required only low-cost DC photo-detectors. One disadvantage of the photonic IFM system was the RF power dependence of the output voltage. Practical use of this system for RF frequency measurement would require knowledge of the RF power level and this may not be practical in the Electrical Warfare environment. As there are two unknowns (RF frequency and RF power), two measurements are required to measure the RF frequency, independent of RF power. These two measurements should also be orthogonal to enable independent frequency and power measurement.

Since a parallel research was being conducted at RMIT university on photonic hybrid coupler [8], this Chapter focusses on employing a photonic hybrid coupler to implement a photonic IFM system with orthogonal measurement. To gain more insight, a theoretical transfer function model is derived in Section 4.2. In Section 4.3, an alternate photonic hybrid coupler approach using a transversal filter scheme is proposed and practicality demonstrated. In Section 4.4 a different approach is used to implement a photonic hybrid coupler using a cascaded grating to improve the latency of the system. This system is practically demonstrated and employed to achieve two sets of orthogonal measurements in the photonic IFM system of Chapter 2, enabling a demonstration of the independent measurement of frequency and amplitude.

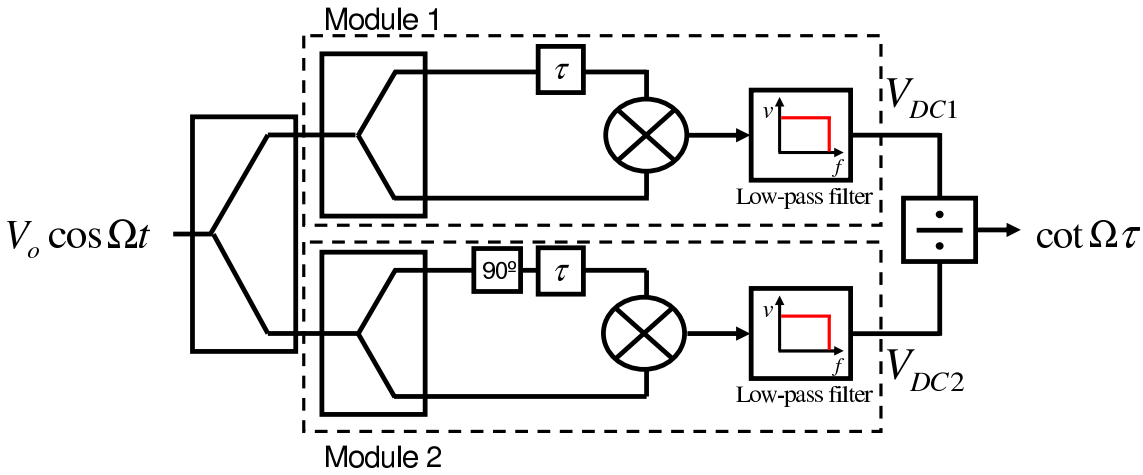

Figure 3.1: Block diagram of an IFM system with two orthogonal signals.

In Section 4.5 a photonic IFM system is developed and practically demonstrated which is capable of producing two orthogonal measurements. Conclusion are drawn on the practically of the proposed system in Section 4.6. The outcome of this work has been published in [70, 78].

3.2 Orthogonal Measurement

Section 2.3 defined an accurate model for the photonic IFM system. This model is summarized in Equation (2.45). Although Equation (2.52) establishes a relation between a DC voltage and frequency, this DC voltage is also a function of input RF power. This makes independent measurement of frequency and power impossible. To solve this problem, two orthogonal measurements are required to independently establish both frequency and RF signal level.

Several IFM systems have been reported incorporating orthogonal measurements [30, 31, 33, 38, 39]. One possibility is presented in Figure 3.1. A single RF tone is divided into two equal portions feeding two modules; Module 1 and Module 2. The configuration within each module, is similar to that described in Section 2.2.2.

In each module the input RF tone is divided into two equal portions. One portion is delayed relative to the other by time τ and the two portions are then multiplied together and the output is low-pass filtered. The DC output of each module is a sinusoidal function of frequency. In this case however, a 90° phase shift is introduced in one arm of Module 2 causing its output to have a sine response while Module 1 has a cosine response. Note that sine and cosine functions are orthogonal. This system should thus enable independent measurement of RF frequency and power. One possibility is to define the outputs of Module 1 and Module 2 to provide a *cotangent* relation which depends only on the RF

frequency and is independent of power.

Having conceived an orthogonal IFM system, a mathematical model is developed to show that the two outputs of the IFM system are indeed orthogonal. The single RF tone can be described as:

$$v_{in}(t) = V_\circ \cos \Omega t \tag{3.1}$$

where $V_\circ$ and Ω are the amplitude and angular frequency of the RF tone, respectively. As the input is divided into two equal portions, the portions present at the input of both modules can be written as:

$$v_1(t) = v_2(t) = \frac{1}{\sqrt{2}} V_\circ \cos \Omega t \tag{3.2}$$

Each portion is further divided by two equal portions within both modules. Thus the voltage present at each arm of each module, is:

$$v_1'(t) = v_2'(t) = \frac{1}{2} V_\circ \cos \Omega t \tag{3.3}$$

Module1

At Module 1, one portion is delayed by amount of τ respect to the other arm, therefore the input voltages of the multiplier inside Module 1, can be described as:

$$v_{1,1}(t) = \frac{1}{2} V_\circ \cos \Omega (t - \tau) \tag{3.4}$$

$$v_{1,2}(t) = \frac{1}{2} V_\circ \cos \Omega t \tag{3.5}$$

where $v_{1,1}(t)$ and $v_{1,2}(t)$ are the upper and lower voltages present at the input of the multiplier of the Module 1, respectively. The output of the multiplier can then be written as:

$$v_{m1}(t) = \frac{1}{4} V_\circ^2 \cos \Omega (t - \tau) \times \cos \Omega t \tag{3.6}$$

where $v_{m1}(t)$ is the output of the multiplier of the Module 1. Using trigonometric relations, Equation (3.6) can be simplified as:

$$v_{m1}(t) = \frac{1}{8} V_\circ^2 \left[\cos \Omega (2t - \tau) + \cos \Omega \tau\right] \tag{3.7}$$

This voltage is then low-pass filtered. Therefore at the output of the low-pass filter of Module 1, the first term of Equation (3.7) will vanish and only the DC term will remain:

$$V_{DC1}(\Omega) = \frac{1}{8} V_\circ^2 \cos \Omega \tau \tag{3.8}$$

where $V_{DC1}(\Omega)$ is the total voltage present at the output of Module 1. Note that $V_{DC1}(\Omega)$ is a function of angular frequency Ω and is not time dependent as it is a DC term.

Module2

At Module 2, one portion is phase shifted by 90° ($\frac{\pi}{2}$) and delayed by time τ respect to the other arm, therefore at the input voltages of the multiplier inside Module 1, can be written as:

$$v_{2,1}(t) = \frac{1}{2}V_\circ \cos\Omega(t+\frac{\pi}{2}-\tau) = -\frac{1}{2}V_\circ \sin\Omega(t-\tau) \tag{3.9}$$

$$v_{2,2}(t) = \frac{1}{2}V_\circ \cos\Omega t \tag{3.10}$$

where $v_{2,1}(t)$ and $v_{2,2}(t)$ are the upper and lower voltages present at the input of the multiplier of the Module 2, respectively. The output of this multiplier can then be written as:

$$v_{m2}(t) = -\frac{1}{4}V_\circ^2 \sin\Omega(t-\tau) \times \cos\Omega t \tag{3.11}$$

where $v_{m2}(t)$ is the output of the multiplier of the Module 2. Using trigonometric relations, Equation (3.11) can be simplified as:

$$v_{m2}(t) = -\frac{1}{8}V_\circ^2 \left[\sin\Omega(2t-\tau) - \sin\Omega\tau\right] \tag{3.12}$$

This voltage is then low-pass filtered. Therefore at the output of the low-pass filter of Module 2, the first term of Equation(3.12) will vanish and only the DC term of Equation (3.12) will remain:

$$V_{DC2}(\Omega) = \frac{1}{8}V_\circ^2 \sin\Omega\tau \tag{3.13}$$

where $V_{DC2}(\Omega)$ is the total voltage present at the output of Module 1. Again, note that $V_{DC2}(\Omega)$ is a function of angular frequency Ω and is not time dependent as it is a DC term.

To remove the RF power dependence the ratio of Equation (3.8) and Equation (3.13) is taken:

$$\frac{V_{DC1}(\Omega)}{V_{DC1}(\Omega)} = \frac{\cos\Omega\tau}{\sin\Omega\tau} = \cot\Omega\tau \tag{3.14}$$

Equation (3.14) is a function of RF frequency but is independent of the RF tone amplitude ($V_\circ$). This establishes an amplitude ($V_\circ$) independent relationship between the IFM output signal and the input RF frequency. Once the determined frequency has been established, the amplitude can also be measured using the output of either Module 1 or Module 2 via either Equation (3.8) or Equation (3.13). As the output signals are DC terms, this system can be implemented using low-cost, low-frequency photo-detectors while still enabling broadband frequency measurement.

Having demonstrated the mathematical concept of orthogonal measurement, it is now possible to develop a photonic IFM system which exhibits two orthogonal measurements.

Using this system it should be possible to independently measure the RF frequency and power. As discussed in Chapter 2 realizing a 90° phase shift over a broad frequency range could be challenging in microwave domain. Recently a broadband microwave photonic 90° hybrid coupler has been developed at RMIT university [8, 70]. It should thus be possible to use this phase shifter in the photonic IFM system of Chapter 2 to achieve two orthogonal measurements.

3.3 Photonic Hybrid Coupler

Quadrature hybrid couplers are important microwave components being used widely in microwave circuits and equipments. They have two outputs which one of them provides a 90° phase shifted signal relative to the other output (reference output).

As discussed in Section 3.2 a wideband 90° phase shift is required to implement an IFM system with orthogonal measurement which could be challenging in the microwave domain [36].

As stated in Section 1.3, microwave photonic facilitates processing the amplitude and phase of wideband microwave signals which result in realizing different types of photonic filters. Since quadrature hybrid couplers exhibit constant amplitude with 90° phase shift, they can be categorized as filters. A photonic filter shall then be used to implement a hybrid coupler in the photonic domain. Through various types of photonic filters, transversal filtering seems to be a good candidate since it is highly reconfigurable and frequency agnostic, for example the same system could be used to achieve a notch filter in both MHz or GHz frequencies.

In this Section, the optical hybrid coupler of [8] is reviewed. This coupler should achieve broad bandwidth, low ripple, and does not require input/output matching network [8]. This hybrid coupler can be employed to achieve orthogonal measurement required for the photonics IFM system.

3.3.1 Transversal Hybrid Coupler

It is well known that if a system has an impulse response of a homographic hyperbola type:

$$h(t) = \frac{1}{\pi t} \tag{3.15}$$

the corresponding frequency response will be:

$$H(j\omega) = -jsgn(\omega) \tag{3.16}$$

which has constant amplitude and a frequency independent 90° phase shift relative to the input. For ideal system performance with infinite, bandwidth, the impulse response must be an infinite continuous time signal. In reality, this is impractical, and thus the impulse response must be truncated in time. Windowing techniques are usually employed to reduce distortions of the system frequency response due to Gibes effect caused by abrupt truncation. In practice, the window used can be manipulated to optimally trade off ripple and bandwidth [79]. In addition, the impulse response exhibits negative time; therefore practical implementation of the hybrid coupler would require a reference which is delayed with respect to the transformed components as shown in Figure 3.2. The impulse response must also be sampled by discrete taps which are effectively delta functions in time. Sufficient samples must be included to avoid aliasing distortion. Having chosen a finite number of discrete taps as samples, the exact number of taps and appropriate window must be designed to realize the desired function.

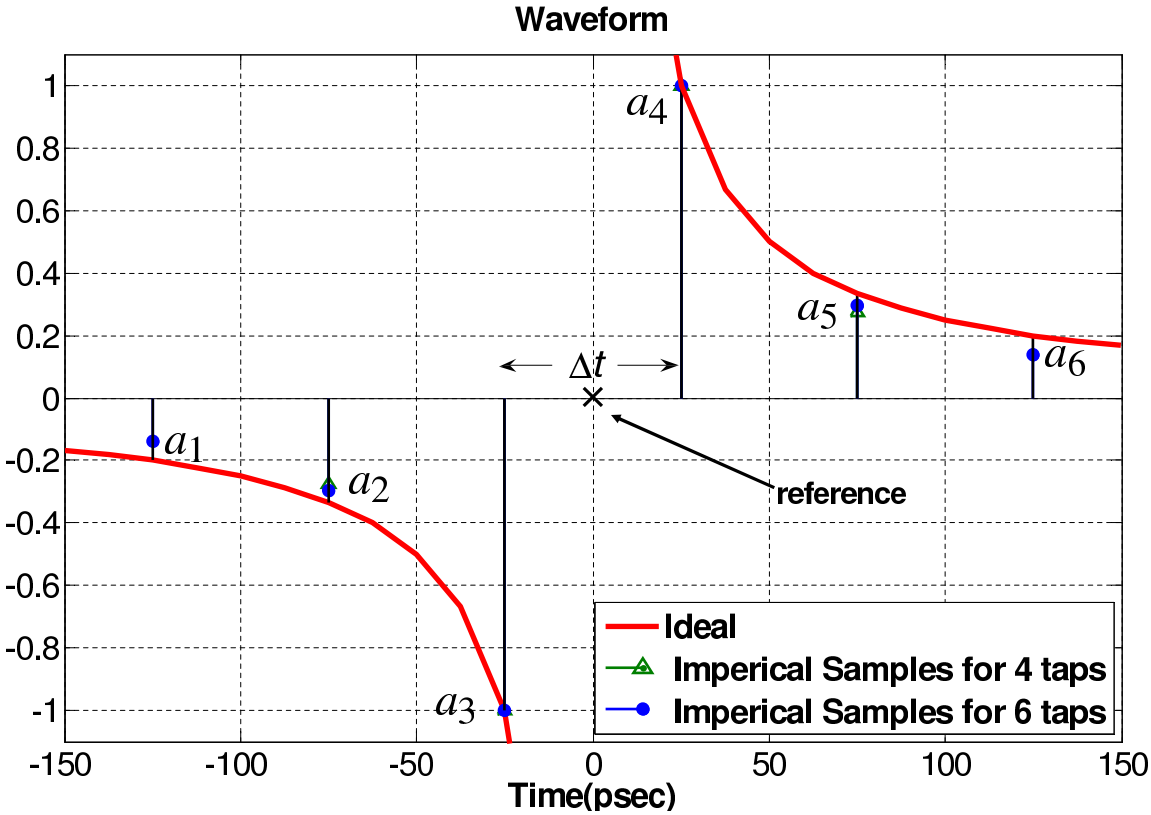

Figure 3.2: Hyperbolic impulse response, ideal, empirically optimized for 4 taps (triangles) and empirically optimized for 6 taps (circles).

3.3.2 Numerical Design Example

To illustrate the hybrid coupler concept presented in Section 3.3.1, a numerical design example of a transversal $90°$ hybrid coupler is presented. The specification chosen for this design are bandwidth of 2.5-17.5 GHz (as most of commercial microwave equipment work in the range of 2-18 GHz), in-band maximum ripple of 2dB (to have 1dB improvement over 3dB traditionally acceptable ripple), and acceptable phase ripple of $5°$. To simplify the design, uniform sampling is assumed. To achieve a passband of 20 GHz, the tap spacing must be $\Delta t \approx 50$ ps to avoid aliasing.

To perform this numerical investigation, it was assumed the continuous hyperbolic impulse response was also shown in Figure 3.2.

This function is sampled by a finite number of discrete taps spaced by 50 ps. The frequency response that can be expected is calculated as the Fourier transform of these sampled taps. The response that could be expected by simply truncating the impulse response at 2, 4 and 6 taps can be seen in Figure 3.3. Truncation and sampling does not impact the phase response which will remain an ideal step function crossing from $+90°$ to $-90°$ at zero frequency. Figure 3.3 indicates that simple truncation does not provide the optimum trade-off between bandwidth and specified amplitude ripple. To better meet the desired hybrid specifications the truncated impulse response must be apodized. This

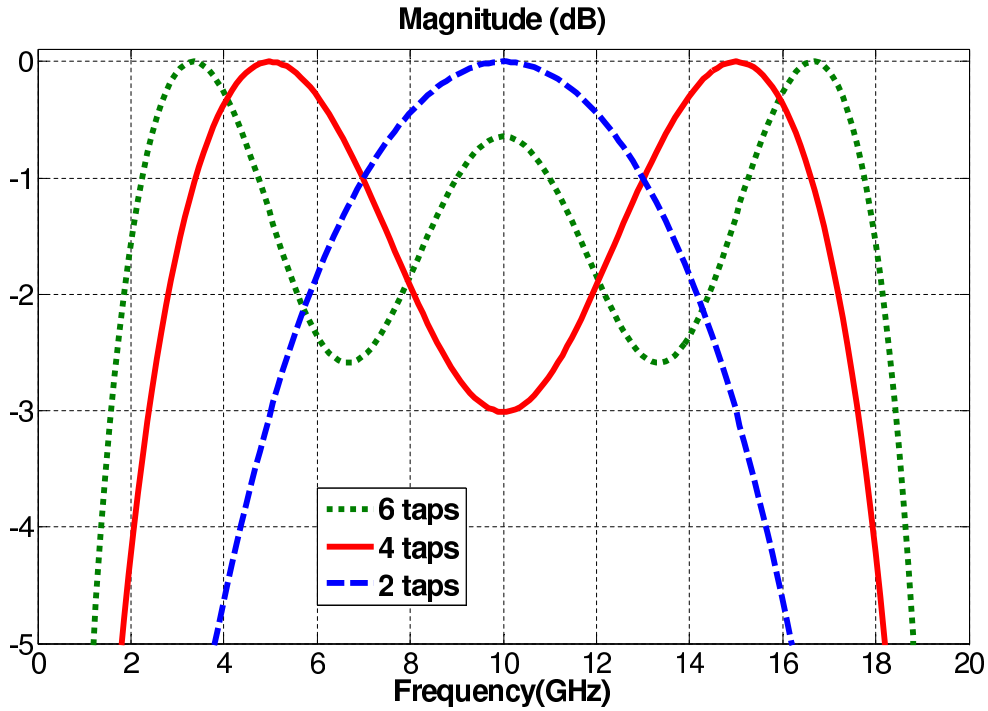

Figure 3.3: Amplitude of the frequency response of the simply truncated ideal response of Figure 3.2. Truncated at 2,4 and 6 taps.

	a_1	a_2	a_3	a_4	a_5	a_6
2	0	0	-1	1	0	0
4	0	-.3328	-1	1	.3328	0
6	-.1397	-.2976	-1	1	.2976	.1397

Table 3.1: Normalized tap weights for 2,4, and 6 tap transversal filter

can be achieved using a range of well established window functions; however, for this investigation, the number of taps is small enough that empirical adjustment of the tap weights is tractable.

A MATLAB program was used to optimize the tap amplitudes in antisymmetric pairs to achieve an in-band amplitude ripple of 3 dB, using the unconstrained nonlinear derivative-free optimization method. As the impulse response has odd symmetry with the two center taps having the largest amplitude, normalizing the tap weights with respect to the center tap amplitude, the tap weights of the two center taps are always $a_4 = -a_3 = 1$. The weights of the other taps, can be chosen to achieve various levels of pass band ripple. The system frequency response was computed by taking the Fourier transform of the impulse response of Figure 3.2.

Now it is demonstrated that a small number of taps can be used to implement a transversal hybrid that meets these specifications. The resulting tap weights for 2, 4 and 6 taps are calculated and shown in Table 3.3.2. Figure 3.4 presents the improved frequency response after computer optimization. As it can be seen a 4-tap transversal filter meets the design specification. Figure 3.5 presents the amplitude response of a 4 tap transversal filter with pass band ripples of 2, 3, and 4 dB. The phase response of the three cases of Figure 3.5 remains ideal, since the impulse response has always odd symmetry. It is evident from Figure 3.5 that the Hilbert transform with 3 dB of ripple meets the set design specification using a 4 tap transversal filter.

Having specified the number of taps, tap weights and tap spacing, it is now possible to develop a practical experiment to demonstrate the optical hybrid coupler.

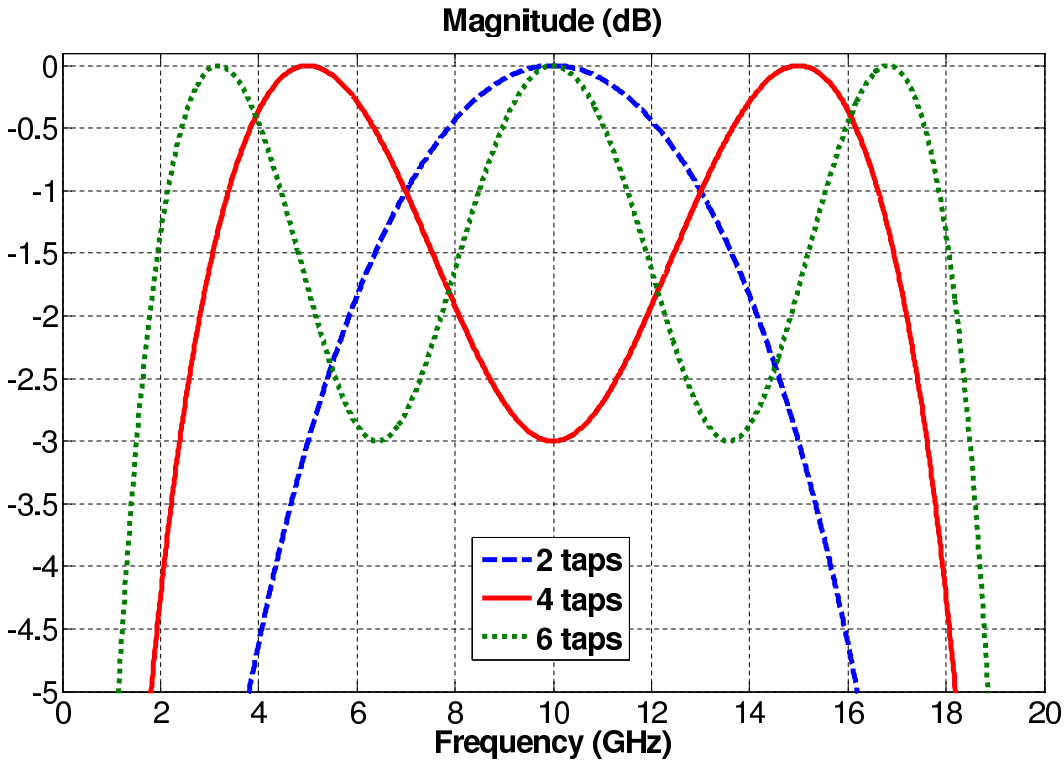

Figure 3.4: Amplitude of the frequency response of the optimized truncated ideal response of Figure 3.2. Truncated at 2,4 and 6 taps.

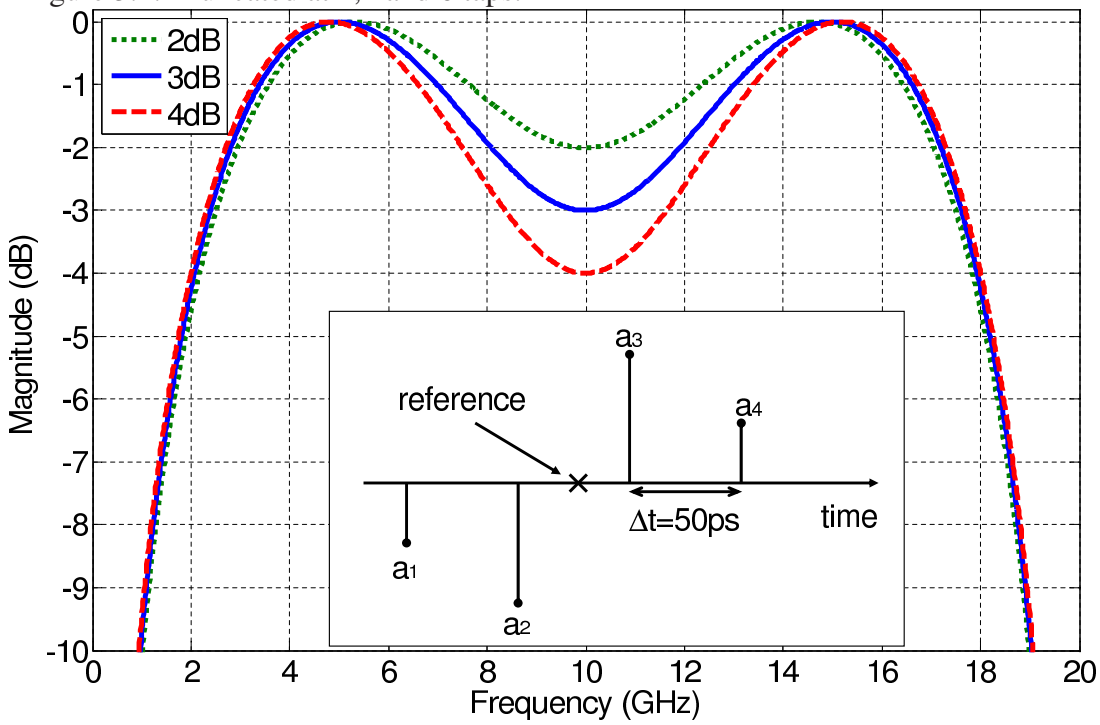

Figure 3.5: Magnitude of impulse response of a 4 tap system.

3.3.3 Experiment Setup

In this Section an experiment is developed to demonstrate that an optical hybrid coupler can be achieved in the optical domain. Figure 3.6 presents a diagram of the system implementation. Four optical carriers were used. These carriers were combined into pairs (λ_1 and λ_2) and (λ_3 and λ_4), and input to MZM1 and MZM2 respectively. To achieve positive and negative taps, MZM1 and MZM2 were biased oppositely at positive (V_q^+) and negative (V_q^-) quadrature. The path lengths were equalized after each modulator using Variable Optical Lines, (VOL1 and VOL2). The taps were then combined and transmitted through a dispersive fiber to impart different time delays to each wavelength. All of the taps were amplified using a single Erbium Doped Fiber Amplifier (EDFA) and then a portion of one tap was separated using a Coarse Wavelength Division Multiplexer (CWDM) coupler. The path lengths were again equalized with VOL3, and VOL4 before detection using broadband photo-detectors. The multi-wavelength output (Out1) formed the 90° phase shifted signal, while the single wavelength output (Out2) provided a 0° reference. The output frequency response was observed with a Vector Network Analyzer (VNA). The power of each laser determined the weight of each tap. As discussed in Section 3.3.2, to achieve a 20 GHz bandwidth, the time spacing of the samples must be $\Delta t \approx 50$ps. This delay was achieved using 2.354 km of single mode fiber (SMF) with dispersion D=17 ps/nm.km. The time spacing and fiber length were used to calculate the wavelength spacing as:

$$\Delta\lambda = DL/\Delta t = 1.25nm \tag{3.17}$$

Since the dispersion was not exactly linear and non-trivial dispersion was contributed by other system components, the actual wavelength of the lasers was empirically fine-tuned to achieve the required time delay by isolating pairs of anti-symmetric taps and adjusting their wavelength spacing to ensure a null in the frequency response at 20 GHz. The resulting wavelength taps were $\lambda_1 = 1543.94$, $\lambda_2 = 1545.3$, $\lambda_3 = 1546.59$ and $\lambda_4 = 1547.69$ nm. Figure 3.7 presents the response of the CWDM. High and low wavelengths are routed to Ports 1 and 2 respectively, with a gradual transition across 1544.2 nm. A wavelength of 1543.94 nm was chosen for the lowest tap such that most of the power was isolated at Port 2 to act as a reference, while a portion remained at Port 1 to contribute to the transversal filter. Only one wavelength was thus required for both functions.

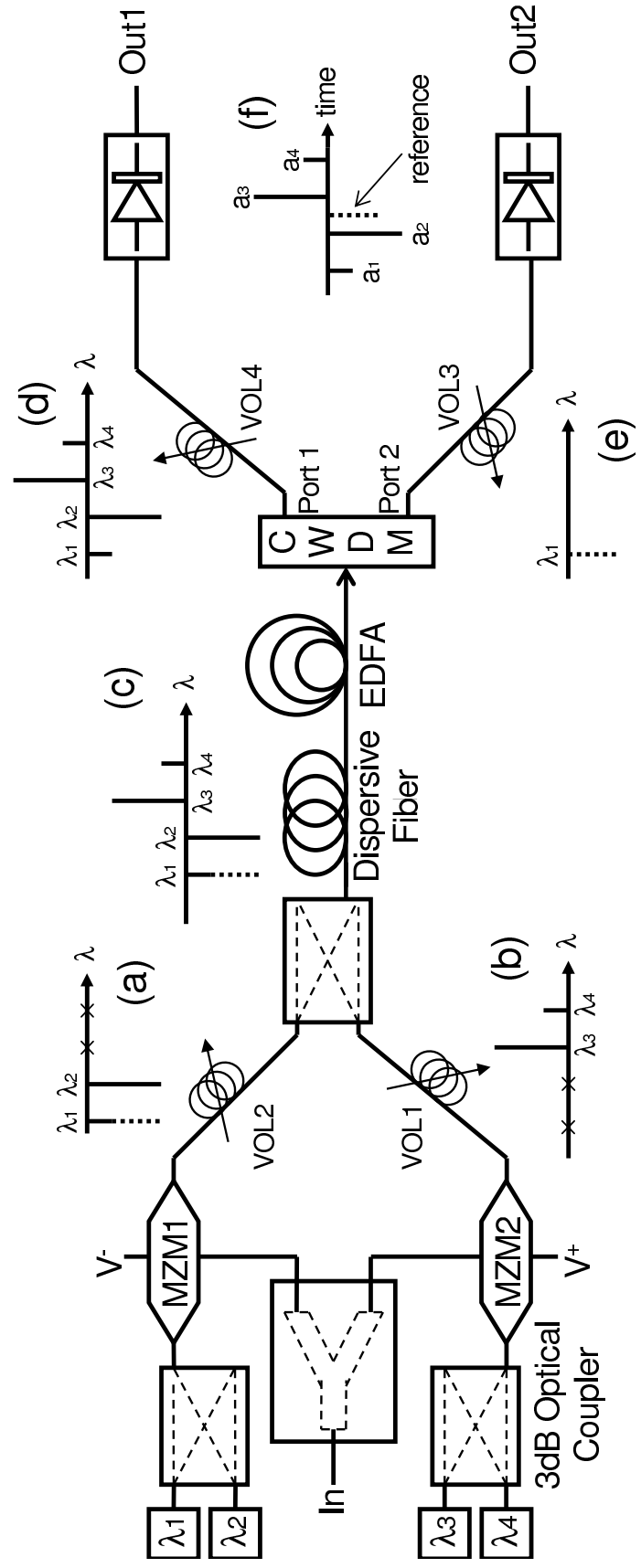

Figure 3.6: Experimental setup of the basic hybrid coupler.

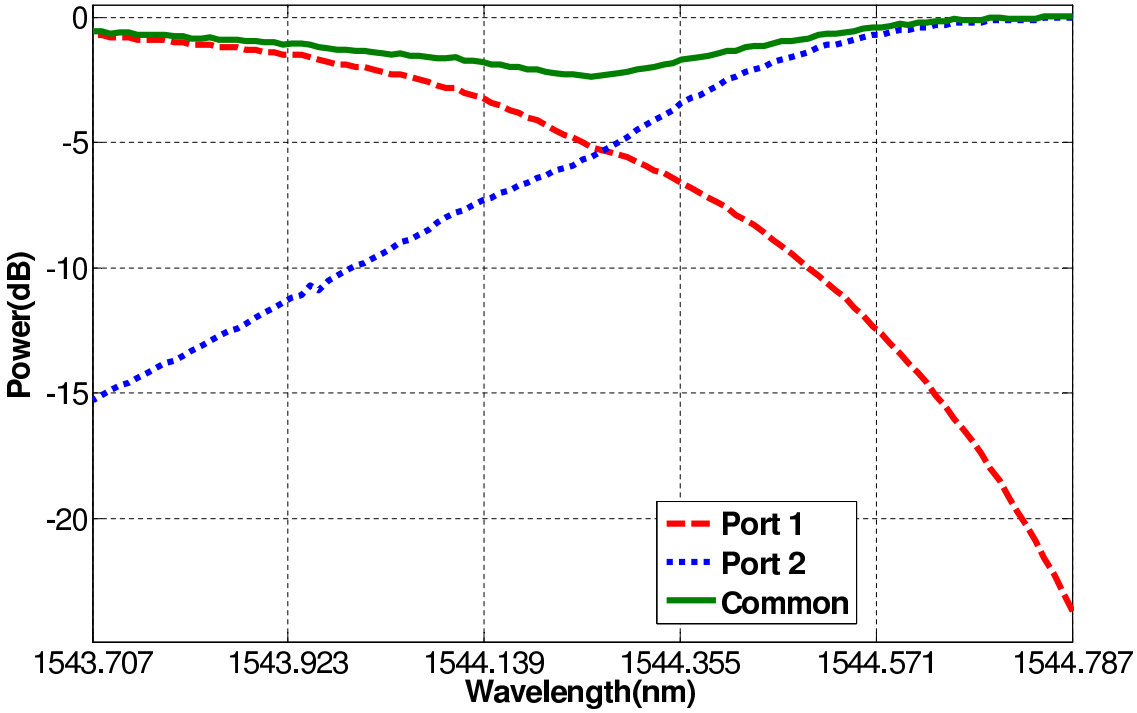

Figure 3.7: Wavelength division multiplexer characteristic.

3.3.4 Results

The experimental system was configured as shown in Figure 3.6. The laser powers were adjusted to achieve the tap weights indicated in Figure 3.2. Fine tuning was achieved by observing the frequency response of anti-symmetric pairs of taps in isolation and adjusting their separation and relative weights to achieve a deep amplitude null at 20 GHz. The relative amplitudes and wavelength spacing of the two pairs of taps was then adjusted to achieve the correct phase and amplitude response. To observe the relative amplitudes and wavelengths of the transversal filter an Optical Spectrum Analyzer (OSA) was used. Figure 3.8 presents an OSA trace indicating the relative wavelengths and amplitudes of the optical carriers used to implement the transversal filter. Note that tap weights correspond to carried RF power. Since MZM2 had a higher half wave voltage (V_π), a slight reduction in the optical power was required for the upper wavelengths. This was done empirically.

The VNA was calibrated to Out2 (the reference arm) and then used to measure the frequency response of Out1. The amplitude and phase response of Out1 is presented in Figures 3.9 (a) and (b) respectively. The simulated response of Figure 3.4 is also presented for comparison. Excellent agreement between the measurement and theory is evident. Amplitude variation less than 2dB has been maintained over 2.9-17 GHz, with less than 5° phase deviation from 90°. The tap weights depicted in Figure 3.8 do not appear to have equal values, despite being empirically optimized because the tap weights are determined

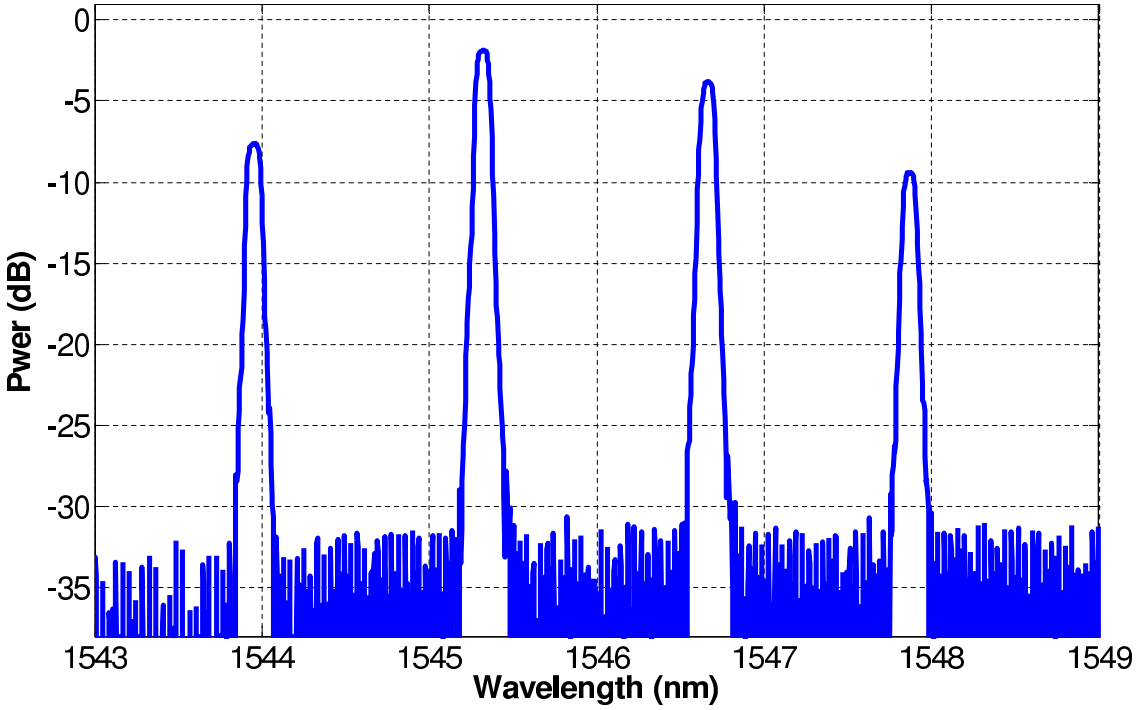

Figure 3.8: Optical Spectrum Analyzer (OSA) trace showing weights and wavelength of each tap.

by the carried RF power, not the peak carrier intensity.

In a practical implementation, outside the laboratory the optimization of channels could be achieved using real time monitoring and numerical control as there are only a small number of variables and clear optimization goals. The phase degradation in Figure 3.9 (b) above 16 GHz could be attributed to very low amplitude response (Figure 3.9). A single balanced modulator could replace the two opposite biased modulators, eliminating the need for an RF splitter. This would also simplify path length equalization, reduce component count and minimize optical splitting losses.

The response of Figure 3.9 compares favorably with traditional microwave hybrids. Further, this photonic implementation offers the flexibility of a customizable passband. The passband ripple and the bandwidth can be dynamically adjusted by changing the tap weights and wavelength spacing. It would be desirable to extend the hybrid operation to 2-40 GHz with less than 3 dB ripple.

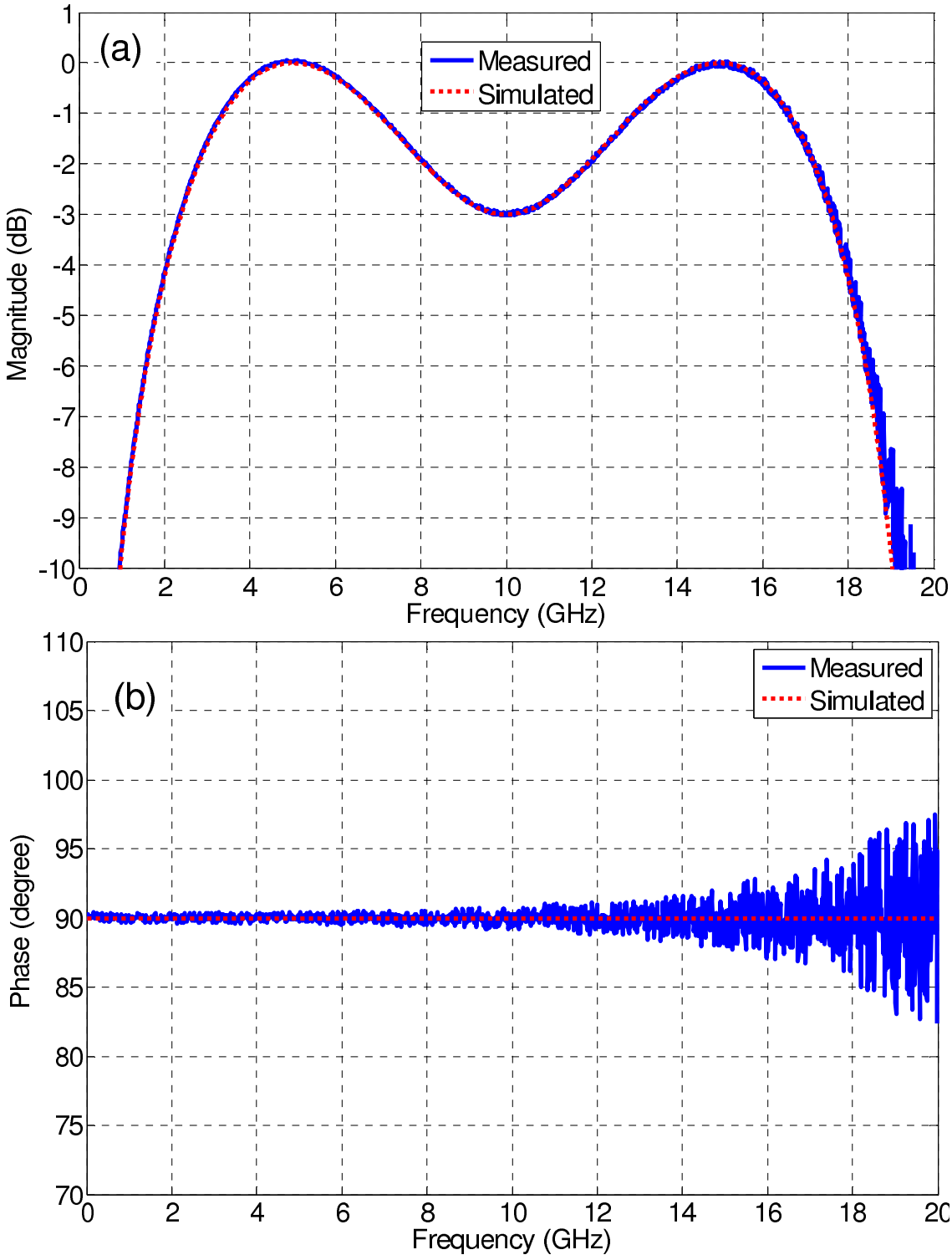

Figure 3.9: Measured and predicted system magnitude and phase response.

3.3.5 Discussion

A photonic technique has been introduced to achieve a 90° phase shift in the microwave domain over a multi-octave frequency range. The system demonstrated good characteristics and the design specifications have been met; however, in some applications having a long Single Mode Fiber (SMF) may result in latency problems since the optical carrier has to traverse a long distance ($\approx$ 2 km) to achieve the required relative delays between taps. Having such a long SMF in the system may also increase the bulk of the system. In some systems requiring polarization maintenance, employing such a long PM fiber, can also increase the system cost. As mentioned in Section 2.2.2, other ways of realizing different delays for different wavelengths are using either cascaded grating, or Wavelength Division Multiplication (WDM) couplers with an array of optical delay lines. Employing optical delay lines together with WDM couplers, could be complex and expensive as two WDM couplers will be needed. It also introduces significant insertion loss. Each WDM coupler introduces a loss of at least 6dB, and a physical delay line has at least 1dB insertion loss, which will result in minimum total loss of 13dB. This could cause Signal to Noise Ratio (SNR) degradation. Instability may also occur in the system as the system relies on delays caused by different paths which may incur phase shifts due to vibration and thermal expansion. As this hybrid coupler is designed to be employed in the IFM system of Figure 2.12, a long optical delay can not be used as it will result in the need for a very long co-axial cable.

On the other hand, utilizing cascaded grating to realize different delays offers the benefits of low insertion loss (3 dB), and reduced cost, complexity and bulk. Maintaining the polarization is also possible using gratings in PM fibers. The overall length of the cascaded grating is much less comparing with the 2.345km fiber which makes it practical for the IFM application. It may also help to improve the latency of the systems addressing the for need for immediate signal processing in, Instantaneous Frequency Measurement (IFM) systems. Therefore, it would be advantageous to implement a hybrid coupler using a cascaded grating.

3.4 Hybrid Coupler Using Cascaded Grating

In this Section the hybrid coupler of Section 3.3 is implemented using cascaded grating as the dispersive medium. As the total length of the cascaded grating and fiber patch cords is less than 5m, a relatively short co-axial cable will be needed which makes the IFM implementation practical. A custom cascaded grating was sourced from Redferm Optical Components (ROC). This cascaded grating was used to give incremental delays of 40 ps.

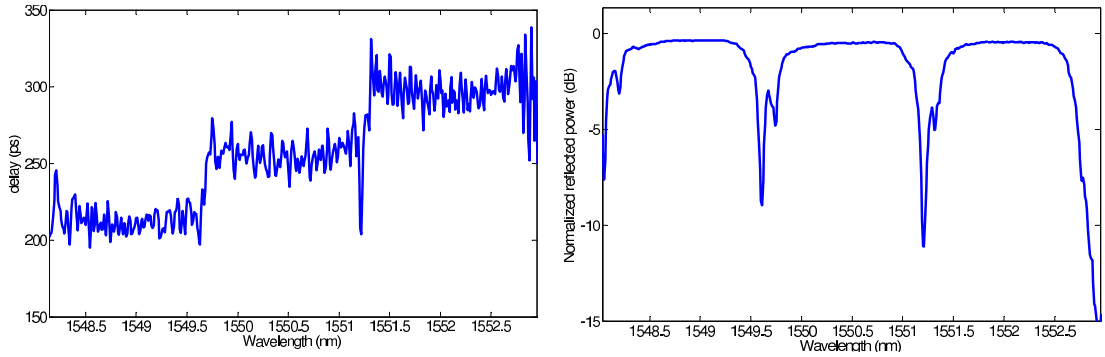

Figure 3.10: Cascaded grating characteristics a) delay, b) reflection.

Figure 3.10 shows the characteristics of the cascaded grating from the company data sheet which was used to implement the hybrid coupler. It has a relatively uniform delay of 40 ps and almost flat reflection response. This cascaded grating was used to implement a two tap transversal filter which resulted in an amplitude frequency response shown in Figure 3.3. The uniform delay of the grating is 40 ps. Since the middle grating was used as the reference, the tap delay is $\Delta t = 2 \times 40 = 80ps$. Therefore the free spectral range of the transversal filter was $1/\Delta t$=12.5 GHz. Hence the hybrid coupler was limited to operation below 12.5 GHz. Having the specification of the cascaded grating, it is now possible to demonstrate the cascaded grating based hybrid coupler.

Figure 3.11 shows the experimental setup of the cascaded grating based photonic hybrid coupler. Three optical carriers ($\lambda_\circ$,λ_1, and λ_2) were used to implement a two-tap (λ_1, and λ_2) transversal filter with a reference tap ($\lambda_\circ$) in between. Carriers $\lambda_\circ$ and λ_2 were combined using a 3 dB optical coupler. Using a 2x1 MZM, the combined signal together with λ_1 were modulated oppositely using a 2x1 MZM to make the desired combination as shown in Figure 3.11 inset (a) (reverse modulation). The modulated signal was then input to Port 1 of an optical circulator. Port 2 of the circulator was connected to the cascaded grating. Each wavelength was reflected with different, but uniformly incremented delays of 40 ps. The dispersed signal was output from Port 3 of the circulator and input to a Wavelength Division Multiplexer (WDM) which separated all wavelengths. Carrier $\lambda_\circ$ remained separated and was used as the reference (Figure 3.11 inset (b)). The carriers λ_1 and λ_2 were again combined using a 3dB coupler to form the two tap transversal filter (Figure 3.11 inset (c)). VOL1, and VOL2 provided path length equalization. Both signals were then detected using broadband photo-detectors. Figure 3.11 inset (d) shows the transversal filter taps with the reference in between.

To test the system of Figure 3.11, the optical carriers were set to $\lambda_\circ$=1550 nm, λ_1=1551.5 nm, and λ_2=1548.5 nm to be placed at the middle of pass bands of the cascaded grating as shown in Figure 3.12 (b). The optical powers corresponding to these three wavelengths were set to $P_\circ$=10 mw, P_1=16.3 mv, and P_2=10 mw.

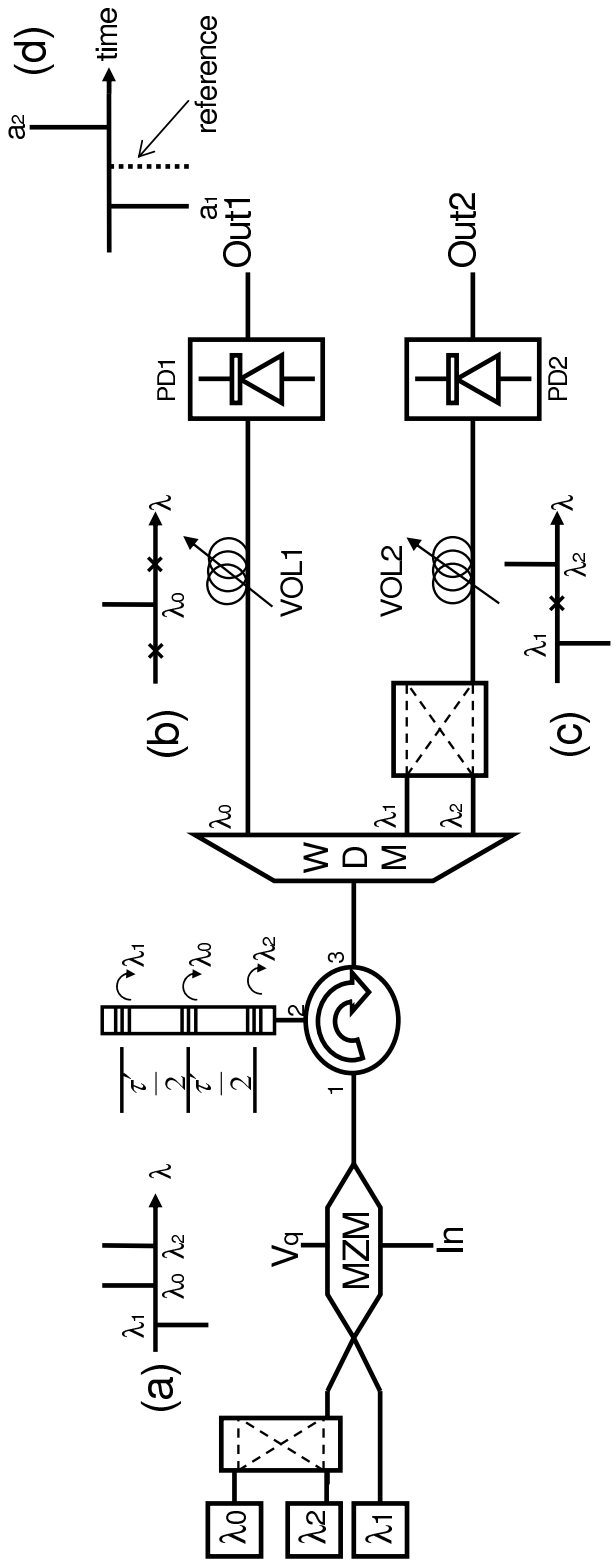

Figure 3.11: Experimental setup of the cascaded grating based photonic hybrid coupler.

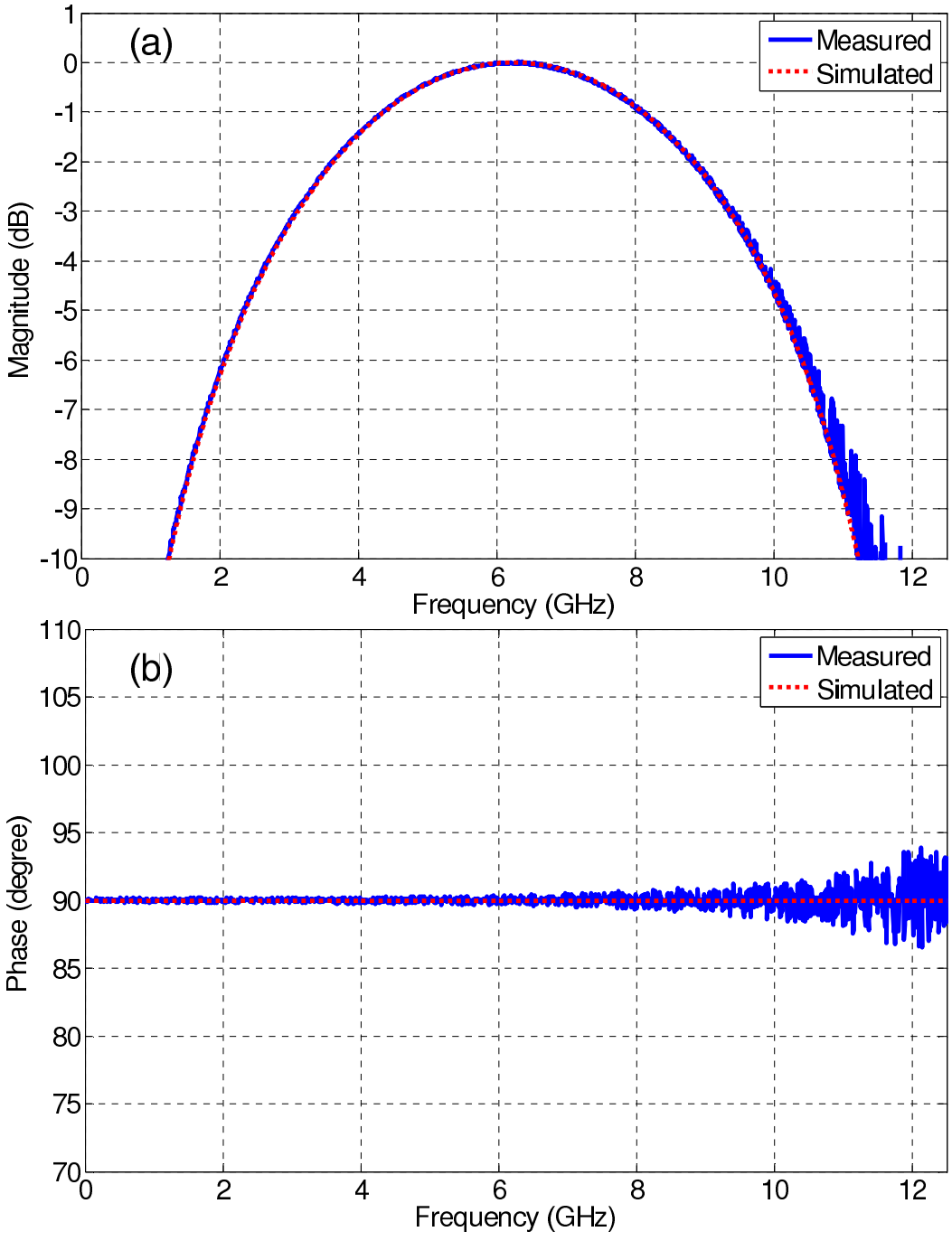

Figure 3.12: Measured and predicted system magnitude and phase response.

To characterize the hybrid coupler, a VNA was used. Port I of the VNA was connected to the RF input of the MZM (In) and Port II was connected to the output of the PD1 (Out1). The VNA was then calibrated and Port II was connected to the output of PD2 (Out2). Figure 3.12 (a) shows the amplitude response of the system. A 3dB bandwidth of 6.4 GHz (3-9.4 GHz) was achieved. A very low noise response inside the pass band is evident. Around 12.5 GHz, the noise increased dramatically due to the amplitude null at 12.5 GHz; however, since the frequency measurement range of the IFM system (1-10 GHz) does not cover this region, this does not affect the pass band characteristics. Figure 3.12 (b) shows the phase response of the system. A phase shift of 90° was achieved for all frequencies. A low phase ripple was achieved in the pass band region (3-9.4 GHz). Due to the null at 12.5 GHz, the phase noise was increased, which does not affect the system performance since it is out of pass band (3-9.4 GHz).

Comparing with the basic hybrid coupler of Section 3.3, the system of Figure 3.11 features better latency and less bulk; however, it has limited bandwidth since it is implemented based on only a two tap transversal filter. This could be solved using a cascaded grating with two additional gratings with uniform delays. A Linearly Chirped FBG (LCFBG) may be considered to implement the Hilbert transformer; however the amount of the delay required would be hard to achieve as a long length of LCFBG would be required particularly if low frequency operation is required. As the Hilbert transformer is required to be wideband, LCFBGs are thus not an ideal solution.

In summary, a cascaded grating based hybrid coupler was proposed and practically demonstrated. Since the optical path length of the whole system is in order of few meters, this hybrid coupler could be employed to implement the orthogonal measurement IFM system. This also ensure a good latency for the system.

3.5 Orthogonal IFM System Implementation

In this Section a photonic approach is introduced that can be employed to implement the orthogonal measurement IFM system of Section 3.2. This system requires a broadband 90° phase shift. As shown in Section 3.3 photonics can be used to implement such a phase shifter over a broad frequency range. Also, as the system is implemented in the photonic domain, it would be advantageous to use the photonic hybrid coupler to achieve the 90° phase shift.

As the system exhibits a frequency dependent DC output, low-cost photo-detectors can be used to reduce the total cost of the system. Also by using photonic elements, a broad frequency detection range can be achieved. To achieve the broadband 90° phase shift required in Figure 3.1, a hybrid coupler can be employed as discussed in Section 3.4

where, a two-tap transversal filter with an additional reference tap is used to make orthogonal to measurements. This provides a broadband 90° phase shift. This Section aims to show that the hybrid coupler of Section 3.4 can be used to achieve orthogonal measurements as discussed in Section 3.2.

3.5.1 Orthogonal IFM System Configuration

Figure 3.13 shows the experimental setup of the photonic IFM with orthogonal outputs. An RF signal generator produced a single RF tone which was divided into two equal portions feeding two arms of the IFM system. These arms are labelled the 'Optical Path' and the 'RF Path' on Figure 3.13. The RF tone in the Optical Path, modulated three wavelengths being used to implement a two-tap (λ_1, and λ_2) transversal filter with a reference tap ($\lambda_\circ$) in between. Carriers $\lambda_\circ$ and λ_2 were combined using a 3dB optical coupler. This combined signal together with λ_1 were modulated oppositely to make the desired combination as shown in Figure 3.13 inset (a) [70]. The modulated signal was then input to Port 1 of an optical circulator. Port 2 of the circulator was connected to a cascaded grating. Figure 3.10 shows the characteristics of this grating. Each wavelength was reflected with different but uniformly incremented delays. The dispersed signal was output from Port 3 and input to MZM2 fed with the original RF tone in the RF Path. Note that both the cascaded grating and the optical circulator were polarization maintaining. This ensured correct polarization at the MZM2 input. The output of MZM2 was then amplified using an EDFA and input to a Wavelength Division Multiplexer (WDM) which separates all wavelengths. Carrier $\lambda_\circ$ remained separated and was used as the reference (Figure 3.13 inset (b)). The arm containing $\lambda_\circ$ is called the reference arm. The carriers λ_1 and λ_2 were again combined using a 3dB coupler to make the two-tap transversal filter (Figure 3.13 inset (c)). This arm was called the 90° arm. Both signals were then detected, low-pass filtered and measured by digital voltmeters.

Having conceived a photonic system capable of producing orthogonal IFM outputs, a theoretical model must now be developed predicting the behavior of the system to validate that two orthogonal measurements are indeed expected.

3.5.2 Orthogonal IFM Model

To validate the ability of the experimental setup of Figure 3.13 to perform orthogonal measurements, a mathematical model must be developed that predicts the frequency dependent DC output. This model builds on the model of Section 3.2 introducing the actual responses of photonic link components to enable exact prediction of photo-detectors output DC voltages. The expression for the reference arm photo-detector (PD1) where only

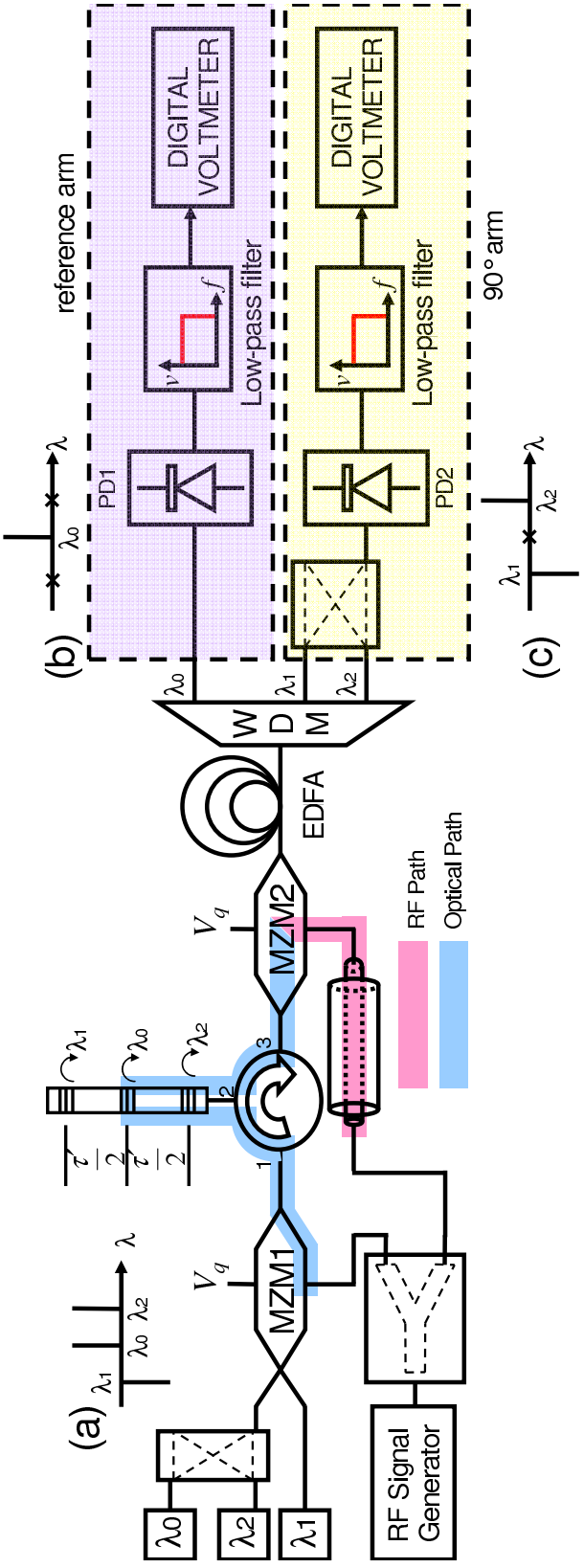

Figure 3.13: Experimental setup of IFM system with orthogonal outputs.

wavelength $\lambda_\circ$ is present, is first derived. In Section 2.3.3 it was assumed that identical MZMs were used, and thus the DC component of the output signal present at the output of PD1 could be can be described by Equation (2.52). Rearranging Equation (2.52), yields:

$$V_{DC_{\lambda\circ}}(\Omega) = \frac{1}{4}GZ_{PD}P_\circ\left[1+\frac{\pi^2(1+M^2)Z_{in}P_{RF}}{4V_\pi^2}\right]+\frac{\pi^2}{4V_\pi^2}GMZ_{PD}Z_{in}P_\circ P_{RF}\cos\phi \tag{3.18}$$

where the factor G can be defined as:

$$G = rG_{LPF}L_{MZM}^2L_{WDM}G_{EDFA} \tag{3.19}$$

where r is the responsivity of the photo-detector, G_{LPF} is the gain of the low-pass filter, L_{MZM} is the MZMs optical insertion loss, L_{WDM} is WDM optical insertion loss, and G_{EDFA} is EDFA gain. For simplicity, the factors $\alpha_\circ$, $\beta_\circ$, $\gamma_\circ$ are defined as:

$$\begin{aligned}\alpha_\circ &= \tfrac{1}{4}GZ_{PD}P_\circ\\ \beta_\circ &= \tfrac{1}{16}GZ_{PD}Z_{in}P_\circ\tfrac{\pi^2(1+M^2)}{V_\pi^2}\\ \gamma_\circ &= \tfrac{\pi^4}{2V_\pi^2}GMZ_{PD}Z_{in}P_\circ\end{aligned} \tag{3.20}$$

Equation (3.18) can then be simplified as:

$$V_{DC_{\lambda\circ}}(\Omega) = \alpha_\circ+\beta_\circ P_{RF}+\gamma_\circ P_{RF}\cos\phi \tag{3.21}$$

At the lower photo-detector (PD2), each wavelength (λ_1, and λ_2), generates its own DC component assuming a linear characteristic for PD2. Therefore, the DC component produced by each wavelength, present at the output of PD2 can be described as:

$$V_{DC_{\lambda1}}(\Omega) = \alpha_{90}+\beta_\circ P_{RF}-\gamma_{90}P_{RF}\cos(\phi+\Omega\frac{\tau'}{2}) \tag{3.22}$$

$$V_{DC_{\lambda2}}(\Omega) = \alpha_{90}+\beta_\circ P_{RF}+\gamma_{90}P_{RF}\cos(\phi-\Omega\frac{\tau'}{2}) \tag{3.23}$$

where $V_{DC_{\lambda1}}(\Omega)$, and $V_{DC_{\lambda2}}(\Omega)$ are DC components produced by wavelengths λ_1, and λ_2 respectively. The delay between λ_1 and λ_2 caused inside the cascaded grating is τ', and factors α_{90}, β_{90}, γ_{90} are defined as:

$$\begin{aligned}\alpha_{90} &= \frac{1}{4}GZ_{PD}P_{90}\\ \beta_{90} &= \frac{1}{16}GZ_{PD}Z_{in}P_{90}\frac{\pi^2(1+M^2)}{V_\pi^2}\\ \gamma_{90} &= \frac{\pi^4}{2V_\pi^2}GMZ_{PD}Z_{in}90\end{aligned} \tag{3.24}$$

where P_{90} is the optical power levels of the both carriers λ_1 and λ_2 which should be equal. The negative coefficients of γ_{90} in Equation (3.22) is achieved by reverse modulation inside MZM1. The total DC component present at the output of PD2, can then be calculated

by adding Equation (3.22) and Equation (3.23) to achieve:

$$V_{DC_{90}}(\Omega) = 2\alpha_{90} + 2\beta_{\circ}P_{RF} - \gamma_{90}P_{RF}\cos(\phi + \Omega\frac{\tau'}{2}) + \gamma_{90}P_{RF}\cos(\phi - \Omega\frac{\tau'}{2}) \quad (3.25)$$

After simplification, Equation (3.25) can be rewritten as:

$$V_{DC_{90}}(\Omega) = 2\alpha_{90} + 2\beta_{90}P_{RF} + 2\gamma_{90}P_{RF}\sin\Omega\frac{\tau'}{2}\sin\phi \quad (3.26)$$

From Equation (3.21) and Equation (3.26), it can be deduced that:

$$\frac{V_{DC_{\circ}}(\Omega) - \alpha_{\circ}}{V_{DC_{90}}(\Omega) - 2\alpha_{90}} = \frac{\beta_{\circ} + \gamma_{\circ}\cos\phi(\Omega)}{2\beta_{90} + 2\gamma_{90}\sin\Omega\frac{\tau'}{2}\sin\phi(\Omega)} \quad (3.27)$$

Equation (3.27), allows calculation of the RF frequency using the measured DC outputs without dependence on the input RF power. Having isolated the RF frequency, the RF power level can also be determined using either Equation (3.21) or Equation (3.26).

Having developed a mathematical model that illustrates the orthogonality of the output voltages of the orthogonal IFM system, it is now possible to experimentally demonstrate the ability of the IFM system to measure both RF frequency and power independently.

3.5.3 Orthogonal Measurement IFM Demonstration

Section 3.5.2 established, in theory, that the system of Figure 3.13 should indeed enable amplitude independent frequency measurement. The IFM performance is now demonstrated experimentally. The system was configured as depicted in Figure 3.13. The optical carriers were set to $\lambda_{\circ}$=1550 nm, λ_1=1551.5 nm, and λ_2=1548.5 nm respectively. The optical powers corresponding to these three wavelengths were set to P_circ=11.7 mv, P_1=17 mv, and P_2=11.7 mw respectively. The factor G in Equation (3.19) was calculated to be $G = 0.95$, and the delay τ' was 80ps corresponding to nulls response at 0 and 12.5 GHz. Both MZMs input impedance (Z_{in}) and photo-detector output impedance (Z_{PD}) were 50Ω. The half wave voltage (V_{π}) of both MZMs was 5V. To validate the model of Section 3.5.2, four different RF power levels ($P_{RF} = 3, 6, 9, 12$ dBm) were used to produce four different measurement conditions for the same frequency. Using orthogonal measurements it is hoped that both RF frequency and RF power can be measured independently. Figure 3.14 shows the measurements taken from digital voltmeters from the reference arm of system of Figure 3.13 along with the predicted voltage obtained from Equation (3.21). Good agreement between predicted and measured results is evident. As the nulls of the transversal filter response (0 and 12.5 GHz) are out of the frequency measurement range (1-10) GHz, this does not affect the IFM operation. Figure 3.15 shows the measurements taken from the digital voltmeter from the 90° arm along with the predicted voltage obtained from Equation (3.26). Good agreement between predicted and

measured results is evident. In both arms, by increasing the RF power level, both constant and sinusoidal terms of the DC components increased as shown by Equation (3.21) and Equation (3.26).

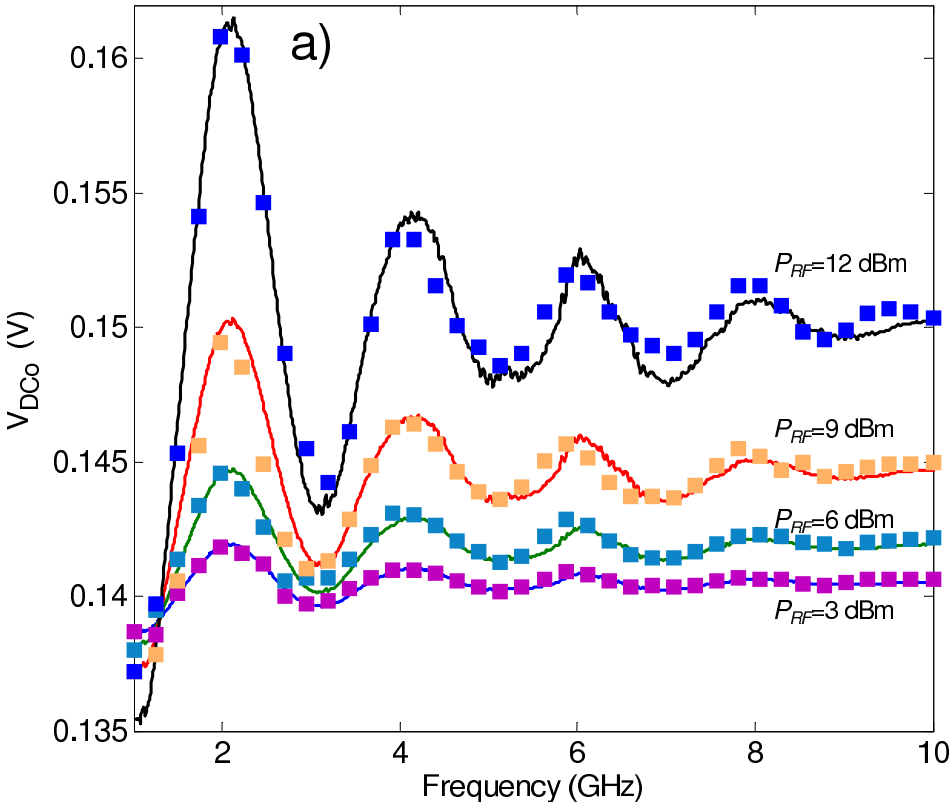

Figure 3.14: Measured and predicted results for the reference tap.

These measurements were then used to predict the RF frequency using Equation (3.27), and the results are shown in Figure 3.16. The RF power level was also predicted using Equation (3.21) and shown in Figure 3.17. Good agreement between measurement and prediction results is evident.

Due to the oscillatory nature of of Equation (3.21), and Equation (3.26), unambiguous frequency measurement is only possible in each half a period of Figure 3.16. This behavior is similar to that observed in Section 2.4. Therefore, there are nine distinct bands within which frequency measurement is unambiguous. Sensitivity is less at edges of each due to zero gradient at the peaks and nulls of the sine curve. Some inconsistencies have occurred which limit the system functionality. This could be attributed to co-axial cable loss at higher frequencies (> 9 GHz). The sinusoidal behavior of Equation (3.21) and Equation (3.26) suggest that by reducing the differential delay τ, the system bandwidth can be increased. Approximating $\phi(\Omega) = \Omega\tau$, it can be easily seen that by reducing τ, the sinusoidal period will increase resulting in a wider frequency measurement range. The system bandwidth can be increased; however, by reducing the differential delay between

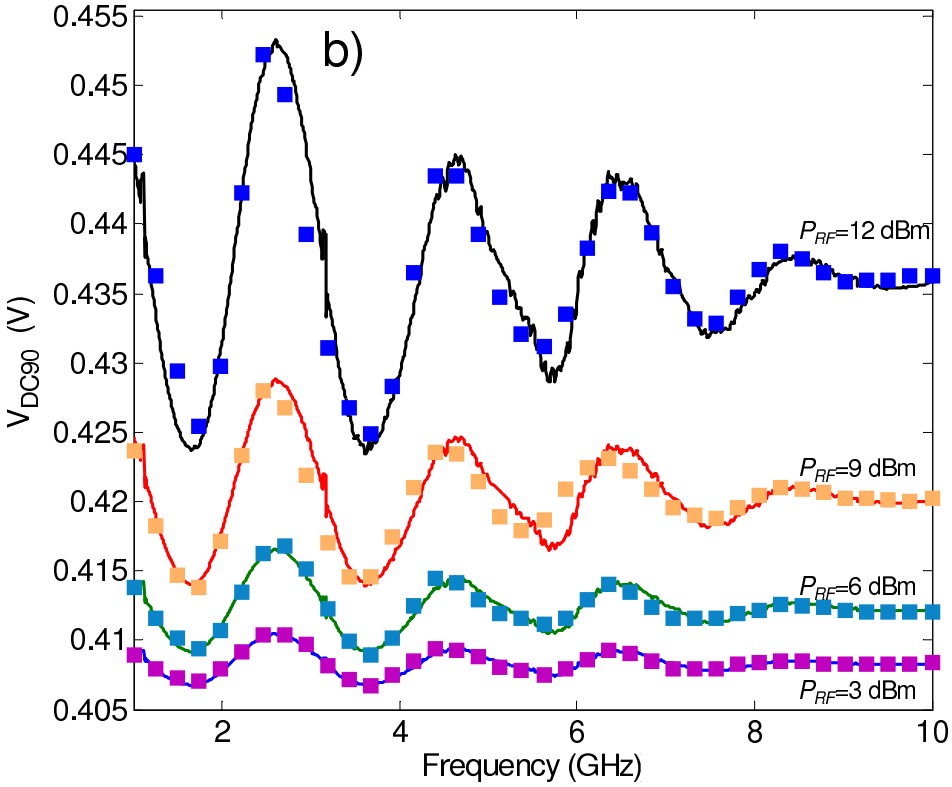

Figure 3.15: Measured and predicted results for the two-tap transversal filter.

the Optical and RF paths through system integration. This comes at the expense of sensitivity. Importantly this system does indeed show the ability to measure both RF frequency and power simultaneously and independently.

In summary an orthogonal measurement IFM system was conceived and practically demonstrated. The system employs a photonic hybrid coupler to generate two sets of orthogonal measurement over a wide frequency range of (1-10 GHz).

3.6 Conclusion

It was concluded in Chapter 2 that a practical IFM systems should be able to independently measure RF frequency and amplitude. In order to do this, two orthogonal measurements were required. To achieve orthogonal measurement, a 90° hybrid coupler or Hilbert transformer is required. However this would need to retain the favorable broadband characteristic of photonics.

A photonic hybrid coupler was then introduced as a solution to address this problem. A technique has been introduced to achieve a 90° phase shift over in the microwave domain over a broad band frequency range. As this scheme is based on non-coherent optics, the system offers very good stability both in phase and amplitude. This implementation

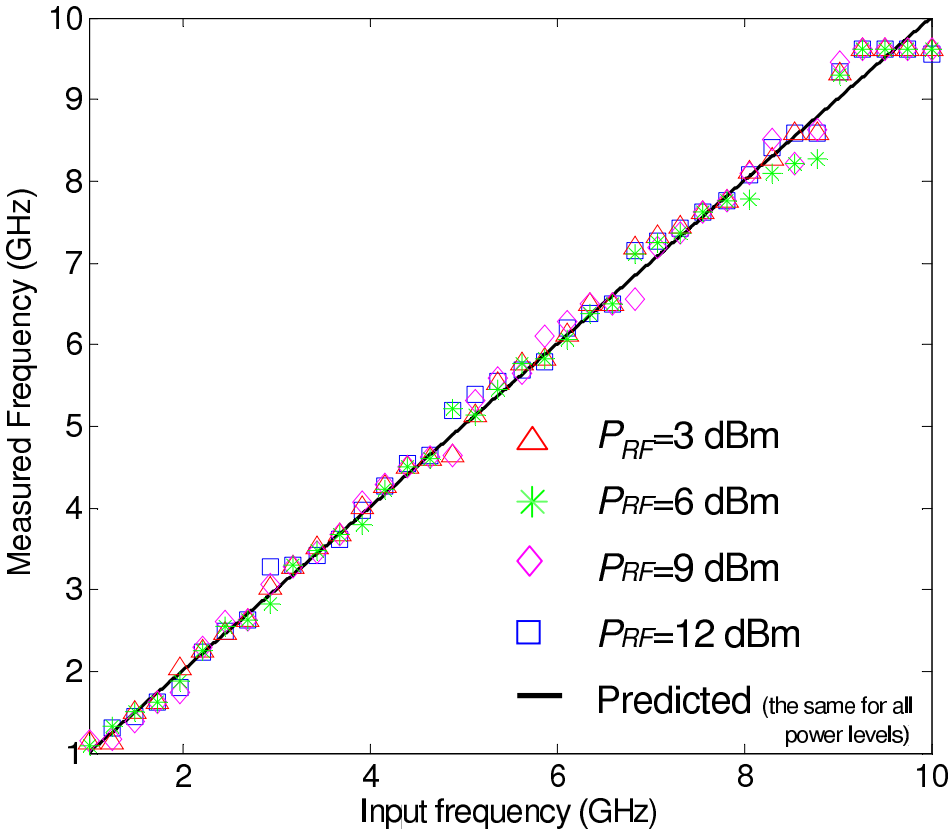

Figure 3.16: Measured frequency vs. input frequency.

offers dynamically adjustable bandwidth and ripple achieved by changing carrier powers in each tap where the absolute laser power needs to be empirically adjusted due to slight differences in MZMs. The isolation between outputs is near perfect as there was no electrical connection between the ports. The impedance of ports is very close to 50Ω for all frequencies and this remains unaffected when loading the ports due to excellent isolation. This is a distinct advantage of over traditional hybrid couplers. Extension to broader bandwidth through introduction of extra wavelength channel taps is possible. Implementing this photonic hybrid coupler, made it possible to achieve two orthogonal sets of IFM measurement. Having two orthogonal measurements provide the possibility of determining both RF frequency and RF power simultaneously and independently.

In summary, using the microwave-photonic hybrid coupler concept a wideband orthogonal microwave-photonic IFM system was conceived and demonstrated practically.

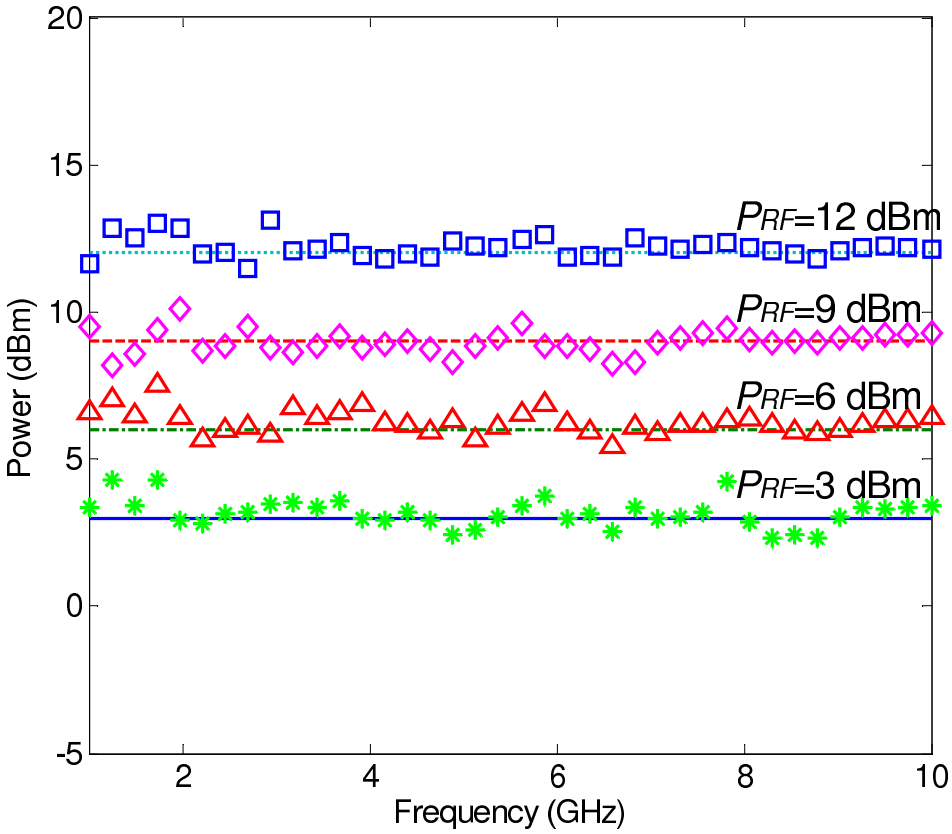

Figure 3.17: Measured and predicted power vs. input frequency.

Chapter 4

Non-Linear Photonic approach to Instantaneous Frequency Measurement (IFM) System

4.1 Introduction

Chapter 2 described a photonic IFM that used low-cost DC photo-detectors. This was possible by mixing the RF frequency to DC in the optical domain using an MZM. One disadvantage with this system was that the loss and limitation of the co-axial cable feeding the second MZM. Since it is necessary to measure in higher bandwidth range, the elimination of the co-axial cable is necessary.

This Chapter will explore how frequency measurement can be achieved, by elimination the co-axial cable and the second MZM and replace that with all optical mixing devices. This demonstration proved that all optical mixing could be effectively utilized to realize a low cost IFM system.

For clarity, the operation of Semiconductor Optical Amplifier (SOA) are first reviewed in Section 4.2. A literature survey focused on non-linearity of the SOA is conducted. In Section 4.3 a new microwave photonic IFM concept is introduced based on employing all optical mixing using SOA as a non-linear device to eliminate the need for any co-axial cable. Section 4.4 proposes and demonstrates a photonic IFM system based on Highly Non-Linear Fiber (HNLF). Section 4.5 draws conclusions on the practicality of the proposed all optical mixing IFM system. The findings of this Chapter have been published in [69, 80].

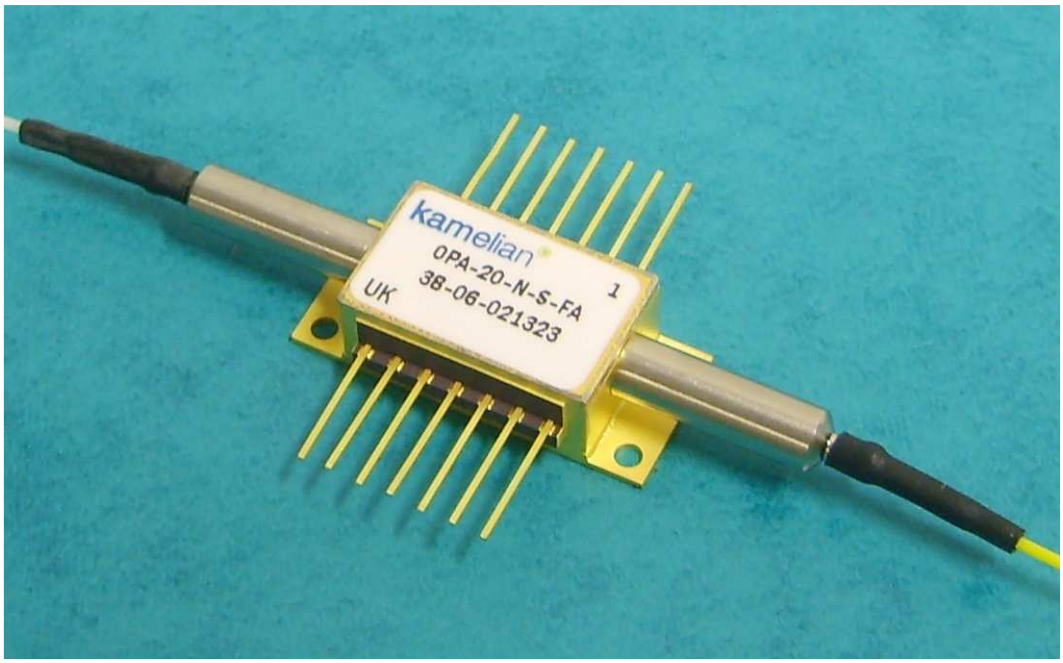

Figure 4.1: Semiconductor Optical amplifier (SOA) from Kamelian

4.2 Semiconductor Optical Amplifier

The Semiconductor Optical Amplifier (SOA) is a useful device that recently has been used in various applications in the fields of telecommunication and optical signal processing [81]. This device has been conceived as an optical amplifier with significant reduced cost and improved components when compared to EDFAs. Recently SOAs have been characterized as non-linear components.

Attempts have been made to analyze and implement cross-gain, cross-phase and Four Wave Mixing (FWM) based wavelength convertors using SOAs. These concepts were then employed to implement wideband microwave up-converters, mixers and frequency doublers.

In one work, cross-gain and cross-phase wavelength conversion in SOAs were analyzed in depth. The influence of saturation filtering on the bandwidth of the converters was explained and conditions for conversion at 20 Gb/s or more are identified. It was shown that for the cross-gain modulation scheme, the extinction ratio degraded for conversion to longer wavelengths [81].

In another work, the main application of SOAs as non-linear optical components were reviewed. Concentrating on FWM, general parameters that are of relevance for signal processing applications have then been defined. It was shown that basic experiments and general simulation procedures can be used to determine optimum operating conditions for the intended applications. An experiment on FWM with picosecond optical pulses was

developed and the results were presented. It was shown that new optimization criteria and advanced theoretical models must be applied for the case of short optical pulses. The possibility to extract the dynamical SOA parameters from the experiments, are also discussed [82].

In another attempt, an experiment to investigate the cross-gain property of SOA was developed. Saturating the SOA, the conversion gain mechanism was changed. This led to an optical mixing effect resulting in mutual exchange of frequency components of optical signals. It was shown that optical feed back saturated amplifiers and cascaded optical amplifiers could have similar performance. Up to 10 dB gain was achieved for two 8 nm apart modulated optical carriers. Both up and down converted RF signals (150 and 650 MHz) were achieved where optical carriers were modulated by RF signals with 250 MHz and 400 MHz frequencies, respectively [83].

In another work, a 20 GHz optoelectronic mixer was implemented and and characterized. More than 70 dB below the IF output third order intermodulation products was achieved. A simple super heterodyne receiver was then implemented utilizing this mixer. The receiver exhibited a -66 dBm tangential sensitivity and a 44 dB compressive dynamic range [84].

In another work, the optical mixing of RF signals by means of exploiting the nonlinearity of an SOA using propagation of photon density and rate equations was proposed. The results show the potential for devices with low conversion losses and even gain and polarization insensitivity and reduced insertion losses [85].

Detailed characteristics for the frequency up-conversion of optical IF signals with the optical heterodyne local oscillator (LO) signals having different wavelengths that can be achieved with SOA cross-gain modulation and square-law photo-detection, were investigated in [86]. A simple analytical expression for the frequency up-conversion efficiency was firstly derived and experimental validation was then conducted. The results showed that the signal frequency up-conversion efficiency was directly attributed by the SOA optical gain and can be optimized by either controlling the optical LO power or selecting the optical IF and LO wavelengths within the SOA optical gain bandwidth. These results will be useful in selecting proper conditions for the optimal frequency up-conversion efficiency.

SOAs have shown the ability to provide broadband signal processing of microwave photonic signals. They provide a high and almost flat conversion gain over a broad frequency range far more better than that of microwave mixers. Therefore, they could be useful in implementing an all optical IFM system. In the next Section an IFM system based on all optical mixing using an SOA is conceived and demonstrated practically. An 18 GHz (2-20 GHz) frequency measurement range has been achieved.

Parameter	Min Spec.	Typical Spec.	Max Spec.
Fiber to fiber gain (Min)	10		
Noise Figure		8	10
Gain recovery time (1/e)		25 ps	
Polarization dependence		1 dB	2 dB
ASE center wavelength	1530 nm		1570 nm
Bias current		300 mA	400 mA
Operating temp	$-5°C$		$70°C$
TEC drive max		.7 A/1.5 V	

Table 4.1: Kamelian SOA specifications (1529-1563 nm with 0 dBm input)

4.3 Photonic IFM System Based on SOA

In this Section a IFM system based on using Non-Linear mixing is conceived and practically demonstrated. This system employs two differentially delayed modulated optical carriers that are mixed using the SOA. The output of the system includes a DC component that varies as a function of frequency. This can be used for frequency measurement purposes. Operation is demonstrated from 2-20 GHz. An SOA from Kamelian (SOA-NL-H1-C-FA) was employed. Table 4.1 shows the characteristics of the SOA.

4.3.1 SOA Characterization

As discussed in Section 4.3 to take advantage of broad bandwidth, long transmission range it is necessary to implement our IFM system using photonic components. Modulation, time delay and detection are straight forward in the optical domain. All-optical multiplication can be achieved using non-linear optical components. In this investigation multiplication is achieved using an SOA. Before proceeding with IFM system implementation it will be necessary to characterize the response of an SOA when used as an all optical mixer.

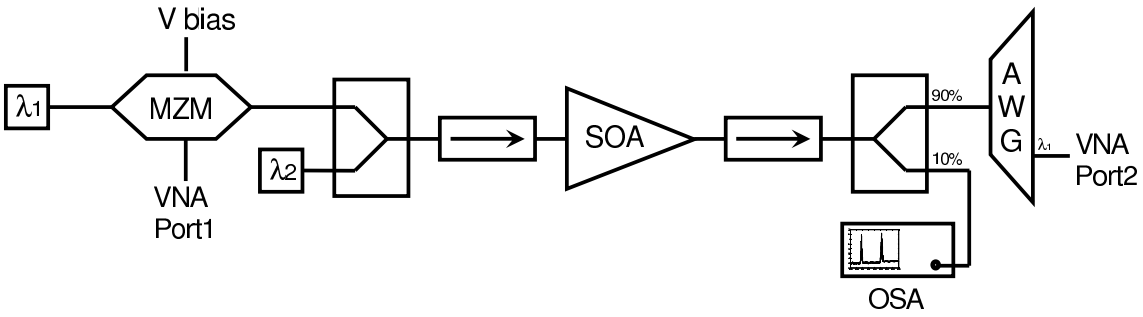

Figure 4.2: Experimental setup for SOA characterization

SOA DC Response

Figure 4.2 presents the experimental setup used to characterize the non-linear response of the SOA. Two laser sources provide two polarized optical carriers at wavelengths $\lambda_1 = 1551.85\ nm$ and $\lambda_2 = 1553.85\ nm$. Carrier λ_1 is transmitted through a high-speed MZM and then combined with carrier λ_2 using a simple 3 dB power combiner. The two optical carriers were then transmitted through the SOA where they were mixed by the SOA non-linear response of this device. Since the SOA also provides gain, optical isolators were used on both sides of the SOA to prevent oscillation. A small portion (10%) of output was tapped to an Optical Spectrum Analyzer (OSA) to enable monitoring of the output optical wavelengths. The remaining optical power was separated into its wavelength components using an arrayed waveguide grating (AWG) and the signal on carrier λ_2 was monitored using a broadband photo-detector. The first characterization experiment aimed to establish

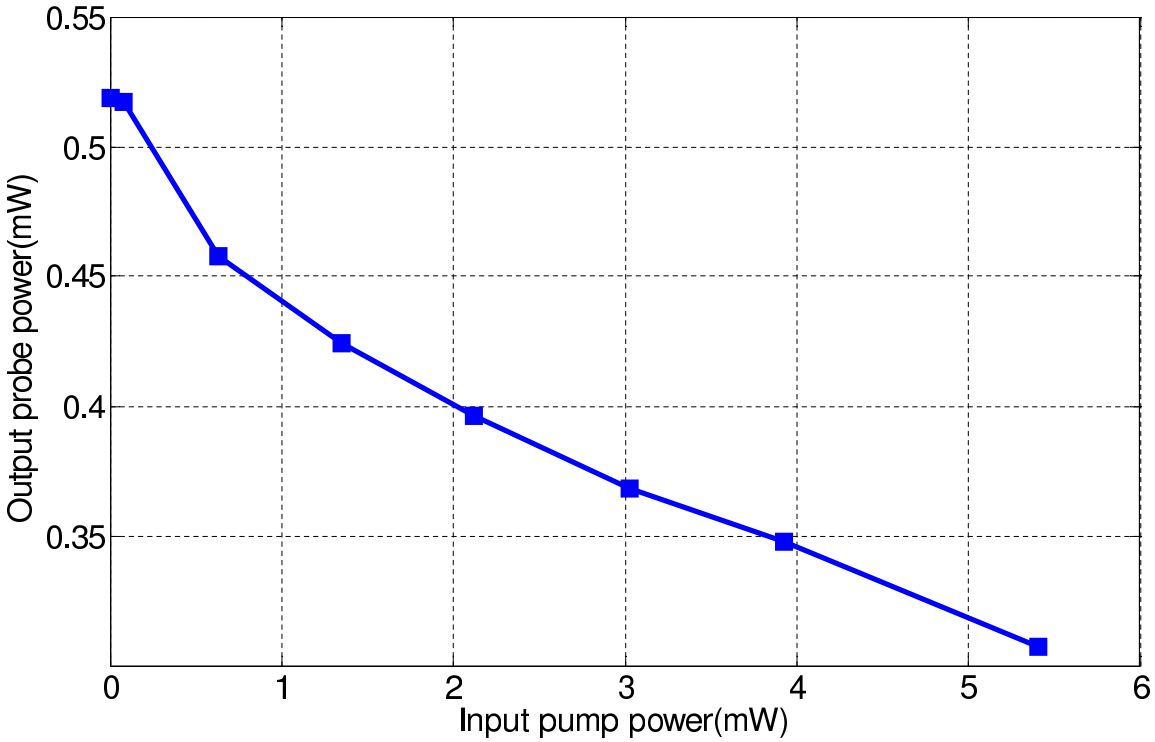

Figure 4.3: DC response of the SOA.

the DC mixing response of the SOA by measuring the output power on carrier λ_2 as a function of the input power on carrier λ_1. The input power at the SOA on carrier λ_2 was fixed at 5mW and the modulator bias was used to adjust the input power of carrier λ_1. The output power on carrier λ_2 was measured using a power meter.

Figure 4.3 presents the measured power on λ_2 as a function of input power on λ_1. As it can be seen there is an almost linear relationship between the input pump power on λ_1 and the output probe power on λ_2. The gradient corresponds to the mixing gain. A pump power of 5mW have been chosen where the gradient is most linear.

SOA Frequency Response

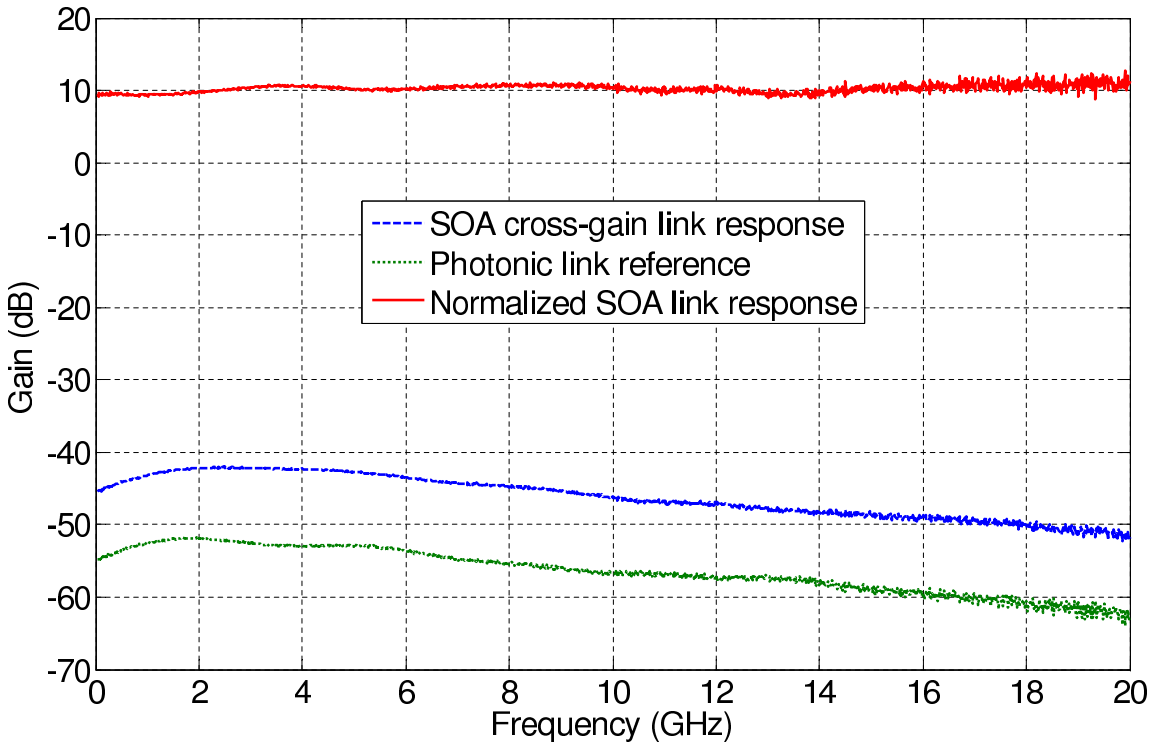

Figure 4.4: Frequency response of the SOA: Photonic Link gain reference response; cross-gain frequency response; normalized cross-gain response

Next step is to establish the frequency response of the SOA mixing response. The configuration of Figure 4.2 was again used. An RF signal from a vector network analyzer (VNA) was input to the MZM and the output was received by a broadband photo-detector and analyzed using the VNA. The system was first calibrated by measuring the photonic link response of carrier λ_1 with the SOA component removed. The SOA was returned and the response of the signal transferred to carrier λ_2 was measured. The RF mixing response of the SOA is presented in Figure 4.4.

The gain level is high and is quite flat over a broad frequency range from 2-20 GHz. The SOA characteristics indicate that it is a good candidate for the mixing component for an IFM photonic implementation.

4.3.2 Photonically Implemented IFM Using SOA

The photonic IFM implementation is presented in Figure 4.5. A 2×1 MZM was used to combine and modulate two polirized optical carriers at λ_1 and λ_2. A length of dispersive fiber was used to achieve a relative time delay between these two carriers. The dispersed optical signal was then traversed through an isolator, the SOA and a second isolator. The output was then split in 10% and 90% portions. The 10% was used to feed the OSA. The 90% portion traversed through an AWG and the detected by a photo-detector. Only the DC component was analyzed at the output.

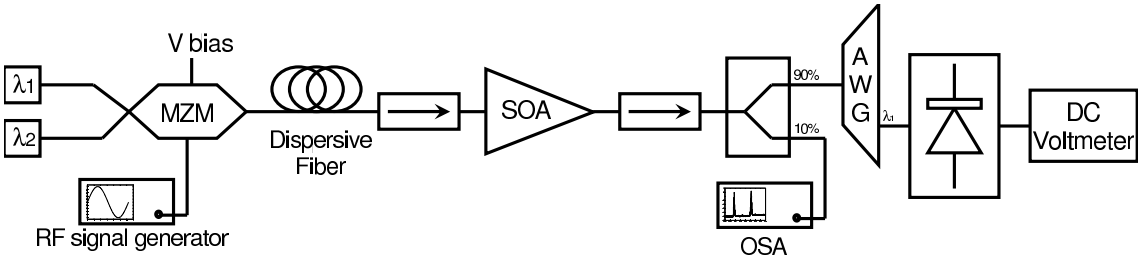

Figure 4.5: Photonically implemented IFM configuration

Model of IFM Using SOA

Before measuring this system, its performance should be predicted. Considering the frequency response of each component of the system, the DC output will be:

$$V(f) = \sqrt{G(f)}cos(2\pi f\tau) + V_{DC} \tag{4.1}$$

where f is the frequency of the signal and $G(f)$ is defined as:

$$G(f) = G^2_{MZM}(f)G_{SOA}(f)G_{PD} \tag{4.2}$$

where $G_{MZM}(f)$ is MZM RF gain response (a simple quadratic function), $G_{SOA}(f)$ is the conversion gain response of the SOA (Figure 4.4), and G_{PD} is the DC gain of the photo-detector.

Since both carriers are modulated, their product includes the modulator response squared. Figure 4.6 presents the response predicted by Equation (4.1). The sinusoidal response required for frequency measurement is evident. The gradually decreasing amplitude is mainly due to the quadratic MZM frequency response.

Implementation of IFM Using SOA

The system of Figure 4.5 was implemented using a dispersive 4.478km fiber (SMF28) which corresponded to a relative time delay of τ=149.165ps between the two optical carriers. Figure 4.6 shows the DC component measured by the digital voltmeter as a function of frequency along with the predicted results. Excellent agreement between measurement and predicted results are evident. The results of Figure 4.6 can be inverted using Equation (4.1) to achieve frequency measurement as shown in Figure 4.7 as with other IFM implementations. Due to the oscillating nature of the response of Figure 4.6, there are six distinct bands within which frequency measurement is unambiguous. Within each band, frequency measurement is reasonably accurate.

However this implementation could suffer from instability as SOAs tends to oscillate. Also SOAs produce Amplified Spontaneous Emission (ASE) which lowers the sensitivity [87]. This could be solved replacing the SOA by a passive non-linear device such a Highly Non-Linear Fiber (HNLF).

In a summary an instantaneous frequency measurement system based on all optical mixing and DC photo-detectors has been demonstrated. The system shows the very wide-band characteristics. The frequency range and sensitivity can be adjusted through use of different lengths of dispersive fiber.

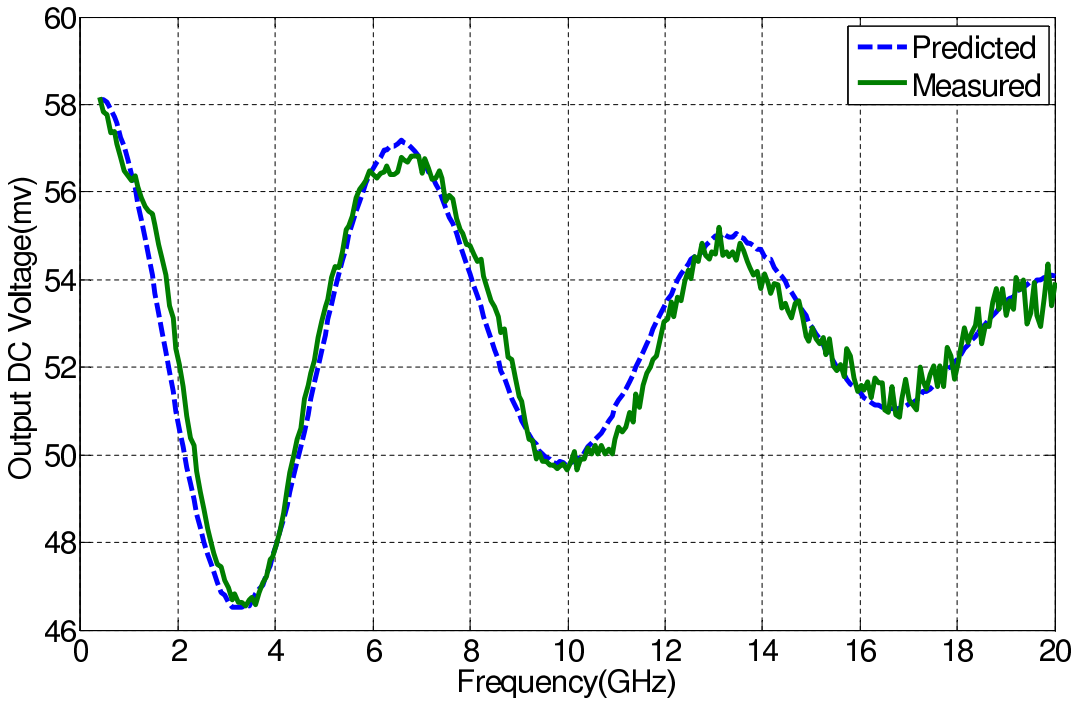

Figure 4.6: Measured and predicted IFM response

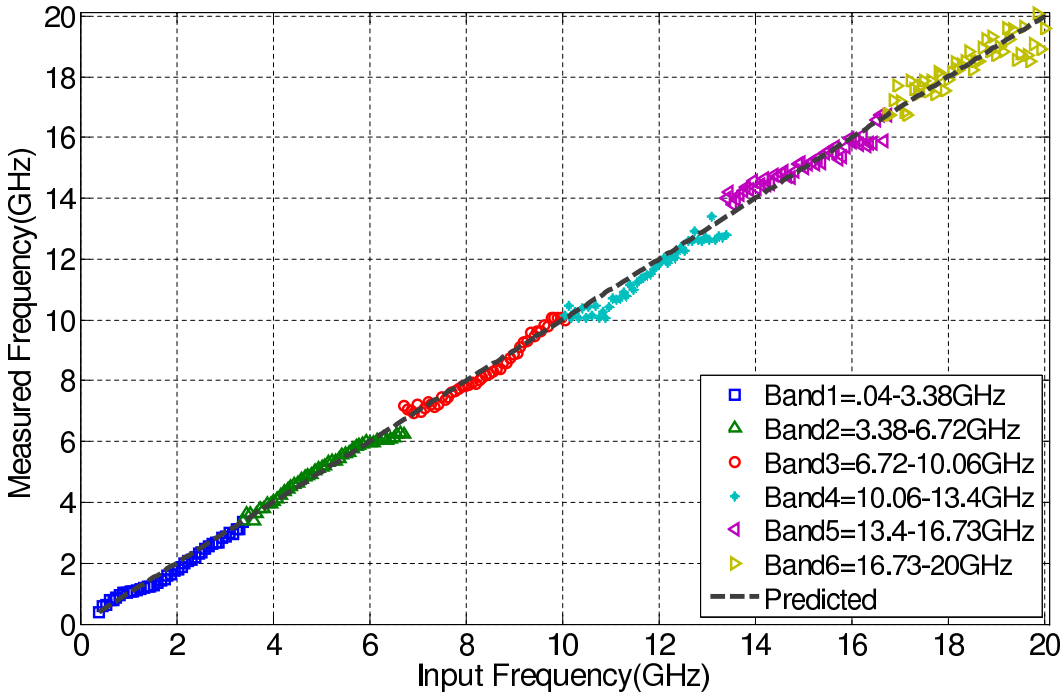

Figure 4.7: IFM frequency response interpreted as frequency measurement (prediction and Measurement)

4.4 Photonic IFM System Based on Non-Linear Fiber

The SOA, being an active component was prone to instabilities and even oscillation. This led to a degree of uncertainty in the frequency measurement. In this Section, a scalable IFM utilizing efficient optical mixing within a length of Highly Non-Linear Fiber (HNLF) is demonstrated. Predictable and highly stable frequency measurement is achieved over the range from 0.5-40 GHz. The HNLF used was an OFS (090161150001). Table 4.4 shows the specifications of the HNLF.

Length	fiber dispersion	fiber dispersion slope	Total loss	Total PMD C-Band
999 m	-.19 $ps/nm/km$	0.01 $ps/nm^2/km$	1.73 dB	0.12 ps

Table 4.2: OFS HNLF specifications (1550 nm)

Figure 4.8 presents this concept graphically and illustrates the optical spectrum of the signals throughout the system.

In Figure 4.8, distinct optical carriers labelled as λ_1 and λ_2 were used for Path 1 and Path 2. Each channel carries an RF signal as sidebands indicated by triangles. Path 1 had an extra time delay compared to Path 2. This results in a frequency dependent phase shift of:

$$\phi(\Omega) = \Omega\tau \tag{4.3}$$

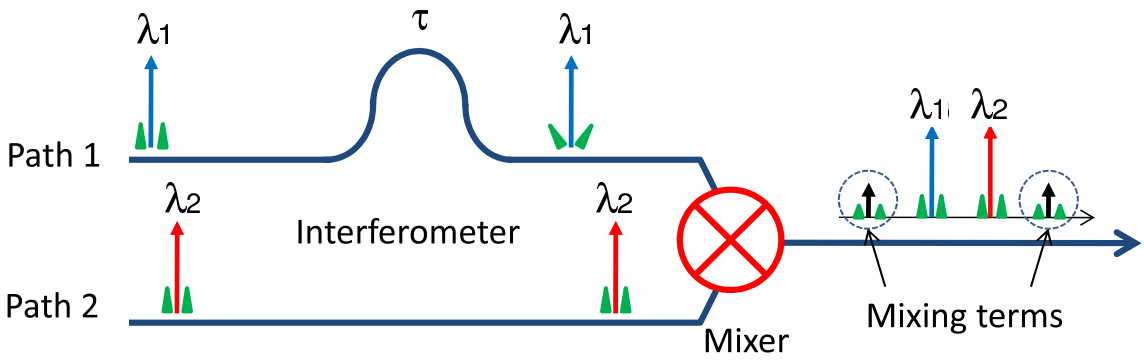

Figure 4.8: Principle of photonic IFM using optical mixing.

between the RF signal on λ_1 relative to the RF signal on λ_2. The two channels are then mixed optically producing new optical wavelengths which also carry the RF signal. These newly created wavelength channels were indicated as the mixing terms in Figure 4.8. It was predicted that the power of the mixing terms including the two sidebands should include a component that varies as $\cos \Omega\tau$ and thus, could be used to measure the input signal frequency Ω.

To achieve the IFM function of Figure 4.8. Two differentially delayed versions of the same signal must become combined. The input field can be written:

$$E = Ae^{j\omega_1 t} + Be^{j(\omega_1+\Omega)t+\phi_1} + Be^{j(\omega_1-\Omega)t+\phi_2} + \tag{4.4}$$

$$Ae^{j\omega_2(t+\Delta t)} + Be^{j(\omega_2+\Omega)(t+\Delta t)+\phi_3} + Be^{j(\omega_2-\Omega)(t+\Delta t)+\phi_4} \tag{4.5}$$

Assuming $B \ll A$, and considering only the idler at ω_2 and its sidebands, the FWM component $(\chi^{(3)})$ can be written as:

$$E^3 = 3A^2 e^{j\omega_2 t}\left[A + 2Be^{j(\Omega t+\phi_1)} + 2Be^{-j(\Omega t-\phi_2)} + Be^{j(\Omega t+\Omega\Delta t-\phi_4)} + Be^{-j(\Omega t+\Omega\Delta t+\phi_3)}\right] \tag{4.6}$$

Note that there is no $(\chi^{(2)})$ component produced in the HNLF. In Equation (4.6) it can be seen that the sidebands include the summation of the RF signals mixed from Path 1 and Path 2. This summation is coherent and hence the optical power itself varies. Thus this nonlinear photonic approach actually implements the summation concept of Figure 4.8. If only the lower idler is measured:

$$P(\omega_2) \propto \left\{A^2 + B^2\left[5 + 4\cos(\Omega\Delta t + \phi_1 - \phi_4)\right] + B^2\left[5 + 4\cos(\Omega\Delta t + \phi_2 - \phi_3)\right]\right\} \tag{4.7}$$

Equation (4.7) shows that the power in the idler oscillates with the RF frequency and thus can be mapped to the value of through knowledge of t. This relationship is the basis

of our IFM system. A low-cost DC photo-detector can be used to measure the power at the output of this IFM system. Having established that, in principle, nonlinear FWM can be used to achieve an IFM function that can be measured with a low-cost photo-detector, we must now characterize the FWM in a practical HNLF to insure that it does indeed behave according to these simple predictions and that it maintains this behavior over the whole RF band from 1-40 GHz.

4.4.1 Characterizations of the Optical Mixing Process

It is proposed that the Four Wave Mixing (FWM) process in HNLF be used to achieve the phase correlation function in Figure 2.3. Here two wavelengths were input to a highly non-linear fiber to produce two new optical wavelengths as mixing products (Figure 4.8). To be confident that the signals carried by the mixing products represented an accurate analog product of the signals modulated onto the original optical wavelengths, it was important to characterize the optical mixing and the photonic link frequency responses.

Channel	1	2	3	4	5	6	7	8
Wavelength	1542.12	1543.73	1545.32	1546.91	1548.51	1550.11	1551.72	1553.32

Table 4.3: Channel numbers and wavelengths (nm)

Figure 4.9 presents the experimental configuration used to perform this characterization. An array of 8 laser diode were available. The wavelength for each channel are shown in Table 4.3. Two laser diodes were used. The longer wavelength channel was labelled as λ_1. The shorter wavelength channel was labelled as λ_2. Channel λ_2 was connected to a broadband MZM. An RF signal generator produced a single RF tone. This RF tone modulated channel λ_2. The modulated optical signal, was then combined with the channel λ_1 using a 3 dB optical coupler. The coupler output was then amplified using an EDFA. The amplified optical signal was then fed to a Highly Non Linear Fiber (HNLF). A narrow band tunable optical filter (JDS Uniphase Grating Filter TB9226) was employed at the fiber output to enable selection of the wavelength band of interest. The filtered optical signal was then split into two portions with the ratio 99:1 using a 1% optical splitter. The smaller portion (1%) was then input to an Optical Spectrum Analyzer (OSA). The other portion (99%) was detected by a photo-detector (PD). The RF output of the photo-detector was measured using an Electrical Spectrum Analyzer (ESA).

To begin characterization of the optical mixing, it was important to identify which pair of the channels would result in the most efficient mixing. This was achieved using the setup of Figure 4.9. The MZM was biased at quadrature to achieve maximum transmission and the signal generator turned off. The lasers powers were set such that two

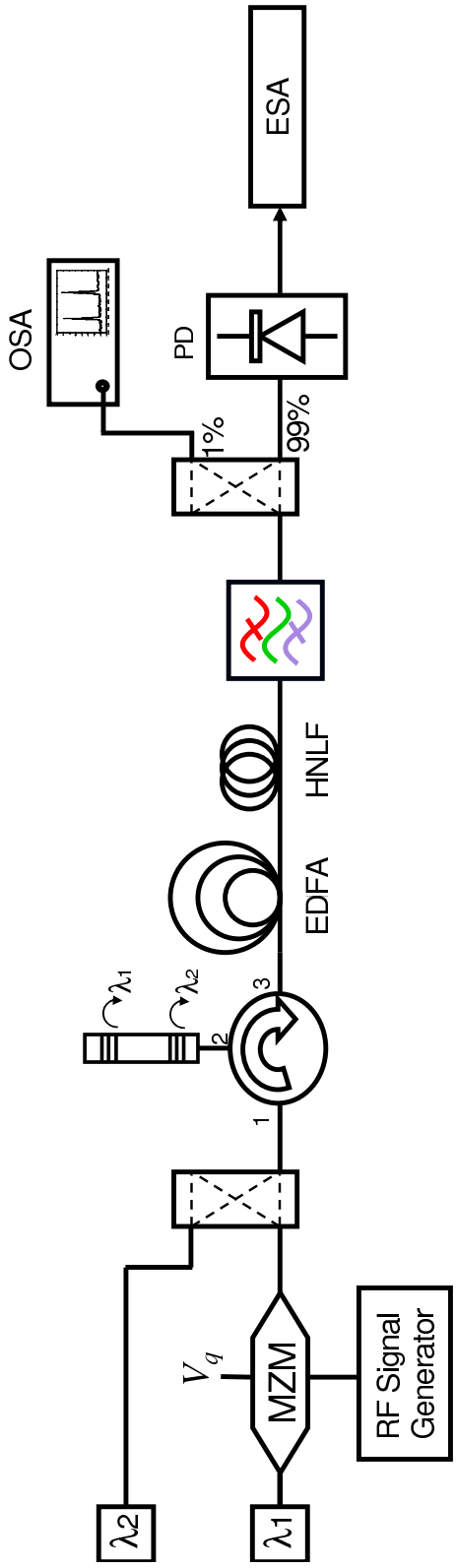

Figure 4.9: Experimental setup for optical mixing characterization.

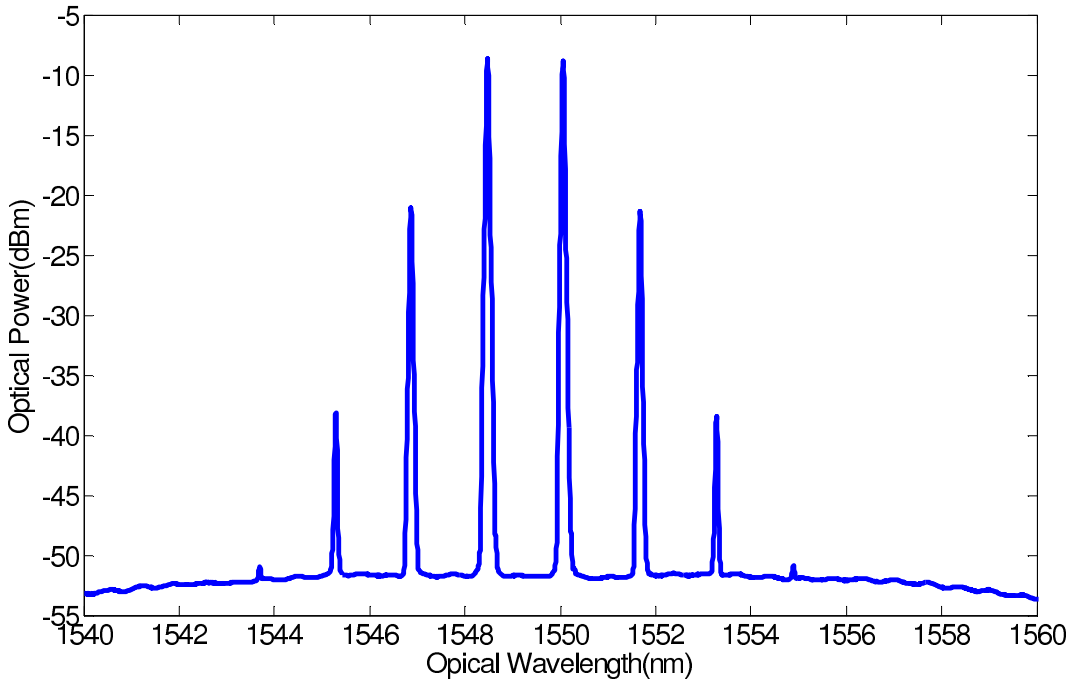

Figure 4.10: Optical spectrum of mixing Channel 5 and Channel 6.

channels had the same power level (20 dBm) to have maximum SNR at the input to the HNLF. The optical spectrum at the output of the HNLF was measured. The mixing efficiency, defined as the power difference between the Four Wave Mixing (FWM) product channels and the pump channels, was calculated from the optical spectrum.

Figure 4.10 presents a typical spectrum at the output of the HNLF when Channel 5 and Channel 6 were used. As it can be seen the non-linearity of the HNLF has resulted in making 3^{rd}, 5^{th} and 7^{th} intermodulation products. Having established that FWM was indeed achieved, the mixing efficiency of this FWM was then analyzed for different channel combinations and the result was shown in Figure 4.11. Only mixing results for adjacent channels are presented since mixing efficiency reduced significantly for larger channel separation due to increase phase mismatch. It is evident from Figure 4.11 that the mixing efficiency was essentially flat throughout the wavelength range between Channel 1 and Channel 8. The most efficient mixing performance was observed between Channels 5 and 6 and thus these channels were selected for frequency response characterization.

Using the setup of Figure 4.9, the lasers were tuned to Channel 5 (1548.51 nm) and Channel 6 (1550.11 nm). The modulator was biased at quadrature and the signal generator output was maintained at 10 dBm throughout the experiment. The lasers were adjusted to provide the same power (20 dBm) at the HNLF input to ensure that the mixing characteristics of Figure 4.11 were attained. The frequency dependence of the photonic link through the system using Channel 5 was measured by turning Laser 2 off and adjusting the optical filter to align with Laser 1.

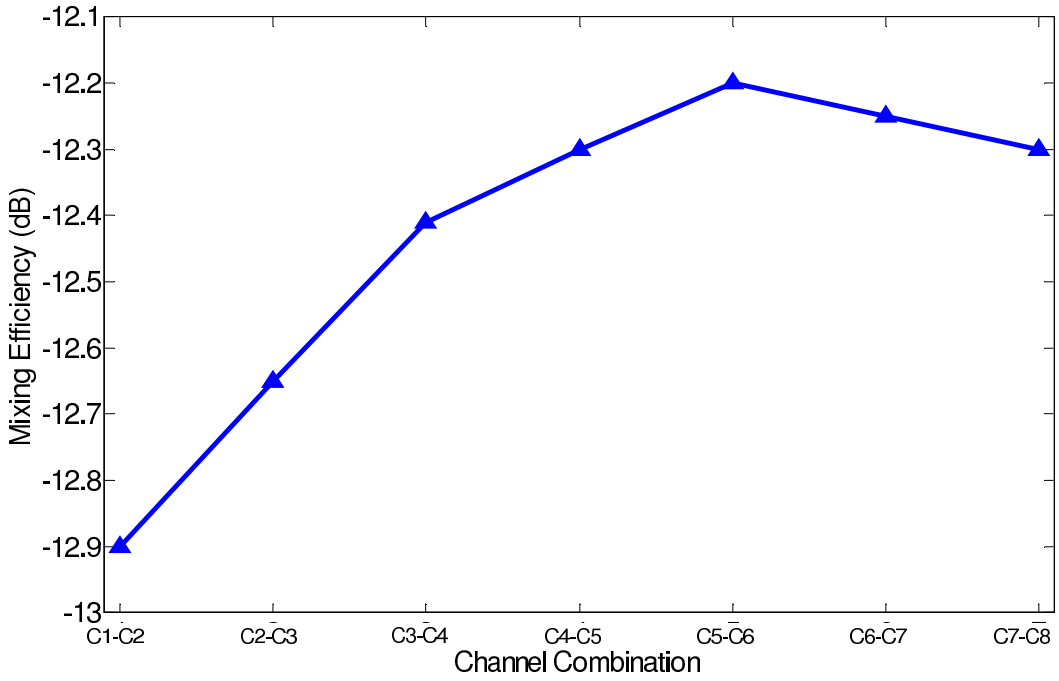

Figure 4.11: Optical mixing efficiency for various channel combinations.

Figure 4.12 presents the measured RF photonic link gain $G(f)$. The predicted link gain is also presented. A link gain of -27 dB gracefully rolling off to -30.5 dB was observed between 2 to 12 GHz. A similar link gain was also observed if Laser 1 was tuned to Channel 6. The frequency response of the optical mixing was obtained by mixing the modulated Channel 5 with the unmodulated Channel 6 and demodulating the selected FWM term of interest. This was achieved using the setup of Figure 4.9 with the optical filter aligned to the selected FWM band. In this case, the filter was tuned to 1546.85 nm (Channel 4) to select the FWM term to the lower wavelength side of Channel 5.

Figure 4.13 presents the measured RF link gain through the FWM term to the left of Channel 5 together with the link gain of Figure 4.12 for easy comparison. The link gain was measured to be -40dB at 2 GHz and reduced to -48dB at 12GHz. It is evident from Figure 4.13 that the FWM link gain roll off was twice as fast as the roll off of photonic link gain $G(f)$. This behavior could be attributed to the combination of Cross-Phase Modulation (XPM) and FWM between Channels 5 and Channel 6 [82].

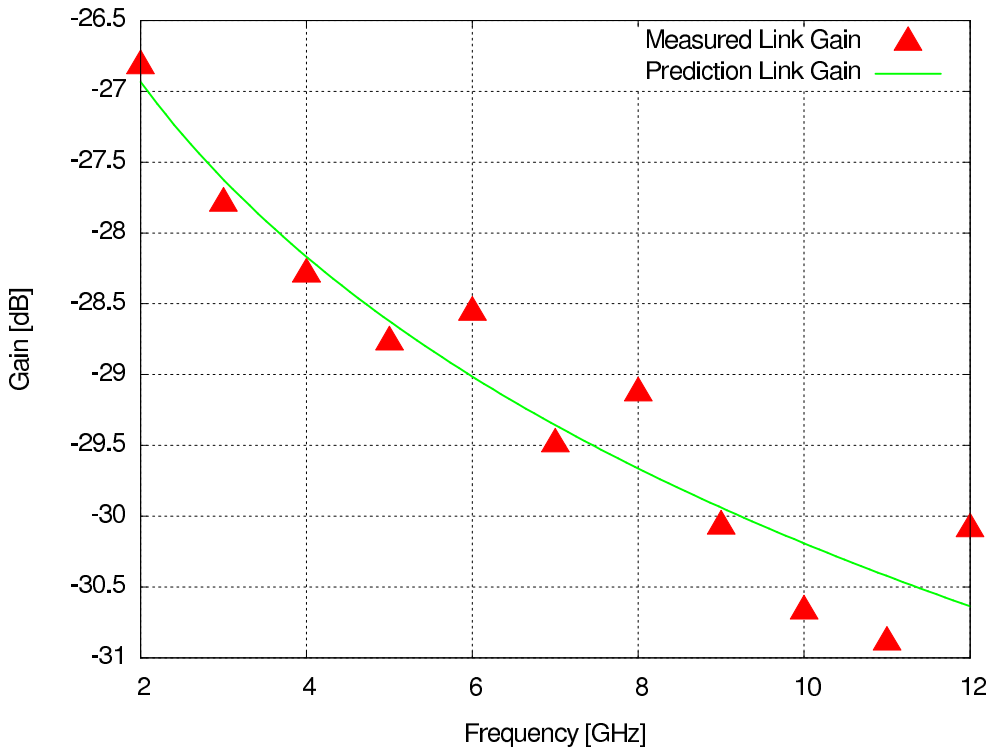

Figure 4.12: Predicted and Measured simple photonic link gain (modulator frequency response $G(f)$).

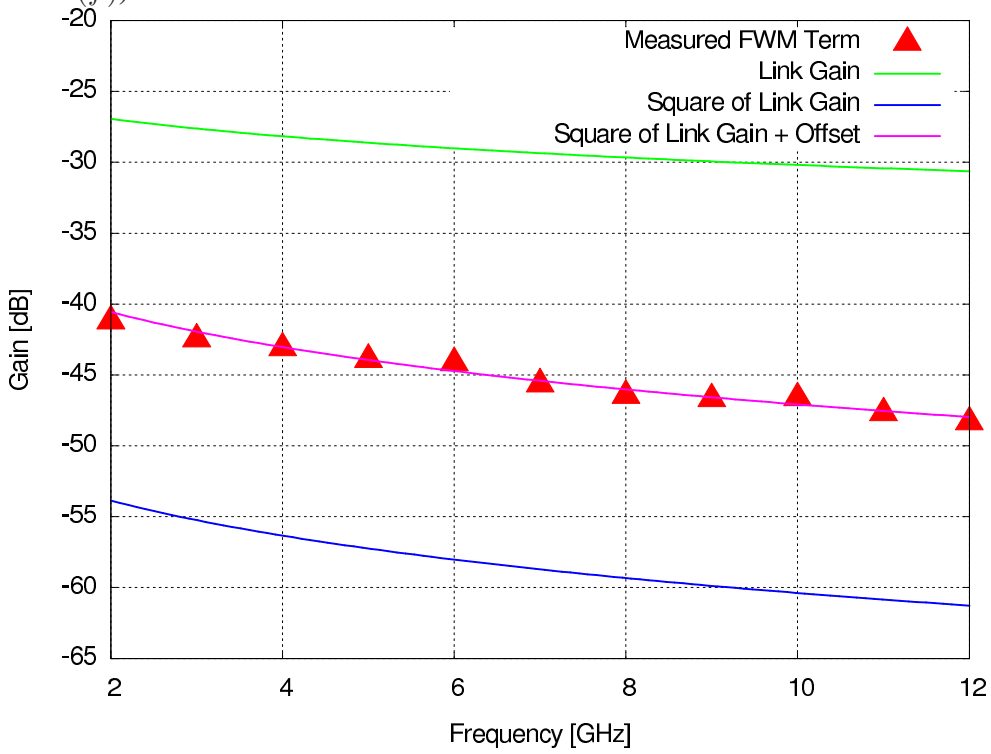

Figure 4.13: Mixing frequency characteristics (predicted and measured) through the first FWM term adjacent to Channel 5 together with the link gain of Figure 4.12 and its square.

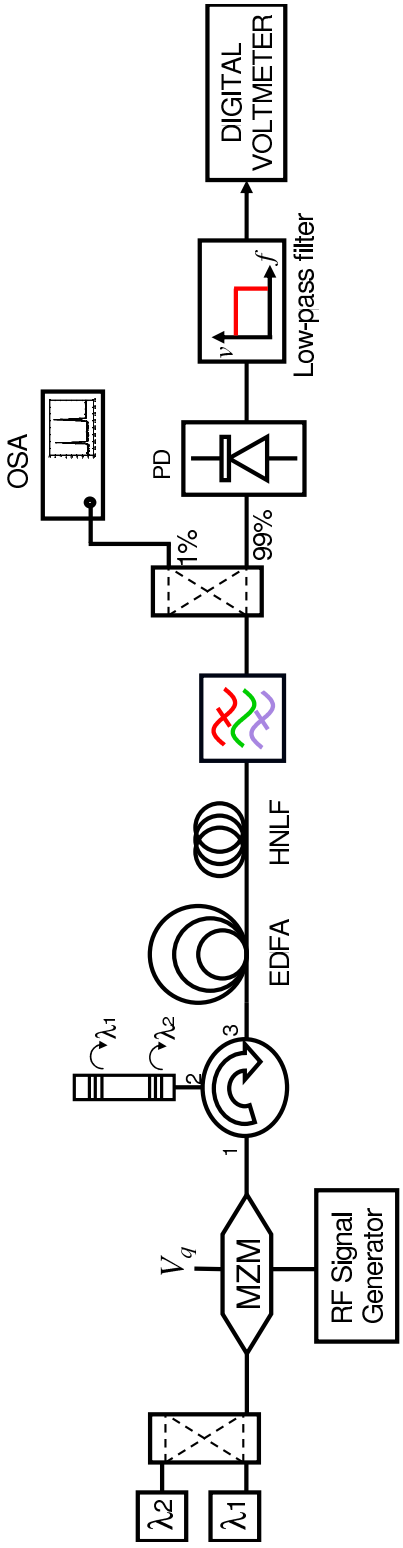

Figure 4.14: Experimental setup for demonstrating the IFM concept using optical mixing in a HNLF.

Photonically Implemented IFM Using HNLF

Having characterized the optical mixing, the photonic IFM could be demonstrated. The experiment setup for the photonic IFM is given in Figure 4.14. Unlike the setup of Figure 4.9, in the IFM setup, both wavelength channels (Channel 5 and Channel 6) were modulated by the same RF signal. The RF signals carried by these channels were delayed by different amounts through a cascaded grating. In particular, Channel 5 has about 40 ps shorter delay than Channel 6. Both channels were amplified by an EDFA to a power level of 20 dBm before being launched into the HNLF. Within the HNLF the two channels were mixed to create several FWM product terms. The RF signal frequency and power were set to 20 GHz, and 0dBm respectively.

Figure 4.15 presents an optical spectrum of the signal emerging from the HNLF after two optical carriers modulated. The mixing products are clearly evident. Unlike a simple RF photonic link with symmetrical sidebands, significant asymmetry between the two sidebands was observed in all optical components. It is hypothesized that complex contributions of FWM, XPM and Self Phase Modulation (SPM) among the spectral components are responsible for this behavior. The optical filter was adjusted to select the spectrum around the 1545.26 nm FWM component. The optical spectrum after the filter is presented in Figure 4.16. This filtered spectrum was detected using a low frequency photo-detector to measure the optical intensity at 1545.26 nm. The photo-detector output was finally obtained with a DC voltmeter.

Figure 4.17 presents the measured output voltage as the frequency of the RF signal varies between 1 to 40 GHz. Also presented in this Figure is the optical mixing transfer function of Figure 4.13 and the predicted IFM response based on Equation (4.7). The output voltage consisted of a constant DC level of approximating 6.7 mV due solely to the carrier mixing of Channel 5 and Channel 6 and a frequency dependent DC part. The value of the frequency dependent DC part was maximum when the RF signals carried by Channel 5 and Channel 6 were in phase (e.g. at low frequency) and minimum when the RF signals were out of phase, (e.g. At 12.5 GHz in Figure 4.17). It can be seen from Figure 4.17 that excellent agreement between the measurement and the prediction has been achieved for RF signal frequencies up to 18 GHz. Beyond 18 GHz, discrepancies between the measurement and the prediction are observed and they are attributed to the roll off the optical filter with a narrow line width of 0.2 nm (approx. 25 GHz). The characteristics oscillating behavior of Equation (4.7) can also be clearly seen in Figure 4.17 from the voltage response with a measured period of 0.5/40 ps=12.5 GHz.

To further demonstrate the characteristics of the IFM given by Equation (4.7), the time delay difference between the two channels was varied. This was achieved by adjusting laser 2 to Channel 7 while leaving laser 1 on Channel 5. The delay difference

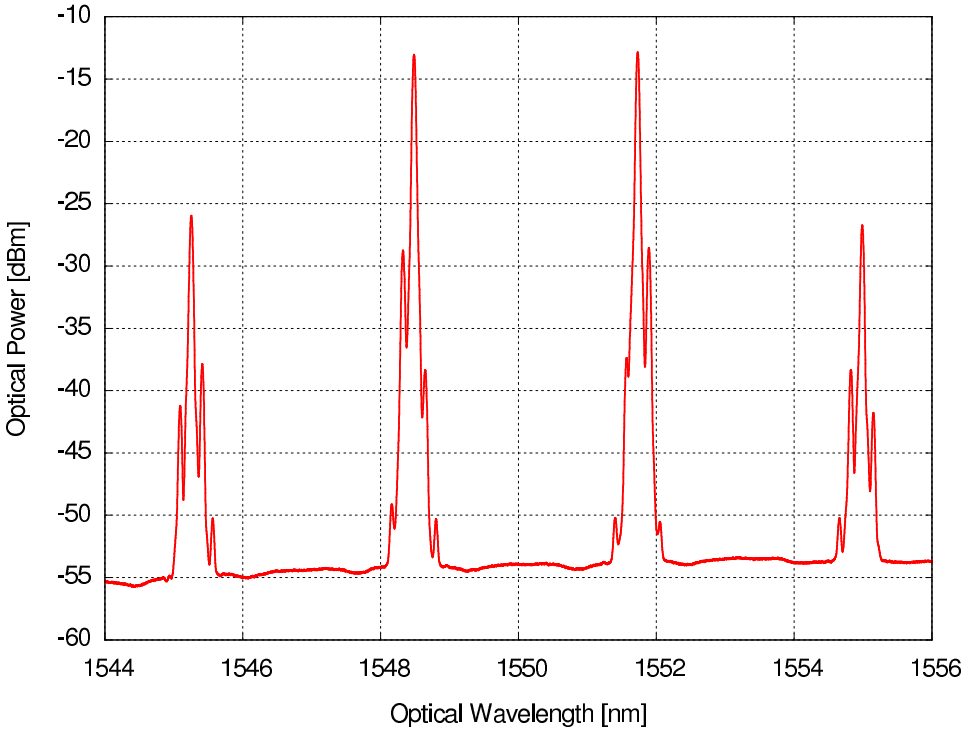

Figure 4.15: Optical spectrum at the output of the HNLF when mixing Channel 5 and Channel 7. RF sidebands of each optical component are clearly visible for RF signal at 40 GHz.

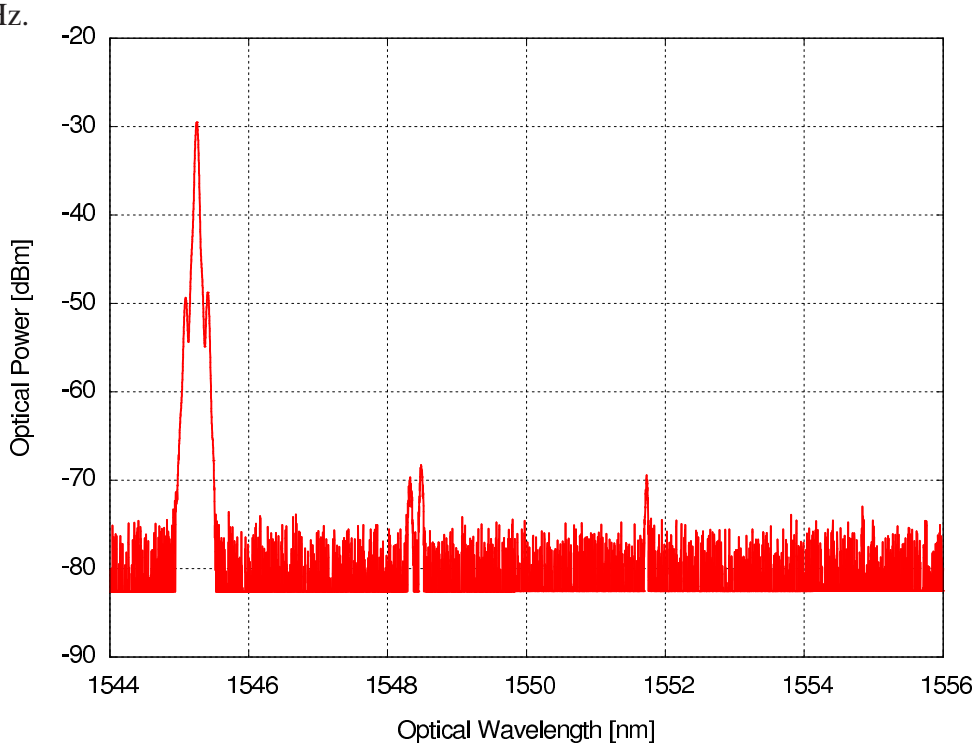

Figure 4.16: Optical spectrum after optical filter of 0.2 nm width centered at 1545.26 nm.

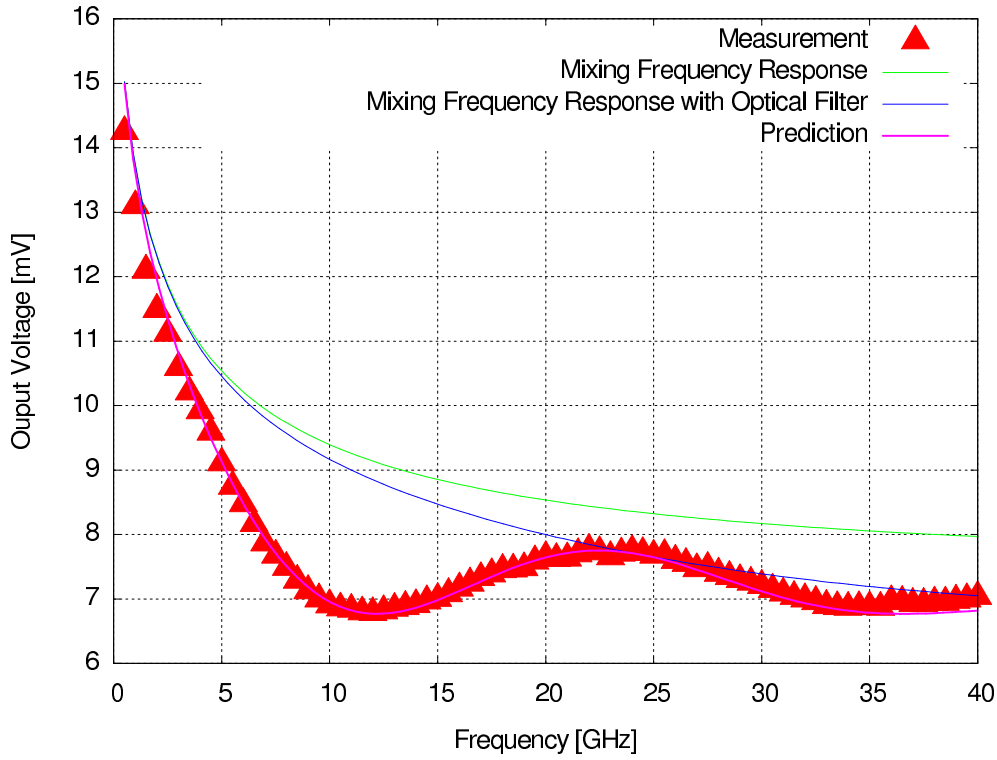

Figure 4.17: Predicted and measured voltage output as a function of the input signal frequency employing optical Channel 5 and Channel 6.

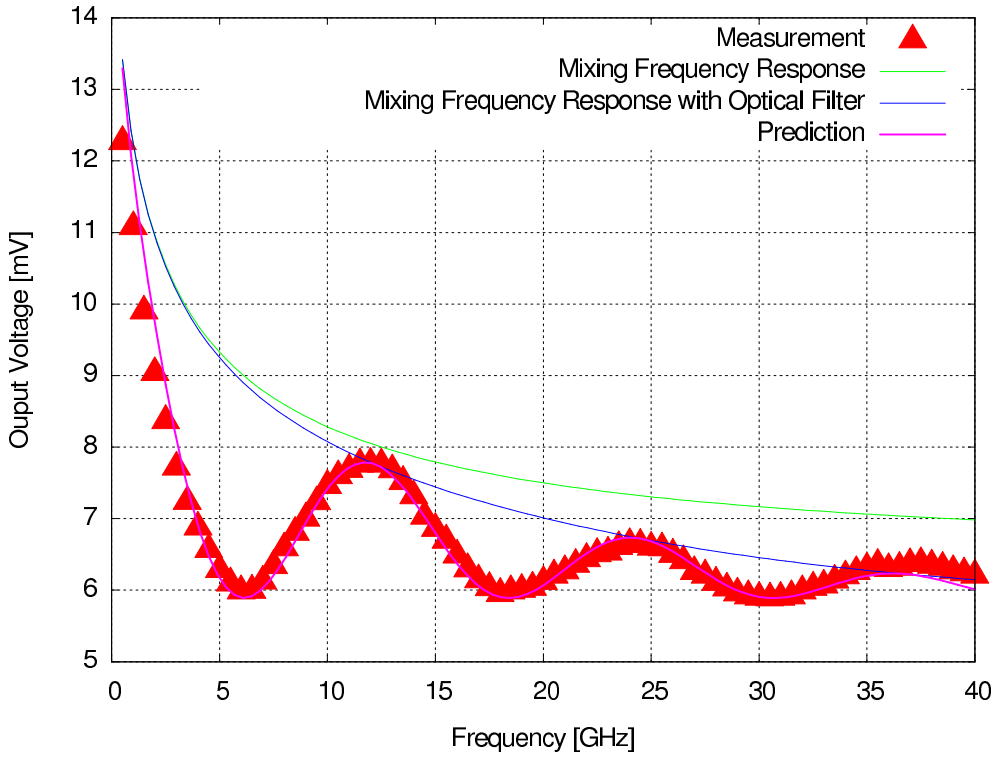

Figure 4.18: Predicted and measured voltage output as a function of the input signal frequency employing optical Channel 5 and Channel 7.

between Channels 5 and Channel 7, produced by the cascaded grating, was 80 ps. The characteristic period of the IFM response was thus predicted to be 6.25 GHz.

The measured response of this later case is presented in Figure 4.18. The optical mixing frequency response and the predicted voltage for this case are also presented. It is evident that the mixing efficiency has slightly reduced due to larger channel separation resulting in a drop in the output voltage. As observed in Figure 4.17 the frequency response of the IFM drops as the square of the simple RF photonic link ($G(f)^2$) It can be seen from Figure 4.18 that excellent agreement between the prediction and measurement was achieved with some deviations for frequency larger than 18 GHz due to the optical filter characteristics.

If the amplitude of the RF signal is known as in this case (10 dBm), the frequency voltage response of Figure 4.14 is fully defined for a given selection of two wavelength channels. This characteristic can thus be employed to map between the measured voltage and the frequency of the RF signal as explained in Section 2. To measure frequency of the RF signal, Equation (4.7) is inverted and then used to map the measured voltage to the predicted frequency.

Figure 4.19 and Figure 4.20 present the measured frequency versus the actual input frequency for cases of Channel 5 and Channel 6 and case of Channel 5 and Channel 7 respectively. In Figure 4.19, there are four distinct bands in which the frequency could be determined without ambiguity. These bands associate with various half cycles of the IFM response of Figure 4.17. In particular, the first band is defined between DC-12.5 GHz, the second band is between 12.5 GHz to 25 GHz, the third band is between 25 and 37.5 GHz and so on. It is evident from Figure 4.19 that excellent measurement accuracy is achieved for the first band. Since the mixing transfer function used for the voltage to frequency mapping does not include the optical filter characteristics, which roll off after ± 12.5 GHz from the carrier, it therefore anticipates that degradation of the measurement accuracy would be observed toward the high frequency end. This is clearly evident in both Figure 4.19 and Figure 4.20.

Having the optical filter response included, the accuracy of the measurement will only be limited by the sensitivity of the voltage meter and by the system noise. Similar to Figure 4.19, Figure 4.20 shows the frequency measurement for Channel 5 and Channel 7. The non ambiguous bandwidth measurement in this case is 6.25 GHz, which divides the frequency range DC-40 GHz to about 7 bands. Excellent accuracy is obtained within the first three bands.

In a summary an instantaneous frequency measurement system based on all optical mixing using HNLF. the system exhibits good stability and a wide frequency measurement range up to 40 GHz.

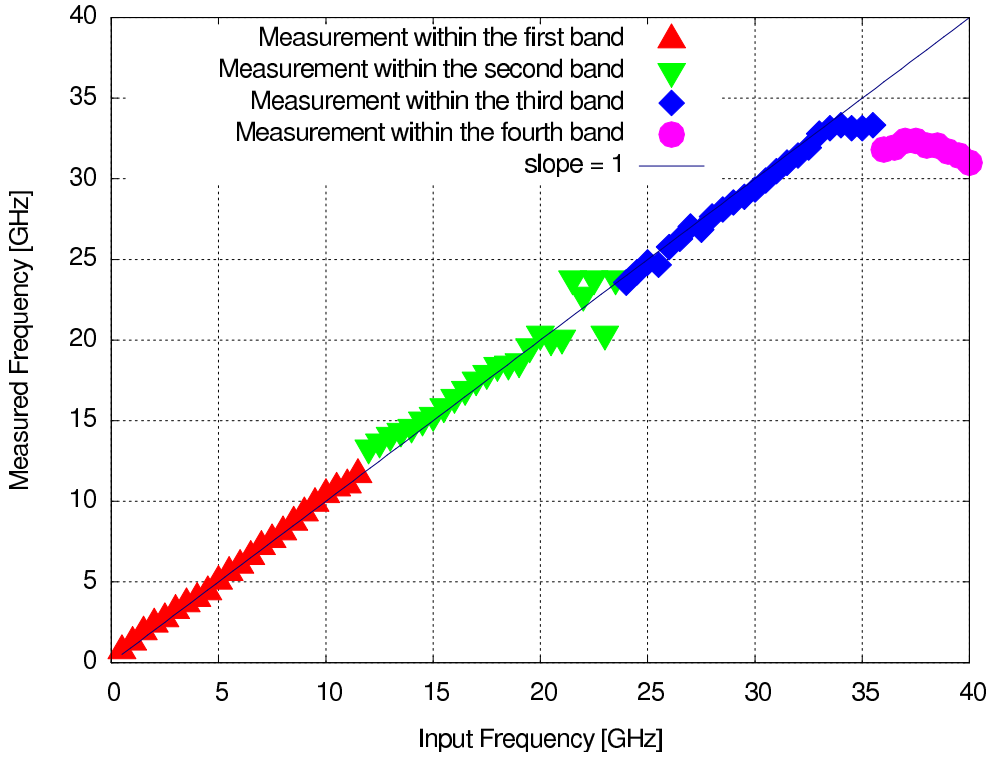

Figure 4.19: Predicted and measured frequency versus the actual signal frequency employing Channel 5 and Channel 6.

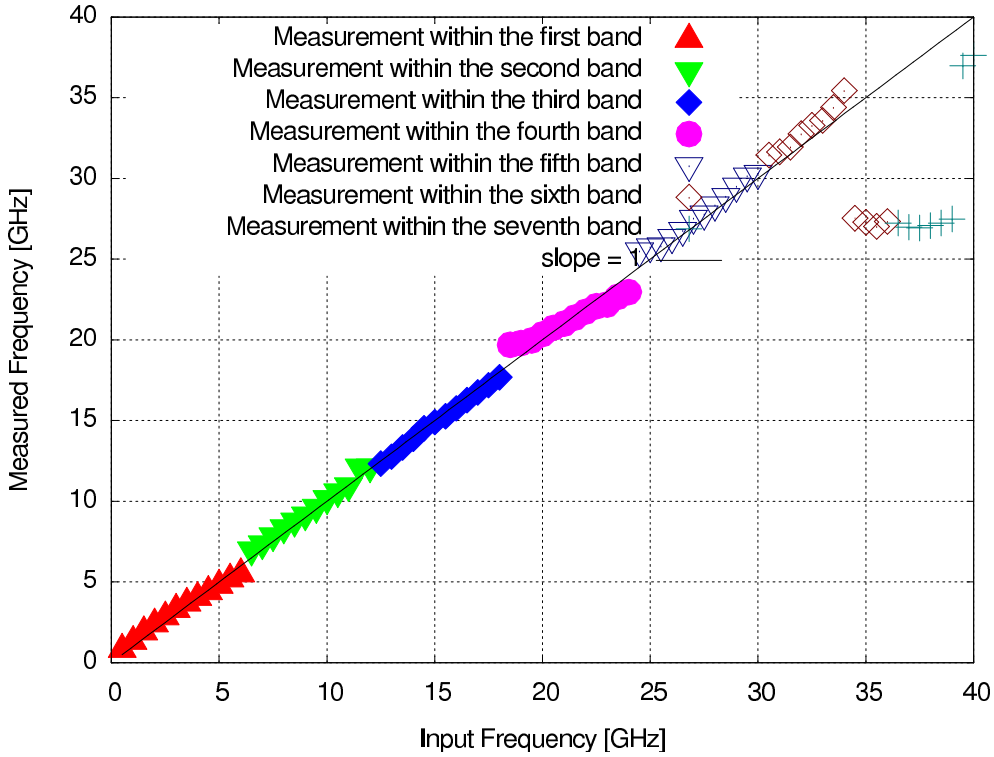

Figure 4.20: Predicted and measured frequency versus the actual signal frequency employing Channel 5 and Channel 7.

4.5 Conclusion

The need to have all optical mixing has arisen in Chapter 2. In this Chapter a new technique based on all optical mixing was introduced to remove the need for the co-axial cable required to compensate the optical length. Semiconductor Optical Amplifier (SOA) was then introduced as a non-linear device. The SOA was then characterized and employed to achieve all optical mixing. A frequency measurement range of 20 GHz was achieved. However, the instable and even oscillating nature of SOA may limit the performance of the IFM system. Also since SOAs produce ASE noise, the sensitivity of such a system may degrade. Highly Non-Linear Fiber (HNLF), was then introduced as an alternative. Being a passive device, HNLF exhibit a better stability comparing with SOA. The HNLF was firstly characterized. The SOA was then replaced by an HNLF. The all optical mixing based on HNLF was then conceived and demonstrated. A 40 GHz frequency measurement range was achieved. It would be imaginable to employ the photonic hybrid concept into the new all optical mixing IFM to achieve orthogonal measurement. It could be shown that an arbitrary numbers of IFM systems, could be implemented using only one nonlinear device (SOA or HNLF). Since in the practical RADAR warning receivers, a bank of IFM systems is required, this would reduce the cost of the whole system.

In summary, by using the microwave-photonic a wideband microwave-photonic IFM system needless of any co-axial cable was conceived and demonstrated practically. This system could provide a broader frequency measurement range comparing with the IFM system of Chapter 2.

Chapter 5

Improved Sensitivity Photonic Measurement Instantaneous Frequency Measurement (IFM) System

5.1 Introduction

In an electronic warfare environment, the RADAR signals received from distant threads could be very low power. Therefore a RADAR warning receiver must have the highest sensitivity possible to be able to detect signals from enemy's RADAR with the largest possible range. To detect very faint signals it is essential that the noise of the detection system is minimized. There has been comprehensive research to increase the Signal to Noise Ratio (SNR) of RF systems including, but not limited, to employing high gain Low Noise Amplifiers (LNAs) at the front-end to improve the total Noise Figure (NF) of the receiver as well as employing high gain antennas to maximize the signal, and using Locked Loop techniques to eliminate noise and other interferences.

In practical electronic warfare applications the photonic IFM system discussed in Chapters 2 and 3 must thus have a sufficient sensitivity to enable comparison with traditional IFM receivers. In low signal environments in order to maximize the sensitivity, noise reduction techniques must be employed to reduce noise of the system.

This Chapter, investigate the sensitivity of the implemented photonic IFM of Chapters 2 and 3.

For clarity, the operation of proof of concept IFM receiver is characterized in terms of sensitivity in Section 5.2. Lock-in amplification technique is utilized to improve the sensitivity of the system in Section 5.3. The sensitivity improvement photonic IFM proof of concept demonstration is shown in Section 5.4. Section 5.5 proposes and demonstrates

a high frequency version of this sensitivity improved photonic IFM system. Section 5.6 investigates the sensitivity improved of the Orthogonal photonic IFM which was implemented in Chapter 3. Section 2.6 draws conclusions on the practicality of the proposed sensitivity improved photonic IFM system. The findings of this Chapter have been published in [72, 88–90].

5.2 Sensitivity of Original Photonic IFM Receiver

Having implemented a low-cost photonic IFM system in the Chapter 2, it is worth investigating the limitation of the sensitivity of the IFM system. To do this investigation, firstly the IFM system of Chapter 2 must be characterized in terms of sensitivity. In this Section the sensitivity of the system is quantified. To do this, the IFM system was characterized in terms of sensitivity. Several measurements were conducted to perform this characterization. In the practical use; however these multiple measurements would not be required and only one measurement would be sufficient to identify the frequency.

Qualitative Sensitivity observation

To establish the sensitivity of the IFM system demonstrated in Section 2.4, sequential measurements of the frequency response were taken with diminishing input RF powers (P_{RF} to be 10dBm, 1dBm and -5dBm). It is predicted from Equation 2.50 that once the RF power is reduced below a certain threshold it will be difficult to be measure due to the presence of the frequency independent offset. This effect will limit the sensitivity of the IFM system.

Figure 5.1 shows the frequency response of the IFM system with input RF powers of 10dBm, 1dBm and -5dBm. In Figure 5.1, at P_{RF} = 10dBm, the sinusoidal transfer function is clearly evident and the amplitude of the variations is a significant proportion of the observed DC offset. At P_{RF} = 1dBm the sinusoidal response is still observable, but the amplitude is significantly reduced. Conversely, the frequency invariant DC offset remains almost unchanged with the reduced RF input power. Reducing the power to P_{RF} = -5dBm resulted in attenuation of the amplitude of the sinusoidal transfer function to the scale of the noise on the DC offset. As it can be seen the sensitivity of the IFM system of Figure 2.4 is not below -5dBm. To gain more insight to the sensitivity problem, a quantitative observation should thus be conducted.

Quantitative Sensitivity Observation

To better illustrate the noise floor behavior, the amplitude of the output was measured as a function of the input RF power. The output signal amplitude was defined as the voltage difference between the first peak and the first null in the oscillating response as illustrated in Figure 5.1. Measurements were taken for input RF powers ranging from 10dBm to -50dBm in 3dB increments. It is clear that the system without lock-in amplification can only achieve a sensitivity of -5dBm.

Figure 5.2 shows the amplitude of the output as a function of the RF input power for the original system of Figure 2.8. A sensitivity of only -5dBm was achieved.

At this power it is no longer possible to measure frequency with this system. Recall that the role of an IFM system in a RADAR warning receiver is to provide early indication of possible threats in an electronic warfare environment. The ability to see distant threats is vital and hence the sensitivity of an IFM system is extremely important.

It has been established that the sensitivity of the experiment of Figure 2.8 is between -5dBm and 1dBm. This poor level of sensitivity would be unacceptable in practical applications. It is thus necessary to explore methods for enhancing the sensitivity of this IFM system if it is to be seriously considered for RADAR warning receiver applications.

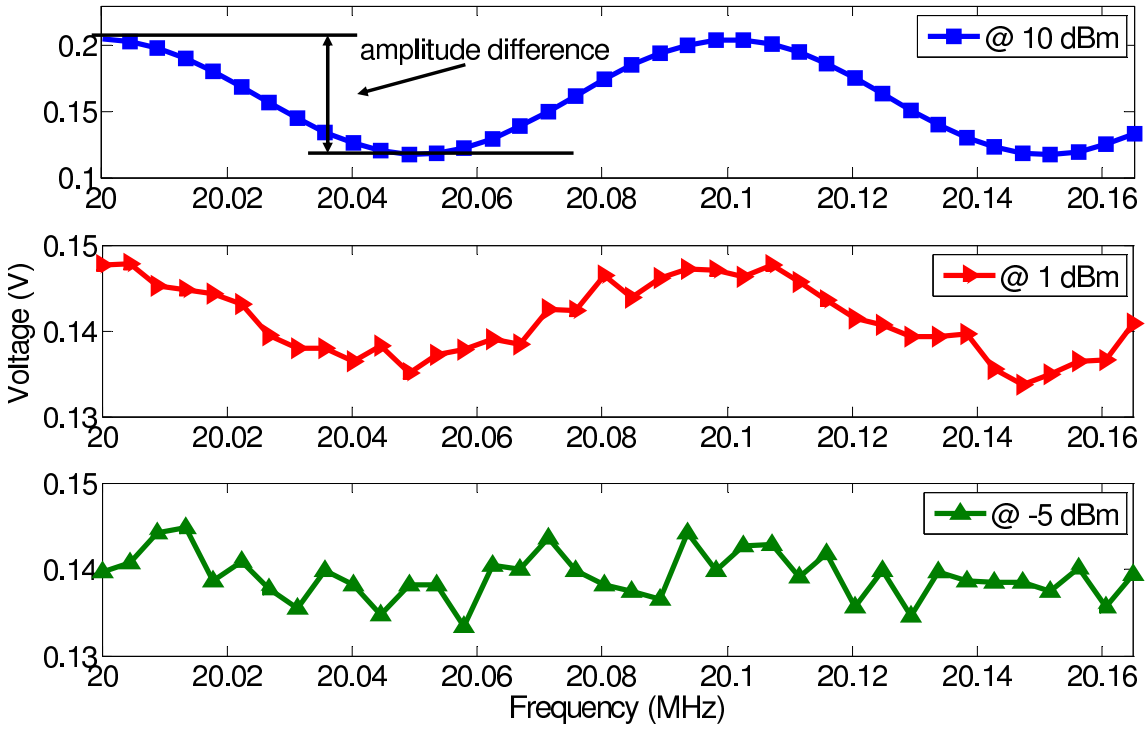

Figure 5.1: Output voltage of original IFM system as a function of frequency. RF input powers of 10dBm, 1dBm and -5dBm.

5.3 Lock-in Amplification

A lock-in amplifier (also known as a phase-sensitive detector) is a type of amplifier which amplifies only the desired portion of a signal and reject interfering components. At the receiver, a signal which is to be measured may be accompanied by strong interference as shown in Figure 5.4 a). The lock-in concept is to modulate only the desired signal component with a reference tone (Figure 5.4 b)). The modulated signal goes to a mixer which is fed by a phase shifted version of the reference tone. This mixing transfers the interference to f_{circ} while transferring the originally modulated signal back to DC. A low-pass filter then isolates the DC signal and it is amplified.

As a result at the output of the mixer there is a DC component which is proportion to the desired signal to be measured (Figure 5.4 c)). This DC component will be isolated from the other harmonics by a low-pass filter. This way as any interference (undesired components which has accompanied the desired signal), are not modulated, at the output of the system, they will not be detected and hence will be rejected. Signal to Noise ratio (SNR) improvement using lock-in amplification can be as low as -60 dB or even less [91].

Having presented a qualitative description of the lock-in amplifier, a mathematical

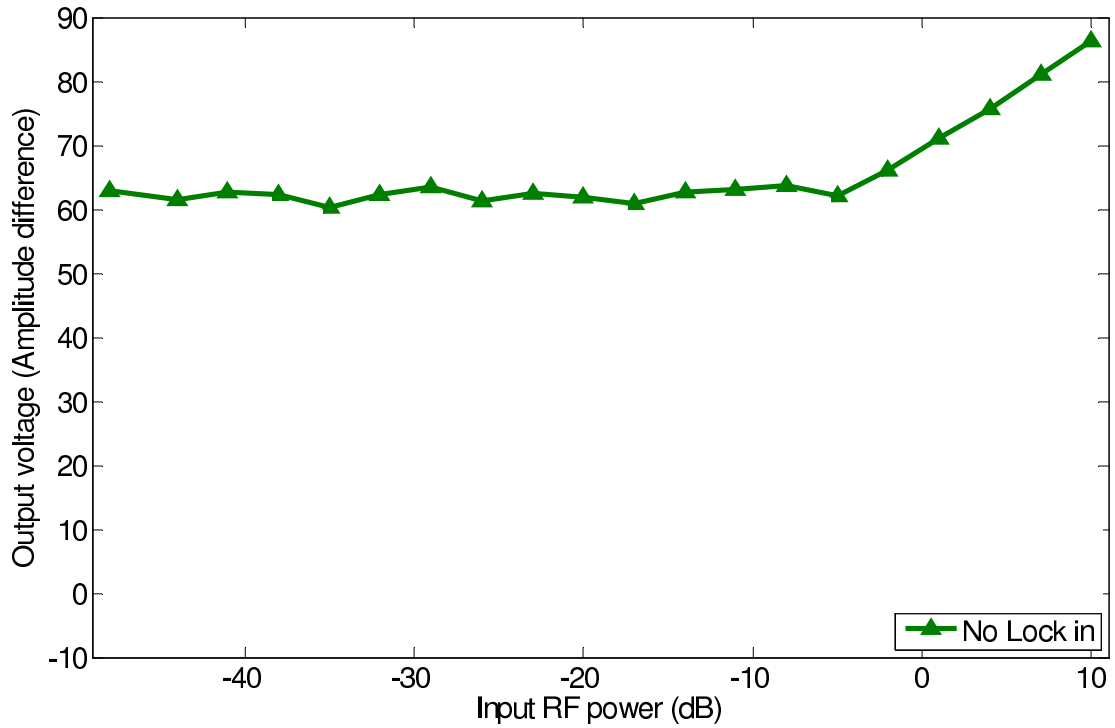

Figure 5.2: Amplitude difference of the output for RF input powers of 10dBm, 1dBm and -5dBm.

Figure 5.3: Lock-in amplifier

model is developed to give the reader a better understanding of lock-in amplification.

Consider the voltage to be measured is A which is accompanied by an interference of B. Modulating only the desired voltage to be measured, the modulated outcome can be written as:

$$v(t) = A(1 + \cos \Omega t) + B \tag{5.1}$$

This signal is then amplified and mixed with the shifted reference tone of :

$$v_{ref}(t) = C(\cos \Omega t + \Theta) \tag{5.2}$$

where Θ is a user-adjustable phase-shift introduced within the lock-in amplifier.

The output will thus be:

$$v_{out}(t) = C[A(1 + \cos \Omega t) + B](\cos \Omega t + \Theta) \tag{5.3}$$

Using trigonometric relation, Equation (5.3) can then be expanded as:

$$v_{out}(t) = C(A + B)\cos(\Omega t + \Theta) + \frac{CA}{2}\cos(2\Omega t + \Theta) + \frac{CA}{2} cos\Theta. \tag{5.4}$$

After low-pass filtering, the DC component of v_{out}, is:

$$V_{DC} = \frac{CA}{2} cos\Theta \tag{5.5}$$

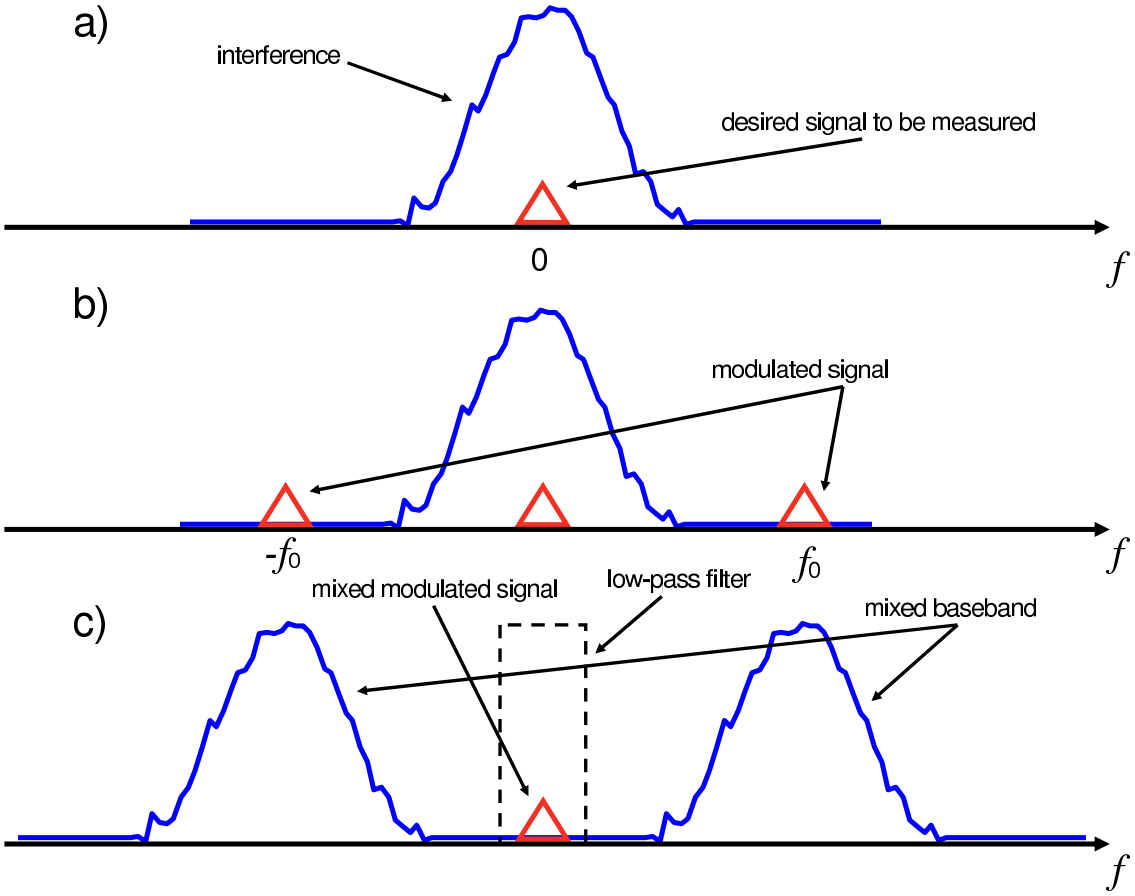

Figure 5.4: Lock-in amplifier concept

Rearranging Equation 5.5:

$$V_{DC} = \frac{C}{2} cos\Theta \times A \tag{5.6}$$

As it can be seen, at the output, there is no term including B, therefore the interference is vanished. The gain of the system can also be calculated as:

$$G = \frac{C}{2} cos\Theta \tag{5.7}$$

As stated in Section 5.1 one of the solutions to reduce the noise is lock-in technique. Attempts have been done to reduce the noise of the photonic link by using lock-in technique.

Lock-in technique has been widely used in several applications needing accurate measurement of interfered or noisy signals such as SNR and dynamic range enhancement in highly noised photothermal experiments, adaptive power line interference extraction, detecting very weak inhomogeneities in materials that are not possible to detect with conventional techniques when coupled to a photothermal detection system, measurements of

nanosecond fluorescence lifetimes, nano indentation and contact stiffness measurement, radio astronomy, measuring photon lifetime and true reflectance in an optical cavity, measuring hydrostatic pressure on membrane processes, transverse surface acoustic wave detection, thin film using scanning probe microscope [92–100].

5.4 Sensitivity Improved Photonic IFM Proof of Concept Demonstration

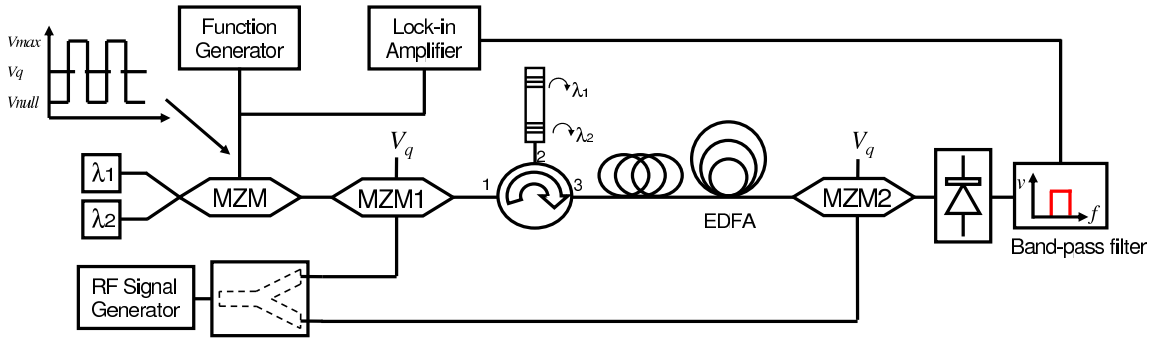

Figure 5.5: Experimental setup of the photonic IFM with lock-in amplifier.

The poor sensitivity shown in Section 5.2, (Figure 5.2) has been attributed to the strong frequency invariant DC component predicted by Equation (2.50) which quickly dominates the output response as the input RF signal amplitude is reduced. If this frequency invariant component could be rejected by the receiver, then a far more sensitive measurement should result. Lock-in amplification is a excellent candidate for rejection of this DC offset.

5.4.1 Lock-In Amplifier Technique

As discussed in Section 5.3 to efficiently use lock-in amplification it is important that the modulated perturbation modifies only the components of the output that are of interest while leaving the background interference unchanged. For the IFM system of Figure 2.8 the quantity to be measured is the RF frequency and this is done by relating the phase accumulated by a fixed time delay τ to the signal frequency. Thus, to effectively use lock-in amplification, this differential time difference must be modulated with a dithering tone. Equation (2.50) shows that perturbing τ will only change the desired frequency dependant component of the output leaving the frequency independent components unaltered. Having established that it is the time delay τ that must be modulated it is now possible to conceive a system that will enable modulation of this delay with sufficient amplitude and

frequency to enable lock-in amplification.

5.4.2 System Implementation

In order to achieve lock-in amplification, the delay τ must be modulated at a rate above a few hundred Hz to avoid interference/noise sources such as 50 Hz AC background and its harmonics. The modulation must also have sufficient amplitude so that the phase change imparted by the varying delay can be observed interferometrically. This means that the physical change in path length must be of the order of 1% of a wavelength at the lowest frequency to be measured. In the case of the experiment of Figure 2.8 the nominal frequency is 20 MHz and so the physical change in length must be a significant fraction of one meter. One might consider electro or thermo-optic phase modulation or even fiber stretching as a means of perturbing the path length [101]; however, these approaches will be insufficient to achieve the large changes in delay required for this investigation. Instead, a physical switching between two paths must be used to achieve the required modulation.

5.4.3 System Setup

Figure 5.5 shows the proposed block diagram of the IFM system. Two optical carriers (λ_1, λ_2) were provided by a laser array. These wavelengths were switched using the first modulator (MZM1), which was biased by a square wave with amplitude of $V_q = \frac{V_\pi}{2}$ and DC offset of $\frac{V_\pi}{2}$. In this way, the output of MZM1 switched from λ_1 to λ_2 with each clock cycle. The same voltage signal was also used to feed the lock-in amplifier. The output of the MZM1 was then mixed with the RF signal using the MZM2 (biased at V_q). The modulated signal was delayed using a cascaded grating which provided different delays for λ_1 and λ_2. The delayed signal was again modulated with MZM2, and detected. A long length of optical fiber (2.3 km) then provided the bulk differential delay of the interferometer. The output of the photo-detector was connected to the lock-in amplifier. Using two different wavelengths, different delays resulting in different output voltages were achieved. It was this difference in output voltage which was measured by the lock-in amplifier.

5.4.4 System Demonstration

Similar to Section 5.2, a qualitative demonstration is first conducted to investigate any possible noise floor improvement. After observing quantitative improvement a quantitative investigation was conducted.

Qualitative Demonstration

The system was setup as shown in Figure 5.5. The optical wavelengths were set to λ_1=1550 ,λ_2=1551.5nm. The laser diode powers were set to P_1=11.7 and P_2=11.75 mW. The RF input power was adjusted sequentially to values of -20dBm, -32dBm and -35dBm.

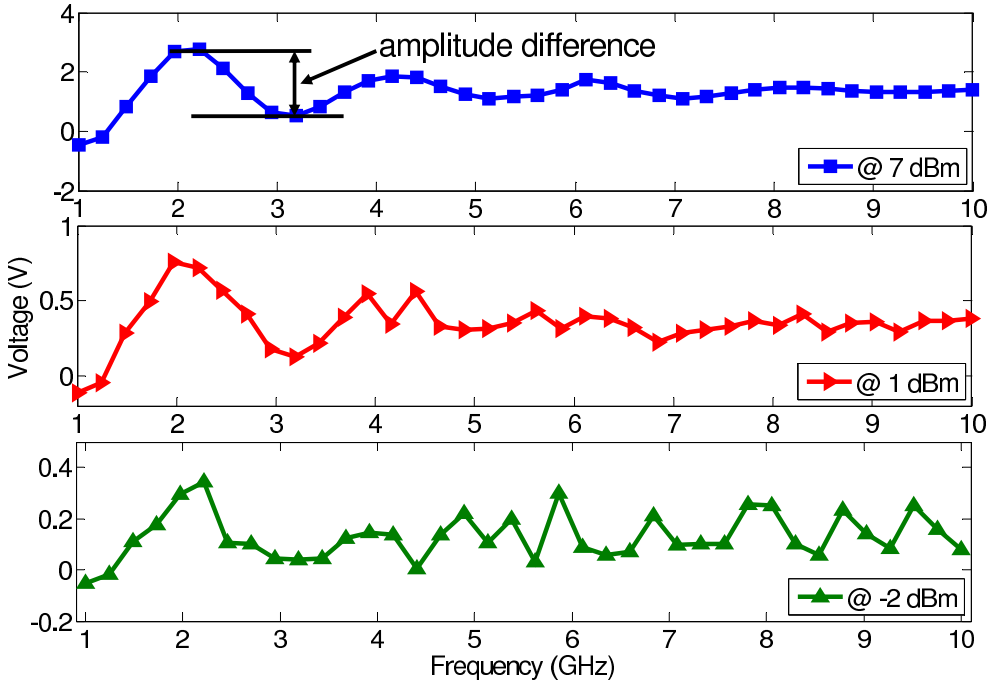

Figure 5.6: Output voltage of Lock-In amplifier (MZM used as switch). RF input powers of -20dBm, -32dBm and -35dBm.

Figure 5.6 presents the frequency response of the system of Figure 5.5 measured for RF input powers of -20dBm, -32dBm and -35dBm. Comparing to Figure 5.1 it is evident that the sensitivity has been improved dramatically. The amplitude of the frequency varying component of the response still dominates even at -20dBm input power. Reducing the input power to -32dBm it is still possible to observe the frequency varying response. At -35dBm, the response has been lost in the noise floor of the system.

It is worth noting that the response still maintains a frequency invariant DC offset which appears to be proportional to RF input power. This is as expected from Equation (2.50).

Quantitative Demonstration

To quantify the noise floor performance, the amplitude of the output was measured as a function of the RF input power. The output signal amplitude was defined as the voltage difference between the first peak and the first null in the oscillating response as illustrated

in Figure 5.6. Measurements were taken for input RF powers ranging from 10dBm to -50dBm in 3dB increments.

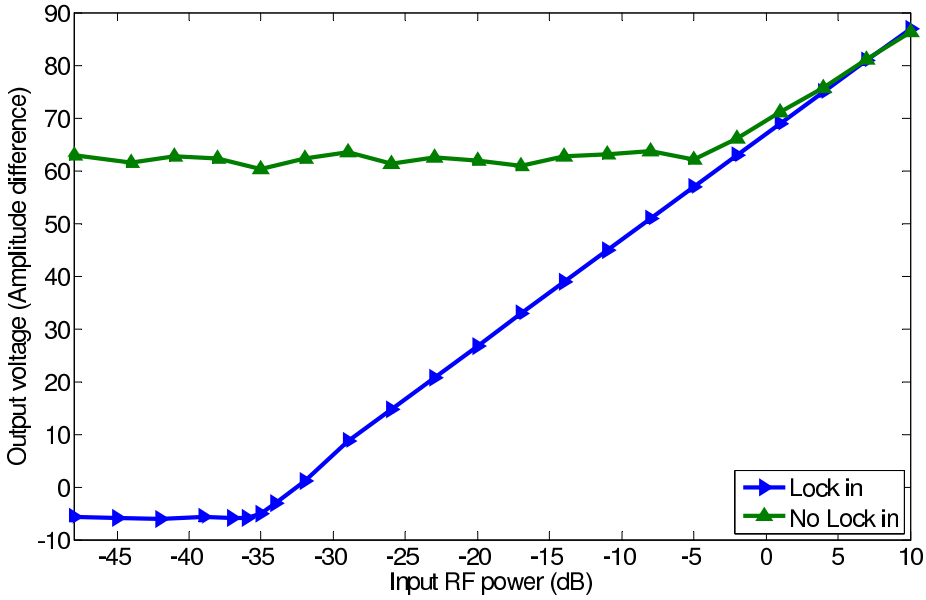

Figure 5.7: Amplitude difference of the output for different RF input powers.

Figure 5.7 shows the amplitude of the output as a function of the RF input power for the original system of Figure 2.8 and the improved sensitivity system of Figure 5.5 using MZM as the optical switch. From Figure 5.7 it is clear that the system without lock-in amplification can only achieve sensitivity of -5dBm, while the locked system can achieve sensitivity of -35dBm. This confirms the estimated noise floor of -35dBm observed in Section 5.4.4.

5.4.5 Summary

A proof of concept sensitivity improved microwave photonic IFM system was proposed and practically demonstrated. A sensitivity of -35dBm has been achieved. Note that this sensitivity is linearly related to the optical power of the laser diodes as Equation (2.50) suggested. The next Section will explore how a high frequency (GHz) sensitivity improved frequency measurement can be achieved [88].

5.5 High Frequency Sensitivity Improved IFM System Demonstration

Having established a method to increase the sensitivity of the original, low frequency photonic IFM system, it is now possible to demonstrate an improved sensitivity IFM

system operating at GHz frequencies.

5.5.1 Noise Floor Observation

To determine the sensitivity of the previously demonstrated system of Figure 2.12, sequential measurements of the frequency response were taken with diminishing input RF powers. Figure 5.8 presents the frequency response of the system with input RF powers of 7dBm, 1dBm and -2dBm. The oscillating response is clearly evident at 7dBm, but becomes unmeasurable at -2dBm. As noted in Section 5.2, this poor sensitivity would be unacceptable for a practical system.

5.5.2 System Implementation

Figure 5.9 shows the experimental setup of the sensitivity enhanced high frequency photonic IFM system. Similar to Section 5.4.2, an RF signal generator produced a single tone. This was split into two equal portions using a Wilkinson power divider. The first portion fed an MZM (MZM1), which was biased at quadrature. Two optical carriers were provided by two laser diodes with wavelengths of λ_1 and λ_2. An optical switch was used to select between two optical carriers, with ideally only one carrier present at the modulator at any time. The output of the MZM1 traversed to the Port 1 of a polarization maintaining optical circulator. Port 2 of the optical circulator was connected to a cascaded grating.

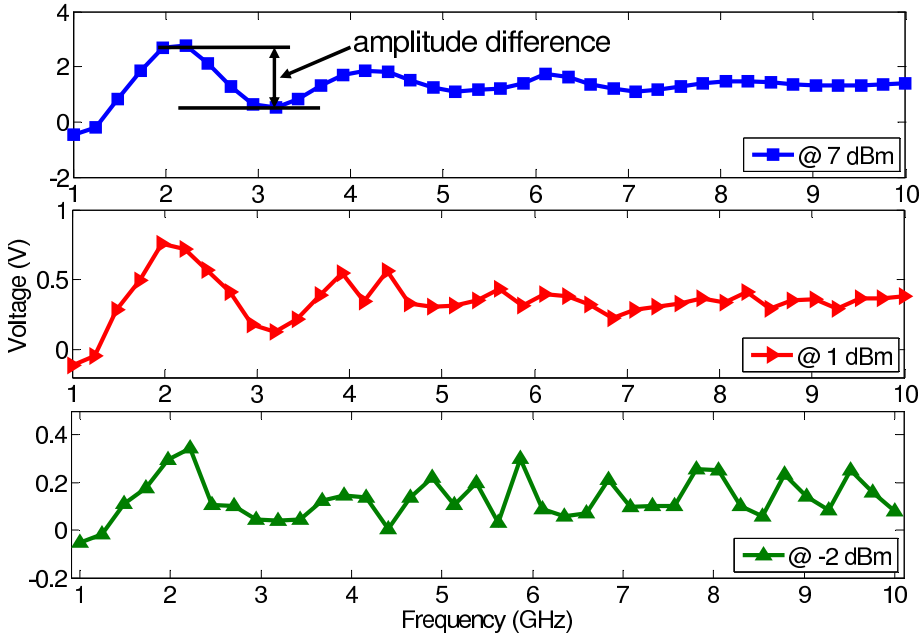

Figure 5.8: Output voltage of high frequency IFM system as a function of frequency. RF input powers of 7dBm, 1dBm and -2dBm.

The cascaded grating provided different delays for different optical carriers λ_1 and λ_2. The reflected signal was output from Port 3 of the optical circulator. unlike Figure 5.5 no excess delay was introduced. The signal was input to the MZM2 directly, where it was modulated a second time. The RF feed for MZM2 was delayed using a co-axial cable to achieve desired differential delay. The output was then low pass filtered and measured by a lock-in amplifier. A dithering tone was applied to the optical switch and this was supplied as a reference to the lock-in amplifier. By carefully adjusting the optical powers for each wavelength such that the optical power received at the output was the same for both wavelengths, it was possible to isolate only the intensity variations that occur as a result of the path length change caused by the cascaded grating. In this way, only the interferometric component of the system output was amplified.

5.5.3 System Demonstration - MZM switch

The system was setup as shown in Figure 5.9. The optical wavelength of the laser diodes were set to λ_1 = 1550, and λ_2 = 1551.5 nm. The laser powers were carefully adjusted to P_1 = 11.7 and P_2 = 11.75 mW respectively to ensure that the power incident on the photo-detector was identical for both wavelengths. The difference in input power can be attributed to varying loss of the cascaded grating. As in Section 5.4, a 2×1 MZM was used as an optical switch. The dithering signal provided by the function generator was a square wave which controlled the MZM bias as shown in the inset of Figure 5.9. The DC offset of the square wave was adjusted to the quadrature voltage of the 2×1 MZM, and the amplitude of the squarewave was set to the quadrature voltage so that switching from peak to null was achieved. The response of the system of Figure 5.9 was measured for RF input powers of -20dBm, -26dBm and -31dBm.

The measured frequency response of the system for several input powers is shown in Figure 5.10. It is evident that the DC offset has reduced dramatically with output voltages measured in mV compared to V in Figure 5.8. The minimum signal level that can be measured has also been significantly improved with measurements at -20dBm input power showing great clarity and loss of measurement certainty only being observed at -31dBm input power. To illustrate the noise floor performance more clearly, the amplitude of the output was measured as a function of the input RF power.

As in Section 5.2, the output signal amplitude was again defined as the voltage difference between the first peak and the first null in the oscillating response as illustrated in Figure 5.11. Measurements were taken for input RF powers ranging from 10dBm to -50dBm in 3dB increments.

Figure 5.11 shows the amplitude of the output as a function of the RF input power

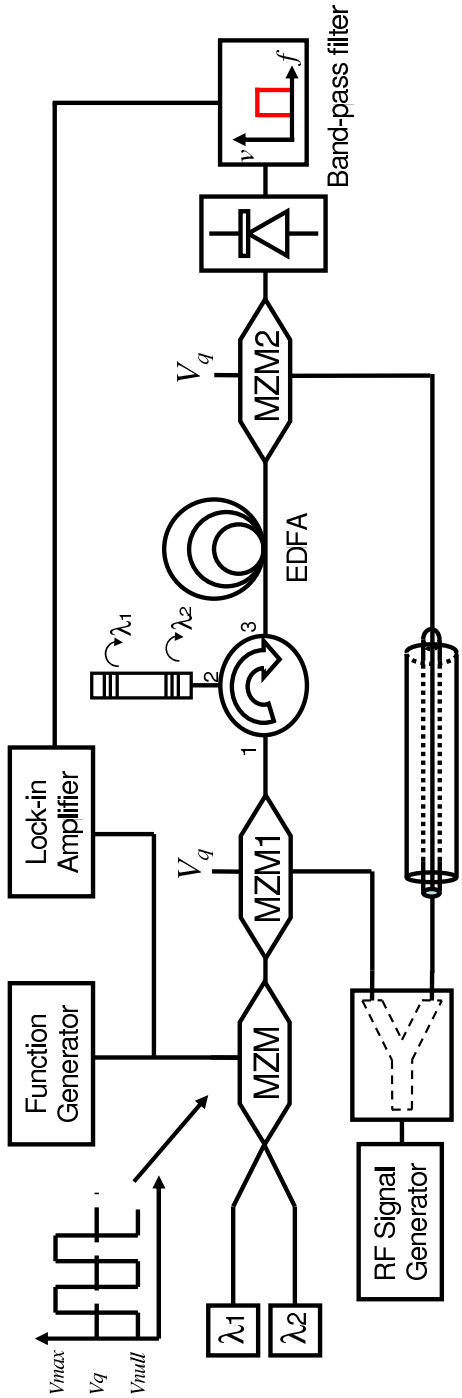

Figure 5.9: Experimental setup of the reduced noise IFM system (MZM as switch).

for the original system of Figure 2.12 and the improved sensitivity system of Figure 5.9 using an MZM as the optical switch. From Figure 5.11 it is clear that the system without lock-in amplification can only achieve sensitivity of -2dBm, while the locked system can achieve sensitivity of -32dBm.

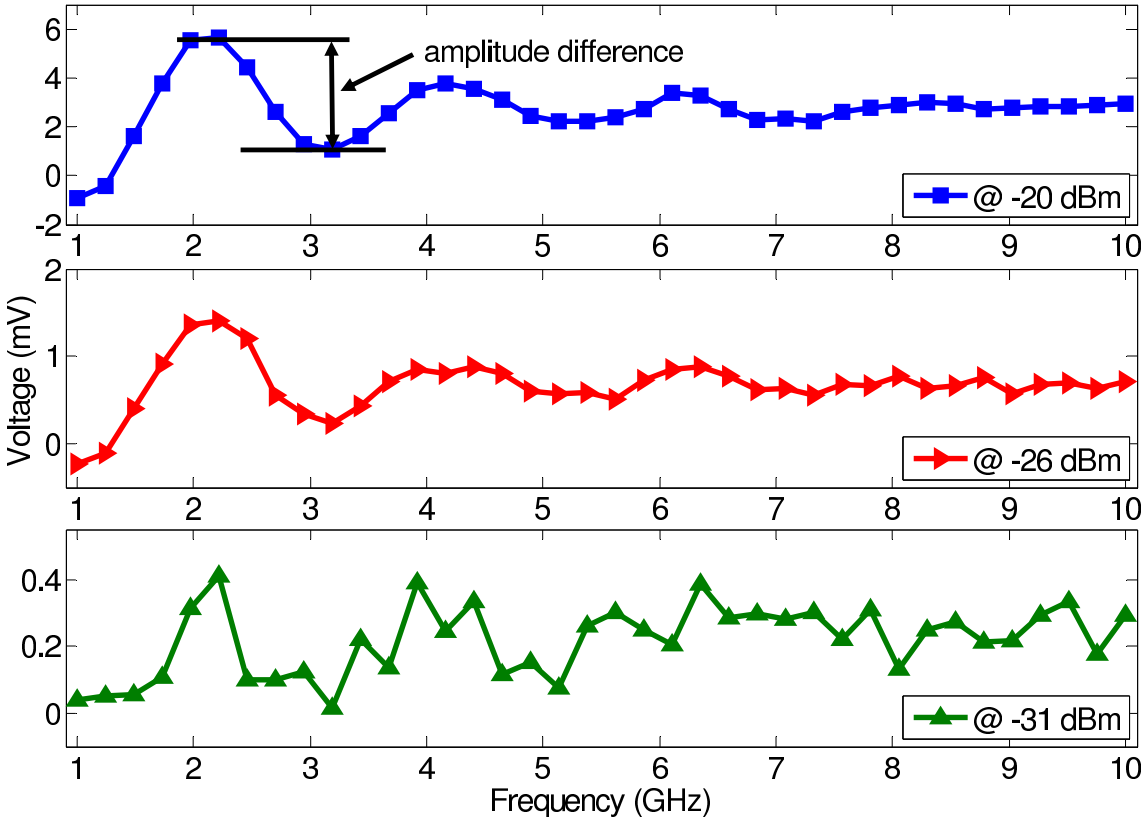

Figure 5.10: Output voltage of lock-in amplifier (MZM used as switch). RF input powers of -20dBm, -26dBm and -31dBm.

5.5.4 Discussion

A sensitivity of -32dBm has been achieved when using MZM as an optical switch in the IFM system of Figure 5.9 while this sensitivity is respectable, it is unlikely that it is a lower limit. It is hypothesized that the finite extinction ratio of the MZM switch (nominally -20dB) and imperfect biasing may limit the sensitivity of the IFM system. This imperfect extinction means that there will always be a portion of both wavelengths at the output and this in turn limits the extent to which the invariant background signal can be cancelled.

Figure 5.12 illustrates the difference between the ideal and non-Ideal switching. To explore whether the finite extinction of the MZM switch could limit the sensitivity, in the next Section the MZM switch will be replaced with a mechanical switch.

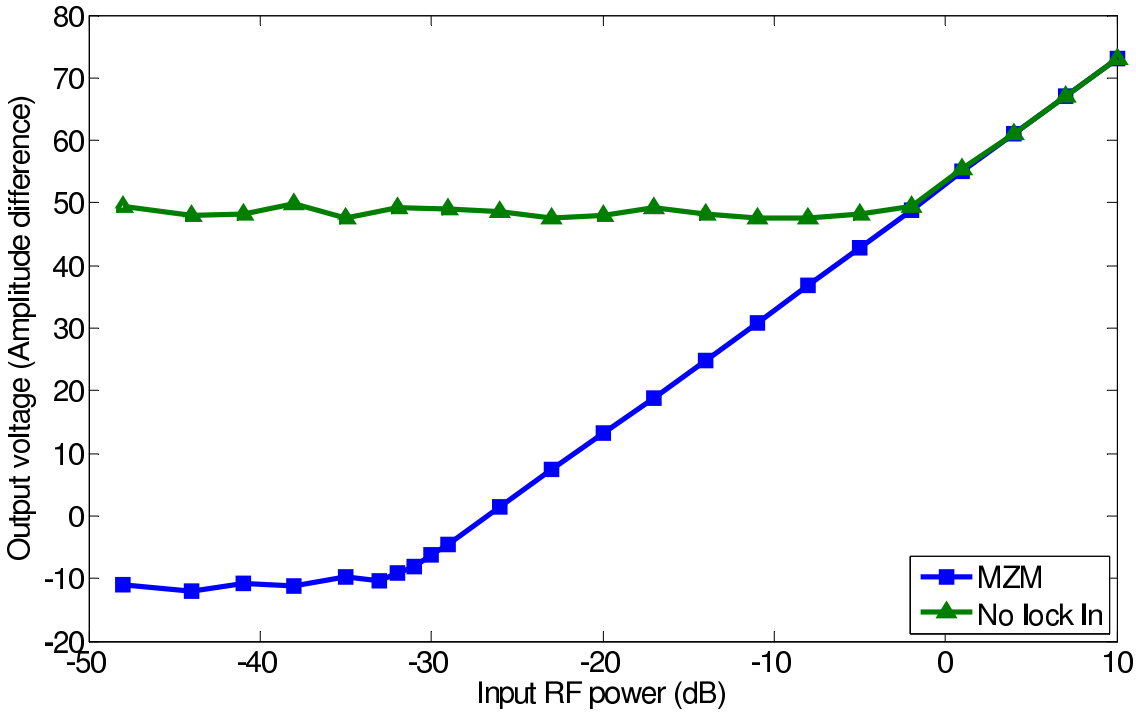

Figure 5.11: Amplitude difference of the the output for different RF input powers.

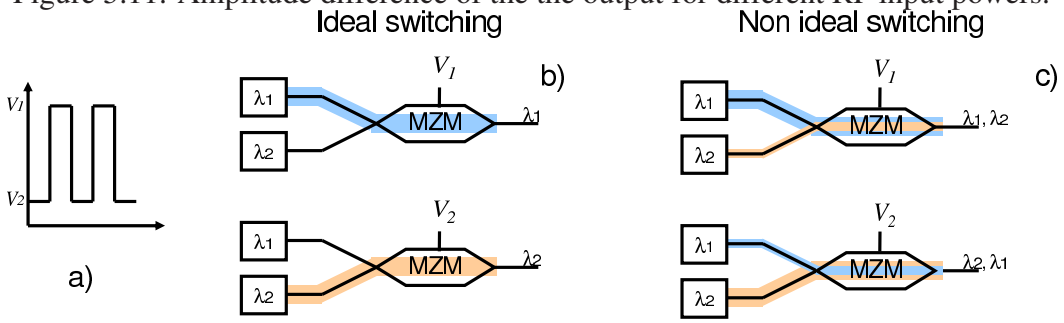

Figure 5.12: Difference between the Ideal and Non-ideal switching.

5.5.5 System Demonstration - Mechanical Chopper

As discussed in Section 5.5.4, the non ideal extinction ration of the 2×1 MZM may place a limit on the effectiveness of the lock-in amplifier. To test this, the 2×1 MZM was replaced by a more ideal switch (Mechanical Chopper).

A mechanical chopper (Figure 5.13) was used to allow only one of the two wavelengths through at a time. The two optical paths were aligned carefully to the apertures of the chopper such that only one path was passed at any time. In this manner the dithering frequency corresponded to the frequency of oscillation between these two paths resulting in only one wavelength present at all time in the input of MZM1. After passing through the chopper the free space optical signal was collected and refocused into separate optical

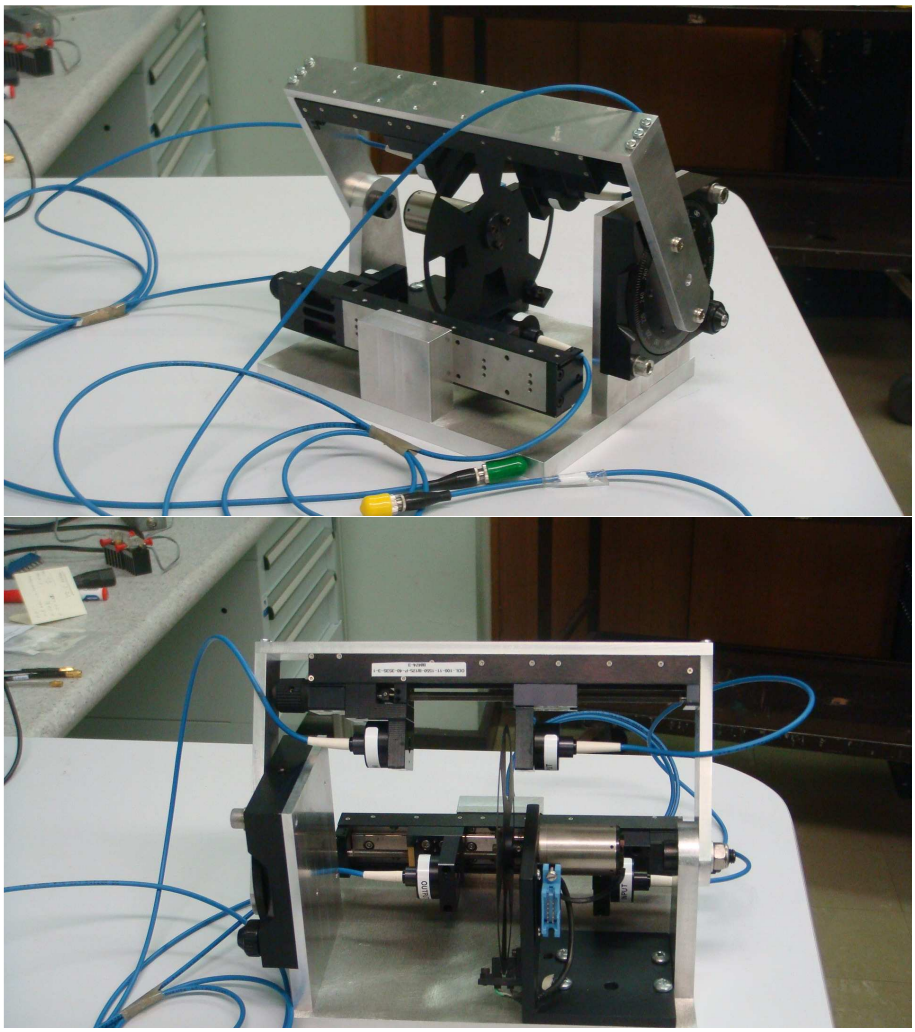

Figure 5.13: Mechanical Chopper

fibers. The experiment of Figure 5.9 was then repeated but this time with the mechanical chopper as a switch as shown in Figure Figure 5.14 . The laser powers were again fine tuned to achieve the same optical power level at the input of the photo-detector for both switching states.

The measurements were repeated over the same frequency range (1-10 GHz). The RF input power was again varied from +10dBm to -50dBm and the output signal amplitude was recorded.

The results for the chopper switched system are presented in Figure 5.15. It can be seen that the system sensitivity has been improved to -41dBm. The observation of Figure 5.15 implies that increasing the switching extinction has indeed improved the sensitivity. This sensitivity is competitive with existing electronic IFM implementations [32].

Figure 5.16 shows the amplitude difference of the output voltage as a function of the RF input power for the original system of Figure 2.12, the improved sensitivity system of

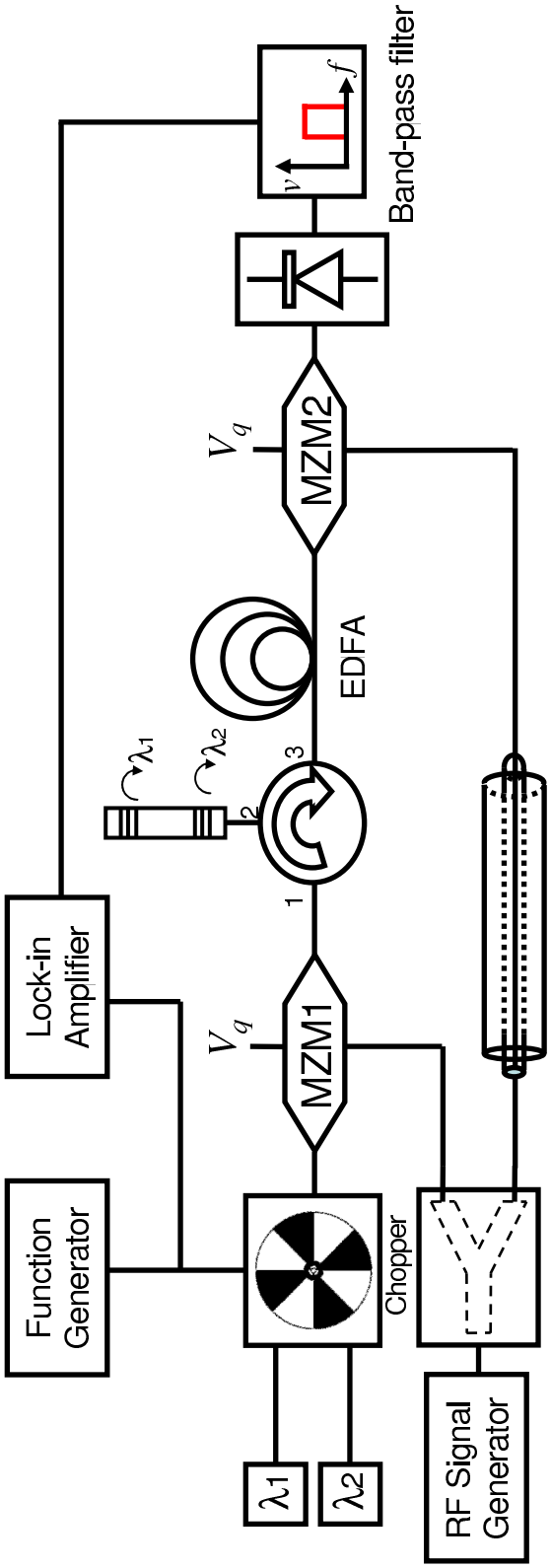

Figure 5.14: Experimental setup of the reduced noise IFM system (Chopper as switch).

Figure 5.9 using MZM as the optical switch and the improved sensitivity of Figure 5.9 using chopper as a switch. Figure 5.16 clearly shows that the system with lock-in amplification and using chopper as a switch has the best sensitivity. This confirms the observations of Figure 5.8 and Figure 5.16. A sensitivity of -41dBm was achieved.

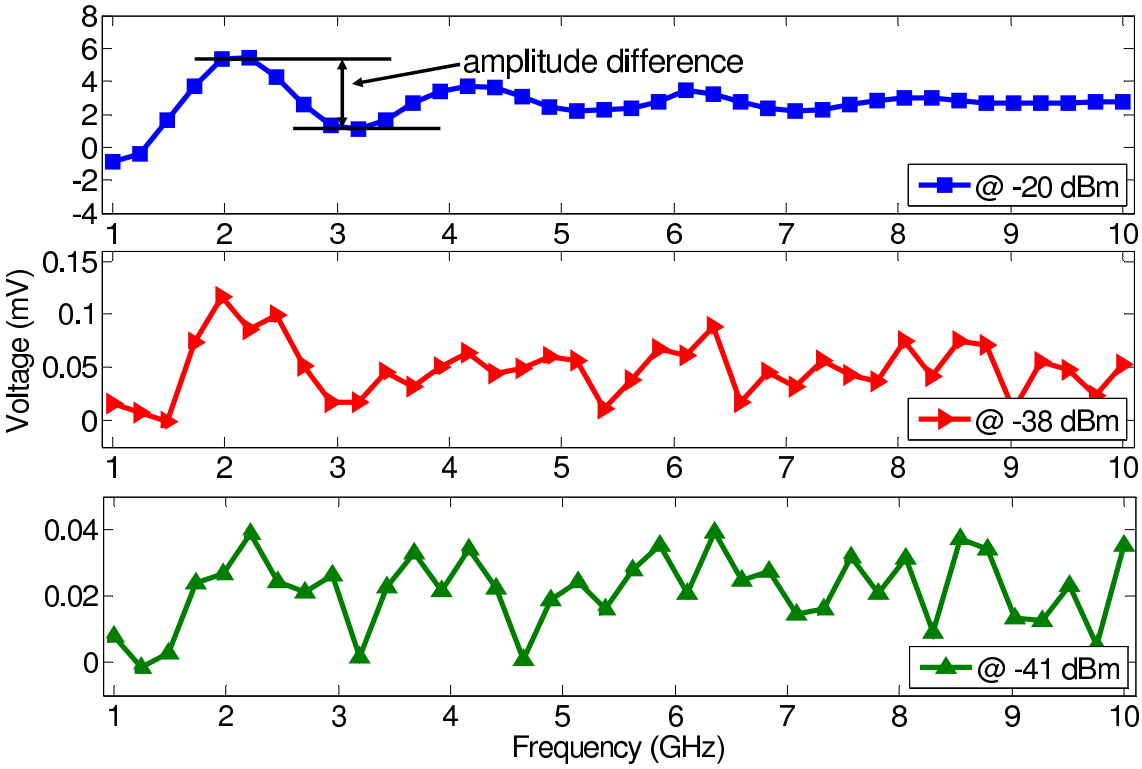

Figure 5.15: Output voltage of lock-in amplifier (used chopper as switch). RF input powers of -20dBm, -26dBm and -31dBm.

5.5.6 Summary

A sensitivity improved microwave photonic IFM system was proposed and practically demonstrated with a sensitivity of -41dBm being achieved for measurements up to 10 GHz. This is competitive with traditional electronic IFM systems. There is scope to extend the frequency range of this IFM into the millimeter range using all optical mixing as demonstrated in Chapter 4. It is conceivable that the sensitivity enhancement techniques demonstrated in this Chapter could be applied to this all optical system creating a very attractive photonic IFM system.

The achieved sensitivity of -41dBm could be attributed to the noise made by the laser diode (RIN noise) and by the photo-detector (shot noise). There is also a thermal noise coming from MZMs which usually has a lower level compared with the other noise sources. It is also observed that the noise floors of the low frequency and high frequency

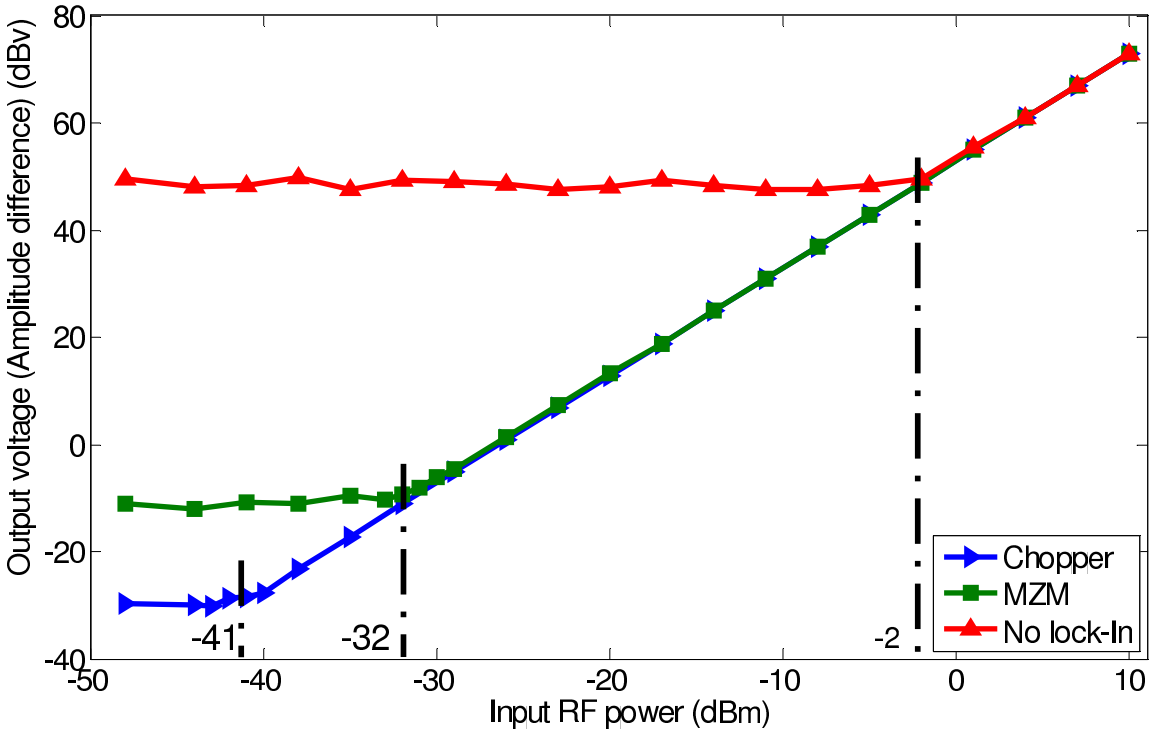

Figure 5.16: Amplitude difference of the the output for different RF input powers.

systems were similar which implies that the bandwidth of the system does not affect the noise floor. This could be due to absence of any RF filter inside the system which removes bandwidth dependence of the noise floor.

A lock-in approach has introduced some complexity to the system. This raises the questions to whether this approach could be practically applied to the orthogonal IFM system or not.

5.6 Orthogonal Instantaneous Frequency Measurement Sensitivity Improved

The aim of this Section is to reduce the noise floor hence, improve the sensitivity of the orthogonal measurement IFM system of Chapter 3. Since more than one wavelength were used in the orthogonal measurement IFM system, switching between all of these optical wavelengths maybe impractical. Therefore a dithering scheme must developed before being applied to the orthogonal IFM system.

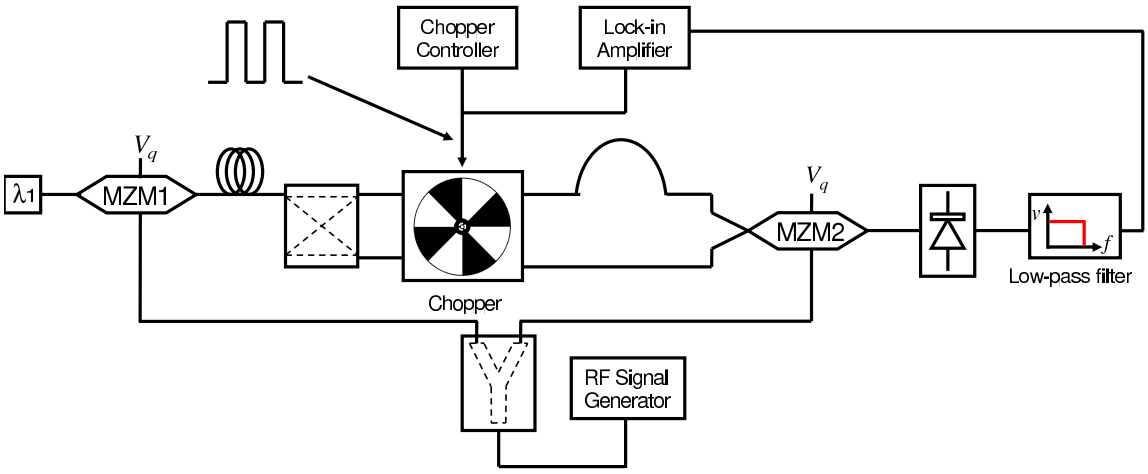

Figure 5.17: Experimental setup of the sensitivity enhanced IFM system.

5.6.1 Dithering the physical length

Since the orthogonal measurement IFM system employs three wavelengths employing the wavelength switching method could be challenging. In this Section a dithering scheme is developed based on switching between physical length. Since no wavelength switching is employed, this system should be able to be employed to reduce the noise floor of the orthogonal measurement IFM system. Figure 5.17 shows the experimental setup of the sensitivity enhanced photonic IFM system. An RF signal generator produced a single tone. This was split into two equal portions using a Wilkinson power divider. The first portion fed an MZM (MZM1), which was biased at quadrature. An optical carrier was provided by a laser diode with wavelength of λ_1. The modulated signal traversed through an optical fiber and was then spilt in two equal portions using a 3dB optical splitter. At this point the light guided within the fibers was collimated and launched into free space. A mechanical chopper was inserted in the path of both beams. The optical paths were aligned carefully to the apertures of the chopper such that only one path was passed at any time. In this manner the dithering frequency corresponded to the frequency of oscillation between these two paths. After passing through the chopper the free space optical signals were collected and both refocused into separate optical fibers. The signals were connected to a 2×1 MZM (MZM2) where the second portion of RF tone re-modulated the already modulated optical carrier. This signal was then detected and band-pass filtered. The output of the low-pass filter was connected to a lock-in amplifier. The clock from the chopper was also input to the lock-in amplifier as the reference frequency. The optical power received in each of the two chopped paths could be tuned by adjusting the bias of MZM2. It was also possible to fine tune the location of the two optical beams relative to the chopper blades to ensure that there was not time at which both beams were transmitted.

Figure 5.18 shows the amplitude difference of the output voltage of the new system

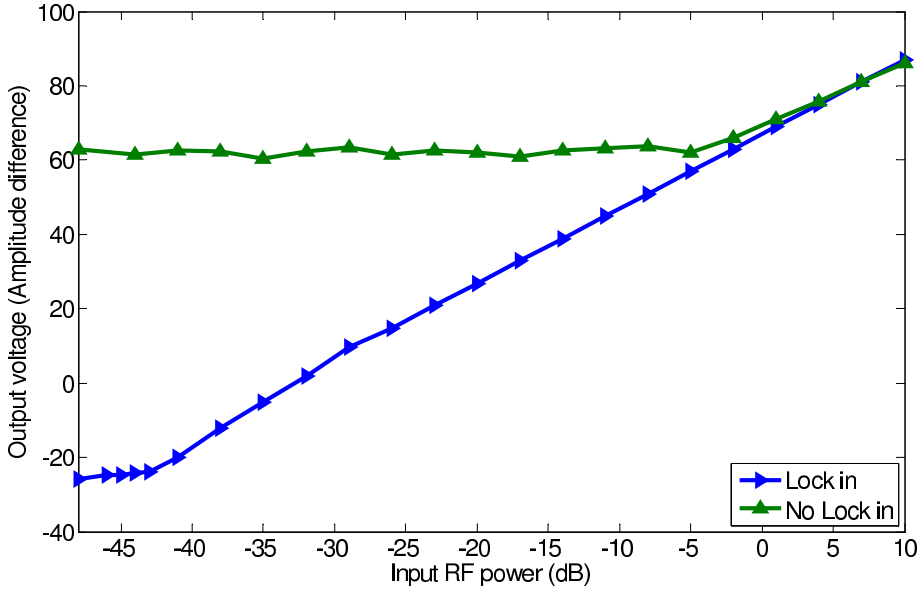

Figure 5.18: Amplitude difference of the the output for different RF input powers.

for different RF input powers. Figure 5.18 shows at least a 35dB sensitivity improvement was achieved using the new technique. This technique should then be a good candidate to be applied to the orthogonal measurement IFM system. It is now possible to adjust the delay of any numbers of wavelengths within a single fiber path.

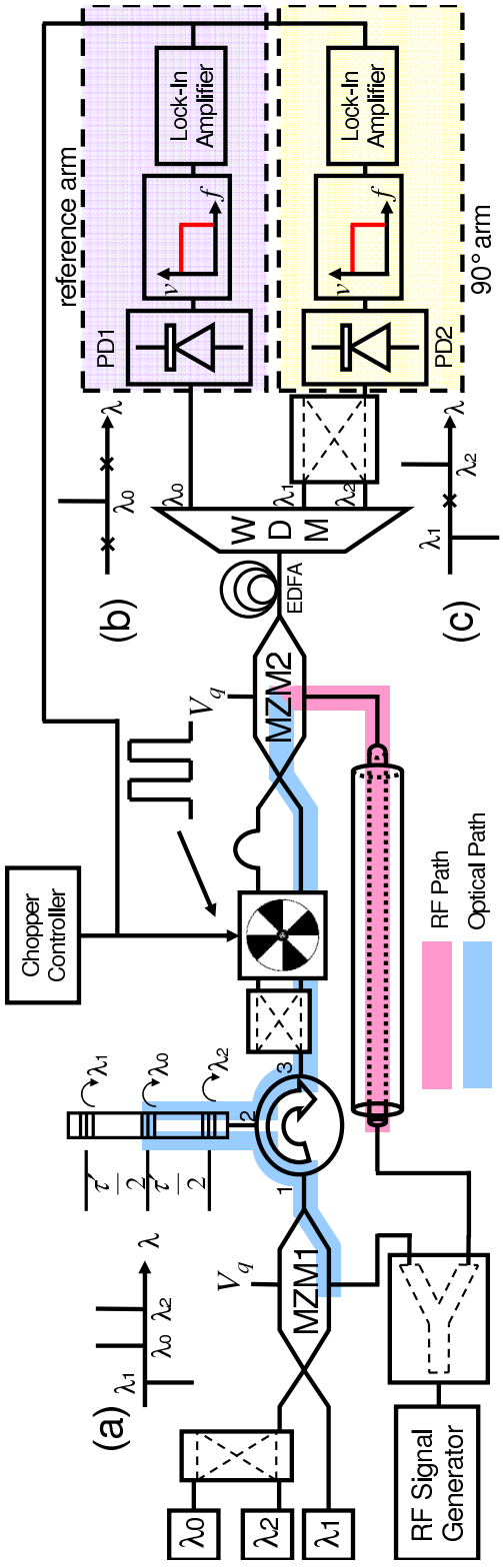

Figure 5.19: Experimental setup of the sensitivity enhanced orthogonal IFM system.

5.6.2 Orthogonal Measurement IFM System Implementation

Since a dithering method was developed needless of wavelength switching, an orthogonal measurement IFM system can now be demonstrated.

Figures 5.19 shows the experimental setup of the sensitivity improved IFM receiver with orthogonal measurement. An RF signal generator produced a single RF tone which was divided into two equal portions feeding two arms of the IFM system. These arms were labelled the Optical Path and the RF Path on Figure 5.19. The RF tone in the Optical Path, modulated three wavelengths being used to implement a two-tap (λ_1, and λ_2) transversal filter with a reference tap ($\lambda_\circ$) in between. Carriers λ_1 and λ_2 were combined using a 3dB optical coupler. This combined signal together with λ_1 were modulated oppositely to make the desired combination as shown in Figure 5.19 inset a). The modulated signal was then input to Port 1 of a Polarization Maintaining (PM) optical circulator. Port 2 of the circulator was connected to a cascaded grating. Each wavelength was reflected with different but uniformly incremented delays. The dispersed signal was output from Port 3 and input to a PM 3dB optical splitter.

Like the experiment of Figure 5.17, the outputs of the splitter were input to the free space with different optical path lengths and the mechanical chopper was inserted in the path of both beams. After passing through the chopper the free space optical signals were collected and both refocused into separate PM optical fibers. The signals were connected to a 2×1 MZM (MZM2) fed with the original RF tone in the RF Path. The output of MZM2 was then input to a Wavelength Division Multiplexer (WDM) which separated all wavelengths. Carrier λ_1 remained separated and was used as the reference (Figure 5.19 inset b)). This arm was called the reference arm. The carriers λ_1 and λ_2 were again combined using a 3dB coupler to make the two-tap transversal filter (Figure 5.19 inset c)). This arm was called the 90° arm. Both signals were then detected, band-pass filtered and measured by a lock-in amplifier which had a reference from the dithering signal controlling the chopper.

Having conceived an improved sensitivity photonic IFM system capable of producing orthogonal measurements, it is now possible to demonstrate the sensitivity improvement of the system.

The system was configured as depicted in Figure 5.19. The optical carriers $\lambda_\circ$, λ_1 and λ_2 were set to 1550, 1551.5, and 1548.5 nm respectively. The optical powers corresponding to these three wavelengths were set to 11.5, 17, and 11.7 mw, respectively. Sequential measurements of the frequency response were taken with incrementally diminishing input RF powers starting from 10dBm to -50dBm. The response of the system of Figure 5.19 was measured for RF input powers of -20dBm, -34dBm and -37dBm and the result is shown in in Figure 5.20. A sensitivity of -37dBm was achieved as expected. Figure 5.21

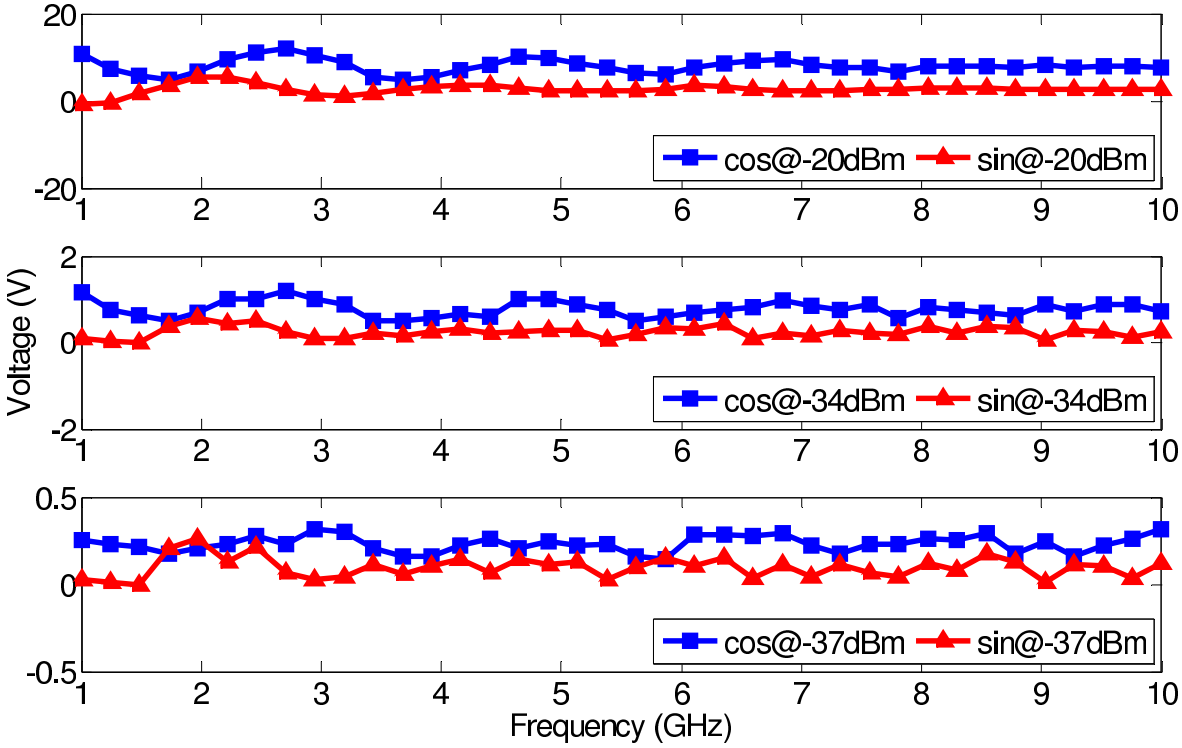

Figure 5.20: Output voltage of IFM system as a function of frequency. RF input powers of -20dBm, -34dBm and -37dBm.

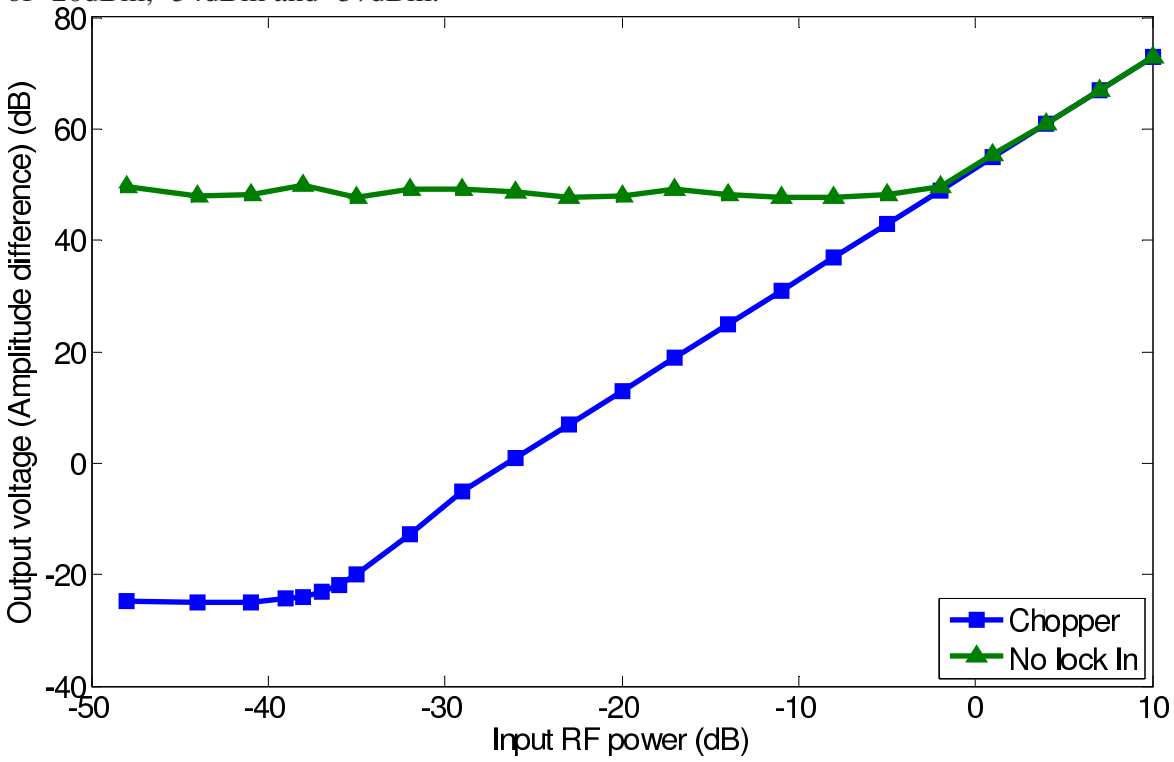

Figure 5.21: Amplitude difference of the output for different RF input powers

shows the amplitude difference of the output for different RF input powers for both locked and unlocked systems. At least 30dB improvement has been achieved using the lock-in technique while achieving orthogonal measurements. Recall from Chapter 3, that due to sinusoidal response of the hybrid coupler the sensitivity should be varied along the pass band of the hybrid coupler and the amplitude response is not ideal. As the nulls of the system are at 0 and 12.5 GHz (as stated in Chapter 3), the system should have the highest sensitivity at 6.25 GHz which is the middle of the band. However, note that the RF path response is frequency dependent and can affect this point as the loss of RF path will increase with frequency increment.

5.6.3 Summary

In summary the sensitivity of a photonic IFM receiver capable of producing orthogonal measurement has been improved using lock-in amplification scheme. This was done based on a new dithering technique where the actual optical lengths were employed along with an optical chopper as a switch to achieve different delays.

5.7 Conclusion

In this Chapter, a technique to improve the sensitivity of the photonic IFM receiver of Chapter 2 was developed and demonstrated practically. It was based on lock-in amplification scheme where a dithering signal was employed to remove the huge DC offset of the IFM measurement. A low frequency version was first developed as the proof of concept. Since the response of the IFM was proportion to the differential delay being caused inside the interferometer, the dithering signal should dither this delay. This was done employing two different wavelengths along with an optical switch and a cascaded grating which provided different delays for different wavelengths. A sensitivity of -35dBm was achieved which is comparable to that of traditional IFM systems. The same technique was applied to the high frequency version of IFM system. While sensitivity was further improved to -41dBm using an almost ideal optical switch. There is scope to extend the frequency range of this IFM into the millimeter range using all optical mixing as demonstrated in Chapter 4. It is conceivable that the sensitivity enhancement techniques demonstrated in this Chapter could be applied to this all optical system creating a very attractive photonic IFM system.

Since the orthogonal measurement IFM system used more than one wavelength, employing a cascaded grating to achieve different delays was not possible in the orthogonal version of the IFM system. A new dithering technique was then developed based

on switching between different physical lengths. This technique was then employed to achieve a dithered delay in the orthogonal IFM system and a sensitivity of -37dBm was achieved. This sensitivity could still be improved further using more taps for the hybrid coupler used inside the IFM system.

Chapter 6

Conclusions

The aim of this thesis was to implement an Instantaneous Frequency Measurement (IFM) system using microwave photonics technology. The photonic IFM system must also have a wide frequency measurement range. Particular emphasis was placed on creating an inexpensive implementation.

An inexpensive photonic IFM was achieved by employing the IFM mixing concept in the optical domain. Down-converting the high frequency RF signals to DC removed the need for high frequency photo-detectors. Since only a DC voltage at the output of the IFM system was required to measure the RF frequency. A proof of concept system able to measure frequencies in the order of MHz was demonstrated. This IFM system was then enhanced to enable measurement of GHz frequencies. Simultaneous measurement of RF frequency and power was then achieved using orthogonal measurements where an optical hybrid coupler was employed to produce orthogonal sets of IFM outputs.

An all optical mixing technique was then used to eliminate the need for undesirable RF cabling. A bandwidth of up to 40 GHz was demonstrated. Finally this sensitivity of the photonic IFM was characterized and lock-in techniques were employed to improve the sensitivity. A sensitivity of -41dBm was achieved which is comparable to traditional IFM systems. Each of these system demonstrations represents a major achievement of this work. A summary of each is presented in the following section.

6.1 Outcomes of This Work

The primary outcome of this work was to develop a microwave photonic IFM receiver. This was achieved in Chapter 2. A new method was introduced to implement an Instantaneous Frequency Measurement (IFM) system based on a photonic scheme where an RF signal was mixed with a delayed version of itself. The output of the system was a DC voltage. This DC voltage depended on the phase between the two mixed RF signal and this, in

turn was RF frequency dependent. The major distinct feature of this system was enabling high frequency measurement using low frequency photo-detectors. This significantly reduced the cost of an IFM unit. This is specifically important when implementing a bank of IFM systems to identify many threat signals independently and simultaneously. One limitation of the system was that measurement of the RF frequency required knowledge of the RF power level.

The IFM system of Chapter 2 relied on knowledge of RF power to identify the RF frequency. In Chapter 3 this problem was investigated and solved. A microwave photonic hybrid coupler was identified and customized for use in this mixed IFM system. Based on the concept of RF hybrids, this photonic configuration provided two outputs, one with 90° phase shift over a broad bandwidth and the other providing a 0° phase reference. This hybrid coupler scheme was achieved using a photonic transversal filtering scheme. Relying on non-coherent optics, the system offered very good stability both in phase and amplitude. Utilizing only a two tap photonic transversal filter, a flat 90° phase shift was achieved over 2-18 GHz frequency range.

Having adopted this wideband photonic hybrid coupler, it was then possible to develop an IFM system which was able to measure both RF frequency and power independently and simultaneously. This transversal photonic hybrid was incorporated into the photonic IFM. This enabled realization of two IFM interferometers with quadrature phase. This resulted in two orthogonal measurements of the same signal enabling two unknowns to be identified. The two unknown measured were RF power and frequency.

Chapter 4 focussed on improving the frequency measurement range using all optical mixing. A Semiconductor Optical Amplifier (SOA) was firstly introduced as a non-linear optical device. The SOA was then characterized and employed to achieve all optical mixing. A frequency measurement range up to 20 GHz was then demonstrated. The unstable nature of SOA was identified as a limit on the performance of the IFM system. ASE noise introduced by the SOA degraded the sensitivity of the IFM system. Highly Non-Linear Fiber (HLNF), was then introduced as a solution. Since HLNF is passive , it exhibits better stability when compared with the SOA. The SOA was then replaced by HLNF and an all optical mixing IFM was then demonstrated up to 40 GHz frequency range. The demonstrated system with HNLF was exceptionally stable.

Chapter 5 explored the sensitivity of the optical IFM system developed in Chapter 2. The sensitivity of the system was characterized first and it was found that the sensitivity was only -2dB. This required improvement. A lock-in amplification scheme was employed to improve the sensitivity of the IFM system. In this technique a dithering signal was used to vary the length of one of the delay lines, and thus the relative delay of the IFM interferometer. Two different wavelengthes were first used along with a cascaded grating

and a double balanced MZM to switch between two different paths. Then a high extinction mechanical optical switch was constructed to switch between two different physical lengths. This led to a sensitivity of -41dBm. This sensitivity improvement technique was also incorporated into the orthogonal measurement IFM system of Chapter 3 leading to a sensitivity of -37dBm. This final demonstration can be considered a practical photonic IFM system.

In summary, a new microwave photonic technique has been introduced to implement an IFM system. This IFM system features wideband frequency range, low cost and good sensitivity comparable to the traditional IFM systems.

6.2 Suggestions for Future Work

The primary goal of realizing a photonic Instantaneous Frequency Measurement were achieved. Providing more taps for the IFM system, would enable wider frequency measurement range and thus better sensitivity. It may also minimize the computer processing time as there would be no need to include the sinusoidal shape of the magnitude of the transversal filter in computer programming.

For the systems of Chapter 2 and Chapter 3 monolithic or hybrid integration could be employed to remove the need for any co-axial cable used for optical path length compensation. This would improve the frequency measurement range of the system. Having achieved a wide frequency measurement range, the IFM system could respond to pulse modulated signals. It also would decrease the bulk of the system dramatically, redesign it practical for use in defence systems.

For the sensitivity improved system of Chapter 5, mechanical choppers are not practical to be used in defence systems. High extinction photonic switches could be employed to stabilize the performance of the system. This would also decrease the size and weight of the system. The lock-in technique could also be employed into the all optical mixing IFM system to improve the sensitivity while achieving very wideband frequency measurement range up to 40 GHz. The photonic hybrid concept could also be incorporated into the all optical mixing approach to achieve broadband independent RF frequency and power measurement. This will result in a complete IFM system featuring broad bandwidth, high sensitivity, and capability of measuring the RF frequency and power independently.

Parallel IFM system could also be implemented. This would require only more optical carriers all combined and traversed through only one MZM. Inexpensive laser diodes could be employed for cost efficiency. Since the photonic IFM system employs only low-cost photo-detectors, the total cost of the system would be relatively low. Employing parallel IFM systems would increase the frequency resolution of the system. It also

enables detection of more than one threat simultaneously.

In the real electronic warfare battle environment, there maybe more than one threat at a time. Multiple IFM systems are then required to obtain sufficient number of measurements to be able to identify all threat signals independently. A similar method to [66] could also be employed to identify simultaneous microwave signals.

Since the photonic IFM system provides reconfigurability, a scanning receiver could also be implemented based on narrowing the bandwidth of the IFM interferometer. It would be imaginable that the same IFM system would first be used to identify the threat frequency and then be employed as a scanning receiver to obtain a high resolution frequency measurements. Such a dynamically reconfigurable photonic IFM system would offer a wealth of research opportunity for future investigations.

References

[1] D. Wake, M. Webster, G. Wimpenny, K. Beacham, and L. Crawford, "Radio over fiber for mobile communications," pp. 157–160, Oct. 2004.

[2] S. Mansoori, "Photonically implemented RF transversal filters using broad band optical source and reconfigurable optical filters," 2004. PhD thesis.

[3] A. Nesic, B. Jokanovic, and N. Popovic, "A miniature surveillance 8-40 GHz radar detector," *Microwave Review*, vol. 10, no. 2, pp. 53–56, 2004.

[4] A. Alexiou and M. Haardt, "Smart antenna technologies for future wireless systems: trends and challenges," *IEEE Communications Magazine*, vol. 42, pp. 90–97, Sept. 2004.

[5] S. A. Vakin, S. A. Shustov, and R. H. Dunwell, *Fundamentals of electronic warfare*. Artech House, 2001.

[6] J. P. Stephen, "Advance signal processing technology for electronic warfare," *IEEE ASE. sytem magezin*, pp. 31 –38, 1996.

[7] I. Hunter, a. B. J. L. Billonet, and P.Gullion, "A review of current and future components for electronic warfare receivers," *IEEE Trans. Microwave Theory Tech.*, vol. 5, pp. 794–805, May 2002.

[8] H. Emami, "Implementataion of a hybrid coupler in optical domain (submitted)," 2008. PhD thesis, Submitted In Nov 2008.

[9] R. A. Minasian, "Photonic signal processing of high-speed signals using fiber gratings," *Opt. Fiber Tech.*, vol. 6, no. 2, pp. 91–108, 2000.

[10] R. A. Minasian, "Photonic signal processing of microwave signals," *IEEE Microwave Theory Tech.*, vol. 54, no. 2, pp. 832–846, 2006.

[11] A. Loayssa and F. J. Lahoz, "Broad-band RF photonic phase shifter based on stimulated brillouin scattering and single-sideband modulation," *IEEE Photon. Tech. Lett.*, vol. 18, no. 1, pp. 208–210, 2006.

[12] M. R. Fisher and S. L. Chuang, "A microwave photonic phase-shifter based on wavelength conversion in a dfb laser," *IEEE Photon. Tech. Lett.*, vol. 18, no. 16, pp. 1714–1716, 2006.

[13] L. A. Bui, A. Mitchell, K. Ghorbani, T.-H. Chio, S. Mansoori, and E. R. Lopez, "Wide-band photonically phased array antenna using vector sum phase shifting approach," *IEEE Trans. Antennas Propag.*, vol. 53, no. 11, pp. 3589–3596, 2005.

[14] H. Zmuda, R. A. Soref, P. Payson, S. Johns, and E. N. Toughlian, "Photonic beamformer for phased array antennas using a fiber grating prism," *IEEE Photon. Tech. Lett.*, vol. 9, no. 2, pp. 241–243, 1997.

[15] R. A. Minasian and K. E. Allameh, "Optical-fiber grating-based beamforming network for microwavephased arrays," *IEEE Microwave Theory Tech.*, vol. 45, no. 8, pp. 1513–1518, 1997.

[16] B. Vidal, J. L. Corral, and J. Marti, "All-optical wdm microwave filter with negative coefficients," *IEEE Photon. Tech. Lett.*, vol. 17, no. 3, pp. 666–668, 2005.

[17] J. Yao and Q. Wang, "Photonic microwave bandpass filter with negative coefficients using a polarization modulator," *IEEE Photon. Tech. Lett.*, vol. 19, no. 9, pp. 644–646, 2007.

[18] D. B. Hunter and L. V. T. Nguyen, "Widely tunable RF photonic filter using wdm and a multichannel chirped fiber grating," *IEEE Trans. Microwave Theory Tech.*, vol. 54, pp. 900–905, Feb. 2006.

[19] E. H. W. Chan and R. A. Minasian, "Photonic RF phase shifter and tunable photonic RF notch filter," *IEEE J. Lightwave Tech.*, vol. 24, no. 7, pp. 2676–2682, 2006.

[20] E. H. W. Chan and R. A. Minasian, "Sagnac-loop-based equivalent negative tap photonic notch filter," *IEEE Photon. Tech. Lett.*, vol. 17, no. 8, pp. 1740–1742, 2005.

[21] J. Capmany, D. Pastor, B. Ortega, and S. Sales, "Optical processing of microwave signals," in *2000 International Topical Meeting on Microwave Photonics, Oxford, UK*, pp. 241–244, Sept. 2000.

[22] A. Seeds, "Optical transmission of microwaves." in the Review of Radio Science, W. Stone, ed. London: Oxfprd University Press.

[23] A. Seeds and K. Williams, "Microwave photonics," *IEEE J. Lightwave Tech.*, vol. 24, no. 12, pp. 4628–4641, 2006.

[24] J. Capmany, B. Ortega, D. Pastor, S. Sales, P.-Y. Fonjallaz, M. Popoy, L. Pierno, and M. Varasi, "Microwave photonic signal processing for wireless systems and optical internet: overview of the current achievement of the ist-labels project," in *Proc. 2004 6th International Conf. Trasnparent Optical Networks, Wroclaw, Poland*, vol. 2, pp. 8–12, 2004.

[25] P. J. Matthews and P. D. Biernacki, "Photonic signal processing for microwave applications," *IEEE Trans. Microwave Theory Tech-S Digest.*, pp. 877–880, June 1999.

[26] J. Marti, M. Fuster, J. L. Corral, F. Ramos, and V. Polo, "Optical processing of microwave signals," pp. 181–184, Jan. 2001.

[27] J. D.Lynch, *Introduction to RF Stealth*. Scitech, 2004.

[28] D.Schleher, *Introduction to Electronic warfare*. Artech House, 1986.

[29] D. C. Puzzo, "Instantaneous frequency measurement apparatus and method." US Patent no. 5168215.

[30] H. Gruchala and M. Czyzewski, "The instantaneous frequency measurement receiver in the complex electromagnetic environment," in *Proceedings of International Conference on Microwave, RADAR, and Wireless Communications (MIKON2004)*, vol. 1, pp. 155–158, May 2004.

[31] J. B. Y. Tsui, "Instantaneous frequency measurement receiver with digital processing." US Patent no. 633516.

[32] "http://www.widebandsystems.com/ifm.shtml."

[33] J. B. Tsui, *Microwave Receivers with Electronic Warefare Applications*. New York: Willey, 1986.

[34] C. Sinclair, "A coplanar waveguide 6-18 GHz instantaneous frequency measurement unit for electronic warfare systems," in *1994 IEEE MTT-S International Microwave Symposium Digest*, vol. 3, pp. 1767–1770, May 1994.

[35] W. G. James, "Instantaneous frequency measurement system." US Patent no. 3939411.

[36] S. Kumar, A. Mohammadi, and D. Klymyshyn, "A direct 64qam modulator suitable for mmic applications," *Microwave Journal*, vol. 40, no. 12, pp. 116–122, 1997.

[37] M. Aikawa and H. Oqawa, "Double-sided mics and their applications," *IEEE Trans. Microwave Theory Tech.*, vol. 37, no. 2, pp. 406–413, 1989.

[38] J. B. Y. Tsui and W. S. McCormick, "Instantaneous frequency measurement (ifm) receiver with only two delay." US Patent no. 4963816.

[39] J. B. Y. Tsui and D. L. Sharpin, "Frequency measurement receiver with bandwidth improvement through synchronized phase shifted sampling." US Patent no. 5198746.

[40] R. B. Sanderson and J. B. Y. Tsui, "Instantaneous frequency measurement receiver with bandwidth improvement through phase shifted sampling of real signals." US Patent no. 5109188.

[41] J. P. Coupez, H. Gruchala, A. Slowik, C. Recko, and A. Rutkowski, "High resolution ifms," in *14th International Conference on Microwaves, Radar and Wireless Communications, 2002. MIKON*, vol. 2, pp. 484– 487, 2002.

[42] J. Capmany and D. Novak, "Microwave photonics combine two worlds," *Nature Photonics*, vol. 1, pp. 319–330, June 2007.

[43] P. J. Matthews and P. D. Biernacki, "Photonic signal processing for microwave applications," in *1999 IEEE MTT-S International Microwave Symposiom Digest*, vol. 3, pp. 877–880, 1999.

[44] J. Capmany, D. Pastor, A. Martinez, B. Ortega, and S. Sales, "Microwave photonic filters with negative coefficients based on phase inversion in an electro-optic modulator," *Opt. Lett.*, vol. 28, pp. 1415–1417, Aug. 2003.

[45] J. Capmany, B. Ortega, and D. Pastor, "A tutorial on microwave photonic filters," *J. Lightwave Tech.*, vol. 24, pp. 201–229, Jan. 2006.

[46] D. Pastor, J. Capmany, B. Ortega, A. Martinez, L. Pierno, and M. Varasi, "Reconfigurable RF photonic filter with negative coefficients and flat-top resonances using phase inversion in a newly designed 2/spl times/ 1 integrated mach-zehnder modulator," *IEEE Photon. Tech. Lett.*, vol. 16, pp. 2126–2128, Sept. 2004.

[47] K. J. Williams, J. L. Dexter, and R. D. Esman, "Photonic microwave signal processing," in *International Topical Meeting on Microwave Photonics, 1997.*, pp. 187–190, 1997.

[48] E. Ackerman and H. Cox, "RF fiber-optic link performance," *IEEE Microwave Magazine*, vol. 2, no. 4, pp. 50–58, 2001.

[49] R. Ramaswami and K. Sivarajan, "Routing and wavelength assignment in all-optical networks," *IEEE/ACM Trans. Networking*, vol. 3, no. 5, pp. 1375–1383, 1995.

[50] O. Tonguz and H. Jung, "Personal communications access networks using subcarriermultiplexed optical links," *J. Lightwave Tech.*, vol. 14, no. 6, pp. 1400–1409, 1996.

[51] C. Cox, E. Ackerman, R. Helkey, and G. betts, "Direct-detection analog optical links," *IEEE Trans. Microwave Theory Tech.*, vol. 45, no. 8, pp. 1375–1383, 1997.

[52] J. Chiddix, H. Laor, D. Pangrac, L. Williamson, and R. Wolfe, "Am video on fiber in catv systems: need and implementation," *IEEE J. Selected Areas in Communications*, vol. 8, no. 7, pp. 1229–1239, 1990.

[53] D. Madris, B. Vidal, V. . P. A. Martinez, J. L. Corral, and J. Marti, "A novel 2N beams heterodyne optical beamforming architecture based on NN optical butler matrices," in *2002 IEEE MTT-S International Microwave Symposium Digest, Seattle, WA/USA*, vol. 3, pp. 1945–1948, 2002.

[54] I. Lin, J. McKinney, and A. Weiner, "Photonic synthesis of broadband microwave arbitrary waveform applicable to ultra-wideband communication," *IEEE Microwave Wireless Components Lett.*, vol. 15, no. 4, pp. 226–228, 2005.

[55] J. Capmany, J. Mora, B. Ortega, and D. Pastor, "Microwave photonic filters using low-cost sources featuring tunability, reconfigurability and negative coefficients," *Opt. Exp.*, vol. 13, pp. 1188–1190, Mar. 2005.

[56] L. V. T. Nguyen and D. B. Hunter, "A photonic technique for microwave frequency measurement," *IEEE Photon. Tech. Lett.*, vol. 18, pp. 1188–1190, May 2006.

[57] H. Chi, X. Zou, and J. Yao, "An approach to the measurement of microwave frequency based on optical power monitoring," *IEEE Photon. Tech. Lett.*, vol. 20, pp. 1249–1251, July 2008.

[58] X. Zou and J. Yao, "An optical approach to microwave frequency measurement with adjustable measurement range and resolution," *IEEE Photon. Tech. Lett.*, vol. 20, pp. 1989–1991, Dec. 2008.

[59] X. Zou, H. Chi, and J. Yao, "Microwave frequency measuremnt based on optical power monitoring using a compementary optical filter," *IEEE Trans. Microwave Theory Tech.*, vol. 57, pp. 505–511, Feb. 2009.

[60] S. F. J. Zhou, P. P. Shum, S. Aditya, L. Xia, J. Li, X. Sun, and K. Xu, "Photonic measurement of microwave frequency based on phase modulation," *Opt. Exp.*, vol. 17, pp. 7217–7221, Apr. 2009.

[61] X. Zhang, H. Chi, Z. zhang, S. Zhang, X. Jin, and J. Yao, "Instataneous microwave frequency measuremnt using an optical phase modulator," *IEEE Microwave Component Lett.*, vol. 19, pp. 422–424, June 2009.

[62] J. Li, S. Fu, J. Q. Zhou, P. Shum, J. Wu, and J. Lin, "Photonic-assisted microwave frequency measurement with higher resolution and tunable range," *Opt. Lett.*, vol. 34, pp. 743–745, Mar. 2009.

[63] X. Zou and J. Yao, "Microwave frequency measuremnt with improved measureemnt range and resolution," *Electron. Lett.*, vol. 45, pp. 497–498, May 2009.

[64] M. V. Drummond, P. Monterio, and R. N. Nogueira, "Photonic RF instataneous frequency measureemnt system by means of a plarization domain interferometer," *Opt. Exp.*, vol. 17, pp. 5433–5438, Mar. 2009.

[65] H. Guo, G. Xiao, N. Mrad, and J. Yao, "Measureemnt of microwave frequency using a monolithically integrated scannable echelle diffractive grating," *IEEE Photon. Tech. Lett.*, vol. 34, pp. 45–47, Jan. 2009.

[66] L. V. T. Nguyen, "Microwave photonic technique for frequency measurement of simultaneous signals," *IEEE Photon. Tech. Lett.*, vol. 21, pp. 642–644, May 2009.

[67] N. Sarkhosh, H. Emami, L. A. Bui, and A. Mitchell, "Reduced cost microwave photonic instantaneous frequency measurement system," *IEEE Photon. Tech. Lett.*, vol. 20, pp. 1521–1523, Sept. 2008.

[68] N. Sarkhosh, H. Emami, and N. a. A. M. L. A. Bui, T, "Low-cost RF frequency measurement using photonic approach," in *Joint International Conference on Optical Internet, 2007 32nd Australian Conference on Optical Fibre Technology. COIN-ACOFT 2007.*, June 2007.

[69] N. Sarkhosh, H. Emami, L. A. Bui, and A. Mitchell, "Photonic instantaneous frequency measurement using non-linear optical mixing," in *2008 IEEE MTT-S International Microwave Symposium Digest*, June 2008.

[70] H. Emami, N. Sarkhosh, L. A. Bui, and A. Mitchell, "Wideband RF photonic in-phase and quadrature-phase generation," *Opt. Lett.*, vol. 33, pp. 98–100, Jan. 2008.

[71] H. Emami, L. A. Bui, and A. Mitchell, "Broadband 90 degree hybrid coupler using photonic transversal approach," in *Proc. Asia-Pacific Microwave Photon. Conf., Kobe, Japan*, vol. 3, pp. 173–176, 2006.

[72] N. Sarkhosh, H. Emami, L. A. Bui, and A. Mitchell, "Microwave photonic instantaneous frequency measurement with improved sensitivity," in *2009 IEEE MTT-S International Microwave Symposium Digest Accepted*, 2009.

[73] S. T. Winnall and A. C. Lindsay, "A fabry-perot scanning receiver for microwave signal processing," *IEEE Trans. Microwave Theory Tech.*, vol. 47, pp. 1385–1390, July 1999.

[74] S. Rani and K. R. Sundaram, "Cots approach shrinks EW recivers," *Cots Journal*, vol. 6, Apr. 2004.

[75] G. Liang, C. Shih, R. S. Withers, B. F. Cole, M. E. Johansson, and L. P. Suppan, "Superconductive digital instantaneous frequency measurement subsystem," *IEEE Trans. Microwave Theory Tech.*, vol. 41, no. 12, pp. 2368–2375, 1993.

[76] G. Liang, C. Shih, R. S. Withers, B. F. Cole, and M. E. Johansson, "Space-qualified superconductive digital instantaneous frequency measurement subsystem," *IEEE Trans. Microwave Theory Tech.*, vol. 44, no. 7, pp. 1289–1299, 1996.

[77] L. V. T. Nguyen, G. Edvell, D. B. Hunter, and M. Englund, "Wideband in-phase and quadrature microwave signal generation utilising a multichannel chirped fibre grating," in *Proc. Australian Conf. on Optical fibre Tech., Melbourne, VIC/Australia*, vol. 3, pp. 25–27, 2006.

[78] H. Emami, N. Sarkhosh, L. A. Bui, and A. Mitchell, "Amplitude independent RF instantaneous frequency measurement system using photonic Hilbert transform," *Opt. Exp.*, vol. 16, pp. 13707–13712, Sept. 2008.

[79] J. F. Kaiser and R. W. Schafer, "On the use of the i_0-sinh window for spectrum analysis," *IEEE Trans. Acoustic, Speech and Signal Processing*, vol. ASSP-28, no. 1, pp. 105–107, 1980.

[80] L. A. Bui, M. Pelusi, T. Vo, N. Sarkhosh, H. Emami, A. Mitchell, and B. Eggleton, "Photonic instantaneous frequency measurement using optical mixing in highly nonlinear fiber." submitted to Opt. Exp.

[81] T. Durhuss, B. Mikkelsen, C. Joergensen, S. L. Danielsen, and K. E. Stubkjaer, "All-optical wavelength conversion by semiconductor optical amplifiers," *IEEE J. of Lightwave Tech.*, vol. 14, no. 6, pp. 942–953, 1996.

[82] S. Diez, C. Schmidt, R. Ludwig, K. O. H. G. Weber, S. Kindt, I. Koltchanov, and K. Petermann, "Four-wave mixing in semiconductor optical amplifiers for frequency conversion and fast optical switching," *IEEE J. Selected Topics in Quantum Electron.*, vol. 3, pp. 1131 –1145, Oct. 1997.

[83] A. C. Bordonalli, J. A. Guimaraes, J. L. Benitez, and a. C. M. G. E. Conforit, "Signal generation by optical mixing in feedbacked semiconductor optical amplifiers," in *SBMO/IEEE MTT-S International Microwave and Optoelectronics Conference*, pp. 111–114, 2001.

[84] A. C. Lindsay, G. A. Knight, and S. T. Winnall, "Photonic mixers for wide bandwidth RF receiver applications," *IEEE Trans. Microwave Theory Tech.*, vol. 43, pp. 2311 –2317, Sept. 1995.

[85] J. Capmany, S. Sales, and a. B. O. D. Pastro, "Optical mixing of microwave signals in a nonlinear semiconductor laser amplifier modulator," *Opt. Exp.*, vol. 10, pp. 183–189, Feb. 2002.

[86] Y.-K. Seo, J.-H. Seo, and W.-Y. Choi, "Photonic frequency-upconversion efficiencies in semiconductor optical amplifiers," *IEEE Photon. Tech. Lett.*, vol. 15, pp. 751–753, May 2003.

[87] K. F. Brennan, *Introduction to semiconductor devices*. Cambridge University Press, 2005.

[88] N. Sarkhosh, H. Emami, L. A. Bui, K. Ghorbani, and A. Mitchell, "Sensitivity improved photonic instantaneous frequency measurement receiver," in *Asia-Pacific Microwave Conf., Hong-Kong*, 2008.

[89] N. Sarkhosh, H. Emami, L. A. Bui, and A. Mitchell, "Improved sensitivity photonic instantaneous frequency measurement," *submitted to Opt. Lett.*

[90] N. Sarkhosh, H. Emami, L. A. Bui, and A. Mitchell, "Sensitivity improved orthognal measurement photonic instantaneous frequency measurement." submitted to MTT.

[91] R. Wolfson, "The lock-in amplifier: A student experiment," *american J. Phys.*, vol. 59, pp. 569–572, June 1991.

[92] A. Mandelis, S. Paoloni, and L. Nicolaides, "Novel lock-in waveform technique for signal-to-noise ratio and dynamic-range enhancement in highly noised photothermal experiments," *J. Analytical Siences*, vol. 17, pp. s5–s8, Apr. 2001.

[93] D. Dobrev, T. Neycheva, and N. Mudrov, "Digital lock-in techniques for adaptive power-line interference extraction," *J. Physiological measurment*, vol. 29, pp. 803–816, June 2008.

[94] T. Hidaka, T. Maruyama, M. Saitoh, N. Mikoshiba, M. Shimizu, T. Shiosaki, L. A. Wills, R. Hiskes, S. A. Dicarolis, and J. Amano, "Formation and observation of 50 nm polarized domains in pbzr1 xtixo3 thin film using scanning probe microscope," *Appl. Phys. Lett.*, vol. 68, p. 2358, Apr. 1996.

[95] G. Behme, T. Hesjedal, E. Chilla, and H.-J. Frhlich, "Transverse surface acoustic wave detection by scanning acoustic force microscopy," *Appl. Phys. Lett.*, vol. 73, p. 882, Aug. 1998.

[96] S. Heinemann, F. Conti, W. Stuhmer, and E. Neher, "Effects of hydrostatic pressure on membrane processes. sodium channels, calcium channels, and exocytosis," *J. General Physiology*, vol. 90, pp. 765–778, Dec. 1987.

[97] J. M. Herbelin, J. A. McKay, M. A. Kwok, R. H. Ueunten, D. S. Urevig, D. J. Spencer, and D. J. Benard, "Sensitive measurement of photon lifetime and true reflectances in an optical cavity by a phase-shift method," *J. Applied Optics*, vol. 19, pp. 144–147, Jan. 1980.

[98] J. A. Giordmaine, L. E. Alsop, C. H. Mayer, and C. Townes, "A maser amplifier for radio astronomy at x-band," *IEEE Proceedings of the Instituite of Radio Engineers*, vol. 47, pp. 1062–1069, June 1959.

[99] S. A. S. Asif, K. J. Wahl, and R. J. Colton, "Nanoindentation and contact stiffness measurement using force modulation with a capacitive load-displacement transducer," *Rev. Sci. Instrum.*, vol. 70, p. 2408, May 1999.

[100] P. Harms, J. Sipior, N. Ram, G. M. Carter, and G. Rao, "Low cost phase-modulation measurements of nanosecond fluorescence lifetimes using a lock-in amplifier," *Rev. Sci. Instrum.*, vol. 70, p. 1535, Feb. 1999.

[101] O. Solgaard, A. A. Godil, B. R. Hemenway, and D. M. Bloom, "All-silicon integrated optical modulator," *IEEE Selected Areas in Communications*, vol. 9, pp. 704–710, June 1991.

Publications

Journal Publications

H. Emami, N. Sarkhosh, E. Lopez, and A. Mitchell, "Photonic phase driver for sinuous antenna," *Opt. Exp. (in preparation)*.

L. A. Bui, M. Pelusi, T. Vo, N. Sarkhosh, H. Emami, A. Mitchell, and B. J. Eggleton, "Photonic Instantaneous Frequency Measurement using optical mixing in Highly Nonlinear Fiber," *Opt. Exp. (Submitted)*.

N. Sarkhosh, H. Emami, L. A. Bui, and A. Mitchell, "Sensitivity improved orthogonal measurement photonic instantaneous frequency measurement system," *IEEE Trans. Microwave Theory Tech. (Accepted)*.

N. Sarkhosh, H. Emami, L. A. Bui, and A. Mitchell, "Sensitivity improved photonic instantaneous frequency measurement system," *Opt. Lett. (Accepted)*.

H. Emami, N. Sarkhosh, L. A. Bui, and A. Mitchell, "Amplitude independent RF instantaneous frequency measurement system using photonic Hilbert transform," *Opt. Express*, vol. 16, no. 18, pp. 13707–13712, Sep. 2008.

N. Sarkhosh, H. Emami, L. A. Bui, and A. Mitchell, "Reduced cost microwave photonic instantaneous frequency measurement system," *IEEE Photon. Tech. Lett.*, vol. 20, no. 18, pp. 1521-1523, Sep. 2008.

H. Emami, N. Sarkhosh, L. A. Bui, and A. Mitchell, "Wideband RF photonic in-phase and quadrature-phase generation," *Opt. Lett.*, vol. 33, pp. 98–100, Jan. 2008.

Conference Publications

N. Sarkhosh, H. Emami, L. A. Bui, and A. Mitchell, "Microwave Photonic Instantaneous Frequency Measurement with Improved Sensitivity," in *2009 IEEE MTT-S International Microwave Symposium Digest, Boston, USA*, June 2009.

N. Sarkhosh, H. Emami, K. Gorbani, L. A. Bui, and A. Mitchell, "Sensitivity Improved Photonic Instantaneous Frequency Measurement," in *Asia Pacific Microwave Conference. Hong Kong*, December 2008.

N. Sarkhosh, H. Emami, L. A. Bui, and A. Mitchell, "RF Photonic Instantaneous Frequency Measurement Using DC Photo-Detection," in *The 2008 33nd Australian Conference on Optical Fibre Technology, Sydney, Australia*, pp. 1–2, July 2008.

N. Sarkhosh, H. Emami, L. A. Bui, and A. Mitchell, "Photonic instantaneous frequency measurement using non-linear optical mixing," in *2008 IEEE MTT-S International Microwave Symposium Digest, Atlanta, USA*, pp. 1–3, June 2008.

H. Emami, N. Sarkhosh, L. A. Bui, and A. Mitchell, "Two output RF hybrid coupler using photonic transversal approach," in *Asia Pacific Microwave Conference. Bangkok, Thailand*, December 2007.

N. Sarkhosh, H. Emami, L. A. Bui, and A. Mitchell, "Low-cost RF frequency measurement using photonic approach," in *Joint International Conference on Optical Internet, 2007 and the 2007 32nd Australian Conference on Optical Fibre Technology. COINACOFT 2007, Melbourne, Australia*, pp. 1–3, 2007.